KTH ROYAL INSTITUTE
OF TECHNOLOGY

Degree Project in Chemical Engineering

Second cycle 30 credits

The Mechanism behind Internal Injector Deposits

JENNY BLOMBERG

Stockholm, Sweden 2023

Author

Jenny Blomberg
Chemical Engineering for Energy and Environment
KTH Royal Institute of Technology

Place for Project

Stockholm, Sweden
Scania CV AB

Date

2023-06-16

Examiner

Associate Prof. Henrik Kusar
Division of process technology
KTH Royal Institute of Technology

Supervisor

Henrik Hittig, Scania CV AB
Mayte Pach, Scania CV AB

Associate Prof. Henrik Kusar, KTH Royal Institute of Technology

Keywords

Biodiesel, deposit formation, engine oil, calcium sulphate, internal diesel injector deposits

Nyckelord

Biodiesel, beläggningsbildning, motorolja, kalciumsulfat, interna dieselinjektorbeläggningar

Abstract

The use of biofuels has increased to reduce the emissions from fossil fuels. However, the use of biofuels results in deposit formation inside the injector, which leads to issues with the drivability of the vehicle. The most believed hypothesis behind the deposit formation is that engine oil contamination in the fuel system leads to formation of calcium sulphate crystals that soft particles adhere to. Moreover, temperature is claimed to have a significant effect on the deposit formation. To ease the shift towards more renewable fuels, more understanding behind the deposit mechanism is needed. Therefore, this study aimed to investigate the mechanism behind internal injector deposits with a newly designed lab scale rig to get a deeper understanding of the mechanism, and especially the role of calcium sulphate and temperature.

The aim was achieved by dividing the experimental work into two parts:

a) Running the test-rig with test fuels followed by analyses of the samples with mainly SEM-EDX and FTIR, to understand the role of temperature, and engine oil for the deposit mechanism.
b) Solubility studies of calcium sulphate to understand the role of calcium sulphate for the deposit mechanism.

The results showed that the newly designed test rig worked well, where the results were consistent with literature and offered repeatability. Thereby, the rig is recommended for future studies of internal injector deposits. A deeper understanding of the mechanism behind the internal injector deposits was successfully achieved. For the first time, a FTIR and SEM-EDX study was performed over a temperature gradient, which made it possible to see the onset temperature for different reactions and to identify deposits in different temperature ranges. It was showed that the deposit formation was temperature dependent with different types of deposits in different temperature ranges. At temperatures below 100°C, zinc sulphate and unreacted metal carboxylates were the dominant species. Above 100°C, the metal carboxylates changed form and became more concentrated while the concentration of zinc sulphate decreased. Moreover, calcium sulphate showed to be formed to a large extent when the temperature exceeded 100°C. The temperature study and results are unique and unknown in the literature. Ostwald ripening has been proposed as a possible mechanism in the literature but turned out to be unlikely. The dissolution of calcium sulphate by engine oil additives followed by precipitation in the fuel showed to be a more likely mechanism. It was also shown that soap deposits promoted the deposit formation of calcium sulphate crystals, which is in line with the field observations since they normally coexist.

Keywords: Biodiesel, deposit formation, engine oil, calcium sulphate, internal diesel injector deposits

Sammanfattning

Användningen av biobränslen har ökat för att minska utsläppen från fossila bränslen. Biobränslen kan dock leda till beläggningar inuti injektorn, vilka påverkar fordonets körbarhet. Den mest trodda hypotesen bakom beläggningsbildningen är att förorening av motorolja i bränslesystemet leder till bildning av kalciumsulfatkristaller som mjuka partiklar fäster till. Dessutom påstås det att temperaturen har en signifikant påverkan på beläggningsbildningen. För att ställa om till mer förnyelsebara bränslen krävs mer förståelse bakom beläggningarnas mekanism. Därför var syftet med denna studie att undersöka mekanismen bakom interna injektorbeläggningar med en nydesignad rigg i laboratorieskala för att få en djupare förståelse av mekanismen, och i synnerhet rollen av kalciumsulfat och temperatur.

Syftet uppnåddes genom att dela upp det experimentella arbetet i två delar:

a) Köra riggen med testbränslen följt av analyser av de körda proverna med huvudsakligen SEM-EDX och FTIR, för att förstå rollen av temperatur och motorolja för beläggningarnas mekanism.
b) Löslighetsstudier av kalciumsulfat för att förstå rollen av kalciumsulfat för beläggningarnas mekanism.

Resultaten visade att den nydesignade testriggen fungerade bra med resultat som överensstämde med litteratur och erbjöd repeterbarhet. Därmed rekommenderas riggen för framtida studier av interna injektorbeläggningar. En djupare förståelse av mekanismen bakom interna injektorbeläggningar uppnåddes framgångsrikt. För första gången utfördes en FTIR och SEM-EDX studie över en temperaturgradient, vilket gjorde det möjligt att se starttemperaturen för olika reaktioner och identifiera beläggningar i olika temperaturintervall. Det visades att beläggningsbildningen var temperaturberoende med olika typer av beläggningar i olika temperaturintervall. Vid temperaturer under 100°C var zinksulfat och oreagerat metallkarboxylat de dominanta ämnena. Över 100°C ändrade metallkarboxylatet form och blev mer koncentrerat medan koncentrationen av zinksulfat minskade. Dessutom visades det att kalciumsulfat bildades i stor utsträckning när temperaturen översteg 100°C. Temperaturstudien och resultaten är unika och okända i litteraturen. Ostwald-mognad har föreslagits som en möjlig mekanism i litteraturen men visade sig vara osannolik. Upplösningen av kalciumsulfat av motoroljans additiv följt av utfällning i bränslet visade sig vara en mer sannolik mekanism. Det visades också att tvålbeläggningar främjade beläggningsbildning av kalciumsulfatkristaller, vilket överensstämmer med fältobservationer då de vanligtvis samexisterar.

Nyckelord: Biodiesel, beläggningsbildning, motorolja, kalciumsulfat, interna dieselinjektorbeläggningar

Acknowledgements

I would firstly like to express a large gratitude to my supervisors Mayte Pach and Henrik Hittig from Scania CV AB, and my examiner Henrik Kusar from KTH. Your guidance has been very appreciated, and the results from my thesis would not have been possible without their help and advice. I would also like to thank all my colleagues at Scania CV AB for your support and help during the thesis work. You made my work much easier. Lastly, I want to thank the companies that have given me advice and guidance during the thesis.

Table of Contents

1. Introduction 13
1.1 Aim 14
1.1 Research Questions 14
1.2 Delimitations 14
2. Background 15
2.1 Biofuels 15
2.2 Engines 17
2.3 Internal Diesel Injector Deposits 19
2.3.1 Causes of the Formation of IDIDs 20
2.3.2 Mechanisms behind the Formation of IDIDs 21
2.3.3 Effects of the Formation of IDIDs 22
2.3.4 Important Parameters on the Formation of IDIDs 23
2.3.4.1 Influence of Temperature on the Formation of IDIDs 24
2.3.4.2 Influence of Engine oil on the Formation of IDIDs 24
2.3.4.3 Influence of Calcium Content on the Formation of IDIDs 25
2.3.4.4 Influence of Fuel Type on the Formation of IDIDs 25
2.3.4.5 Influence of the Preparation of the Test Fuel on the Formation of IDIDs 25
2.3.4.6 Influence of Additives and other Components on the Formation of IDIDs 25
2.3.4.7 Influence of Water Content on the Formation of IDIDs 26
2.3.4.8 Influence of Sodium Content on the Formation of IDIDs 26
2.4 Instrumental Setups 27
2.5 Analysis Techniques 27
2.5.1 SEM-EDX 28
2.5.2 FTIR 29
2.5.3 Pyrolysis GC-MS 30
2.5.4 Ion Beam Milling 31
3. Methodology 31
4. Experimental Setup 32

4.1 Investigation of Hypotheses 32
4.1.1 Investigation of the Solubility of Calcium Sulphate 32
4.1.2 Investigation of Ostwald Ripening 34
4.2 Investigation of Deposit Formation in the TDT 35
4.2.1 Preparation before the Experiments 38
4.2.2 General Procedure of the TDT 38
4.2.3 Reference Level 39
4.2.4 Investigation of Temperature in the TDT 39
4.2.5 Investigation of Tilted Apparatus in the TDT 40
4.2.6 Investigation of Engine Oil in the TDT 41
4.2.6.1 Investigation of Fresh Engine Oil with Sulphuric Acid 41
4.2.6.2 Investigation of Used Engine Oil 42
4.2.7 Analysis of the Samples from the TDT 43
5. Results and Discussion 44
5.1 Investigation of Hypotheses 44
5.1.1 Investigation of the Solubility of $CaSO_4$ 44
5.1.2 Investigation of Ostwald Ripening 47
5.2 Investigation of Deposit Formation in the TDT 48
5.2.1 Investigation of Temperature in the TDT 49
5.2.2 Investigation of Tilted Apparatus in the TDT 56
5.2.3 Investigation of Engine Oil in the TDT 60
5.2.3.1 Investigation of Fresh Engine Oil with Sulphuric Acid and Addition of Concentrate 60
5.2.3.2 Investigation of Fresh Engine Oil with Sulphuric Acid without Addition of Concentrate 64
5.2.3.3 Investigation of Used Engine Oil with Addition of Concentrate 67
5.2.3.4 Investigation of Used Engine Oil without Addition of Concentrate 73
5.3 Comparison with Field 77
6. Conclusions 78
7. Future studies 79
8. Reference List 80

Appendices....83
Appendix A: Temperature Profile inside the Rig....83
Appendix B: Calculation on H_2SO_4 for the Fresh Engine Oil TDT Experiments....84
Appendix C: Investigation of the Solubility of Calcium Sulphate Dihydrate in Engine Oil....85
Appendix D: Investigation of the Solubility of Calcium Sulphate Anhydrous in Engine Oil....85
Appendix E: Investigation of the Solubility of Calcium Sulphate in B7....86
Appendix F: Comparison of Composition with Temperature for each Element....86
Appendix G: Comparison of Composition between Tilted and Non-tilted....87
Appendix H: Comparison of Composition in the Trials on Fresh Oil Addition....88
Appendix I: Comparison of Composition with and without Oil Addition....89
Appendix J: Comparison of Composition with Fresh Engine Oil without Concentrate....90
Appendix K: Comparison of Composition with Fresh Engine Oil with and without Concentrate....91
Appendix L: Comparison of FTIR spectra with Addition of Fresh Engine Oil with and without Addition of Concentrate....92
Appendix M: Comparison of Composition in the Trials on Used Oil Addition....93
Appendix N: SEM-EDX Mapping of the Cross-sectional Area with Used Engine Oil with Concentrate....94
Appendix O: Comparison of Composition with Used Engine Oil without Concentrate....95
Appendix P: Comparison of Composition with Used Engine Oil with and without Concentrate....96
Appendix Q: FTIR spectra from the investigations on Used Engine Oil without Concentrate....97

List of Figures

Figure 1: Chemical structure of a FAME molecule. R represents a hydrocarbon chain. 16
Figure 2: Production of biodiesel from oils through transesterification. R represents hydrocarbon chains. 17
Figure 3: Schematic of the four strokes in the diesel engine [26]. 18
Figure 4: Schematic of an injector. 19
Figure 5: Setup of the Ostwald ripening experiment with a nitrogen atmosphere. 35
Figure 6: The total setup of the TDT. 35
Figure 7: The feed unit of the process setup. 36
Figure 8: Components of the processing unit. 37
Figure 9: The cooling circuit of the process setup. 37
Figure 10: Setup of the tilted apparatus. 40
Figure 11: Results of the investigation of Ostwald ripening with an oxygen atmosphere. 47
Figure 12: Results of the investigation of Ostwald ripening with a nitrogen atmosphere. 48
Figure 13: Comparison of the deposit size at 95°C (left) and 185°C (right) in trial 1 at the setting temperature 250°C. The deposits are the dots seen in the images. 49
Figure 14: Comparison of the deposits at 90°C in trial 2 at a setting temperature of 120°C and the deposits at 95°C in trial 3 at a setting temperature of 250°C. 50
Figure 15: Average composition of the deposits at different positions and temperatures. The upper points in the figure belong to a setting temperature on the heating plate of 250°C and the lower points to 120°C. 51
Figure 16: Comparison of composition of deposits formed at different temperatures for the four main elements. 51
Figure 17: FTIR spectra from trial 1 at a setting temperature of 250°C. The intensity has been normalised to the peak at 2828 cm^{-1}. 52
Figure 18: Closer view of the peak increase and decrease in trial 1 at a setting temperature of 250°C. The intensity has been normalised to the peak at 2928 cm^{-1}. 53
Figure 19: FTIR spectra of the test fuel, B100 and B7. The intensity has been normalised to the peak at 2858 cm^{-1}. 53
Figure 20: FTIR spectra from trial 1 at a setting temperature of 120°C. The peaks have been normalised to the peak at 2858 cm^{-1}. 54
Figure 21: Estimation of the height of the deposit at a temperature of 110°C in the investigations on a setting temperature of 250°C. 55
Figure 22: Spectrum from pyrolysis GC-MS at a setting temperature of 120°C. The unit of the time is minutes. 55
Figure 23: Comparison of the deposits in the horizontal (left) and tilted (right) rig at a temperature of 190°C. 56

Figure 24: Average composition of the deposits at different positions and temperatures in the tilted rig. The upper points in the figure belong to the setting temperature 250°C and the lower points belong to 120°C. 57
Figure 25: Comparison of composition at different temperatures for the four main elements when the rig was tilted. 58
Figure 26: FTIR spectra from trial 1 in the tilted rig at a setting temperature of 250°C. The peaks have been normalised to the peak at 2858 cm^{-1}. 59
Figure 27: FTIR spectra from trial 3 in the tilted rig at a setting temperature of 120°C. The peaks have been normalised to the peak at 2858 cm^{-1}. 59
Figure 28: Comparison of size in the investigation of preheated fresh oil addition with sulphuric acid at a setting temperature of 250°C. The left image is at the temperature 50°C and the right at the temperature 190°C. 60
Figure 29: Comparison of the deposits between the preheated and unheated fresh engine oil at a temperature of 150°C. The left image is the unheated oil, and the right is the preheated oil. 61
Figure 30: Comparison of composition at different temperatures for the main elements in the experiments regarding fresh oil addition. The second trial was disregarded due to deviating results. 62
Figure 31: FTIR spectra from trial 1 in the experiments with fresh oil addition at room temperature at a setting temperature of 250°C. The peaks have been normalised to the peak at 2858 cm^{-1}. 63
Figure 32: FTIR spectra of the $CaSO_4$ dihydrate and $CaSO_4$ anhydrous. 63
Figure 33: FTIR spectra from trial 3 in the experiments with fresh oil addition at 80°C at a setting temperature of 250°C. The peaks have been normalised to the peak at 2858 cm^{-1}. 64
Figure 34: Comparison of size between 90°C and 190°C in trial 3 in the investigations regarding addition of fresh engine oil with sulphuric acid but without addition of concentrate. 65
Figure 35: Comparison of composition at different temperatures for the main elements in the experiments regarding fresh oil addition without concentrate. 66
Figure 36: FTIR spectra at the temperature 190°C for the three trials at the setting temperature 250°C on fresh engine oil with sulphuric acid without addition of concentrate. 67
Figure 37: Comparison of size between 60°C (left) and 190°C (right) in the investigation of used engine oil. 68
Figure 38: Comparison of formation of crystals between fresh oil with sulphuric acid (left) and used oil (right). 68
Figure 39: Comparison of composition at different temperatures for the main elements in the experiments regarding used oil addition. 69
Figure 40: FTIR spectra at a setting temperature of 120°C in the experiments with used engine oil. The intensity has been normalised to the peak at 2828 cm^{-1}. 70
Figure 41: FTIR spectra at 95°C at a setting temperature of 250°C in the experiments with used engine oil. The intensity has been normalised to the peak at 2828 cm^{-1}. 71
Figure 42: FTIR spectra from trial 2 in the experiments with used oil addition at a setting temperature of 250°C. The peaks have been normalised to the peak at 2858 cm^{-1}. 71

Figure 43: SEM-EDX mapping of the cross-sectional area of the sample from trial 1 at a setting temperature of 250°C. Ion milling was performed at the location with a temperature of 150°C. 72
Figure 44: Estimation of the height of the deposits of trial 1 in the experiments with used engine oil and concentrate at a setting temperature of 250°C. 73
Figure 45: Comparison of the deposit formation in the investigations of used engine oil with (left) and without (right) concentrate at a temperature of 170°C. 73
Figure 46: Comparison of composition at different temperatures for the main elements in the experiments regarding used oil addition without concentrate. 74
Figure 47: FTIR spectra at 190°C at a setting temperature of 250°C in the experiments with used engine oil without addition of concentrate. The intensity has been normalised to the peak at 2828 cm^{-1}. 75
Figure 48: FTIR spectra from trial 3 in the experiments with used oil addition and concentrate at a setting temperature of 250°C. The peaks have been normalised to the peak at 2858 cm^{-1}. 76

List of Tables

Table 1: Most investigated parameters in the studies of deposit formation in the injectors. 23
Table 2: Specifications of the trials in the investigation of the solubility of $CaSO_4$ in the engine oil. The trials with ‘di’ represents $CaSO_4$ dihydrate the trials with ‘an’ represents $CaSO_4$ anhydrous.....33
Table 3: Specifications of the trials in the investigation of the solubility of $CaSO_4$ in the B7. 34
Table 4: Reference level in the TDT experiments. 39
Table 5: Method specifications of the trials within the investigation of temperature.....39
Table 6: Method specifications of the trials within the investigation of a tilted rig. 40
Table 7: Specifications of the two types of engine oil used in the TDT experiments with engine oil addition. 41
Table 8: Method specifications of the trials within the investigation of fresh engine oil with addition of concentrate. 42
Table 9: Method specifications of the trials within the investigation of fresh engine oil without addition of concentrate. 42
Table 10: Method specifications of the trials within the investigation of used engine oil with addition of concentrate. 42
Table 11: Method specifications of the trials within the investigation of used engine oil without addition of concentrate. 43
Table 12: Results of the investigation of the solubility of $CaSO_4$ dihydrate in the engine oils. A negative solubility represents an increase of powder. 44
Table 13: Results of the investigation of the solubility of $CaSO_4$ anhydrous in the engine oils. 45
Table 14: Results of the investigation of the solubility of $CaSO_4$ in the B7. A negative solubility represents an increase of powder. 46

List of Abbreviations

2-EHN	2-ethylhexyl nitrate
ABS	Alkylbenzene sulfonate
BIB	Broad ion beams
$CaSO_4$	Calcium sulphate
DDFT	Diesel deposit formation test
DDSA	Dodecenylsuccinic acid
EHT	Electron high tension
FAME	Fatty acid methyl esters
FIB	Focused ion beams
FKM	Fluorine kautschuk material
FTIR-ATR	Fourier-transform infrared spectroscopy-Attenuated total reflectance
GC-MS	Gas chromatography-Mass spectroscopy
GHG	Greenhouse gas
HVO	Hydrotreated vegetable oil
IDID	Internal diesel injector deposits
JFTOT	Jet fuel thermal oxidation tester
PIBSI	Polyisobutylene succinimide
RME	Rapeseed methyl ester
SDG	Sustainable development goal
SE	Secondary electrons
SEM-EDX	Scanning electron microscope-energy dispersive X-Ray
TDT	Thermal deposit test
TEM	Transmission electron microscopy
ULSD	Ultra-low sulphur diesel
ZDDP	Zinc dialkyldithiophosphates

$ZnSO_4$ Zinc sulphate

1. Introduction

The world is facing climate change with severe consequences such as high temperatures, extreme weather, drought, reduced biodiversity, and threatened food security. The major contributor to climate change is the use of fossil fuels, which represents above 75% of the global greenhouse gas (GHG) emissions. Fossil fuels are used in several applications such as transportation, industry, and electricity and heat generation [1]. There is a need for fossil fuels to meet the world's energy demand where a reduced use could result in food, energy, and water crises. However, due to climate change and the fact that fossil fuels are finite resources, renewable and climate-friendly resources are needed [2].

Transportation is the major contributor to the emissions from fossil fuels where it accounts for about 30% of the energy-related carbon dioxide emissions globally and almost 25% of the total GHG emissions in Europe [1], [3]. Road transport has the largest contribution, as it represented over 70% of the GHG emissions from transport in Europe in 2014. In Europe, work is ongoing to shift to transports with low emissions where GHG emissions must be 60% lower in 2050 than in 1990 [3]. In 2020, the EU implemented a regulation on CO_2 emission performance standards for cars and vans. Moreover, in 2021, the European Commission proposed legislation for the achievement of climate neutrality in the EU by 2050. The proposals include a target where a 55% net reduction of GHG emissions should be reached by 2030. These regulations contribute to achieving the Paris Agreement, reducing fuel costs, and strengthening competitiveness in the vehicle industry [4].

To reduce the GHG emissions in the EU, one priority area within the transport sector is to use low-emission alternative energy sources such as biofuels, electricity, hydrogen, and renewable synthetic fuels. Blends of biodiesel with fossil fuels or pure biodiesel can contribute to a significant reduction of the GHG emissions [5]. The use of biofuels promotes several of the sustainable development goals (SDGs). One connected goal is SDG 7 since it includes an increased use of renewable energy. Moreover, SDG 11 about sustainable cities, in which the environmental impact of cities should be reduced, is favoured using biofuels. There is also a connection to SDG 12 since it involves the use of natural resources. Lastly, SDG 13 can be connected, which is focusing on climate action, and as mentioned the use of biofuels result in reduced net GHG emissions [6]. However, besides the benefits with biofuels, blends with fossil fuels lead to solubility issues in the injector, which affects the performance of the engine. The use of, for example, fatty acid methyl esters (FAME) and hydrotreated vegetable oil (HVO) as drop-in fuels increases the risk of precipitation of easily degradable impurities of the fuel, which can lead to formation of deposits in the injector and damage the engine [7].

Vehicles have faced issues with the drivability such as rough idling, high fuel consumption, power loss, and failures. A reason for this is that formed deposits inside of the injector make the movement of the injector restricted. Therefore, the injector needle get stuck, and failures occur [7]–[9]. Research has been performed to achieve an understanding about the deposit formation to be able to prevent it. However, the issue is not solved, and more research is needed, which acts as a basis for this study.

1.1 Aim

The aim of this study was to investigate the mechanism behind internal diesel injector deposits (IDID) to increase the understanding of deposits and why they are formed. The focus was to understand the affect of temperature, inclination, and addition of engine oil with help of a modelled lab scale injector, called thermal deposit test (TDT). Variations of the temperature, inclination, and addition of engine oil made it possible to gain a deeper understanding of the deposit formation. Moreover, the study aimed to examine if the deposit formation could be a consequence of engine oil contamination in the fuel system.

1.1 Research Questions

To answer the aim of the study, the following research questions were answered in the study:

- Is it reasonable that soluble $CaSO_4$ is transferred from the engine oil to the fuel and then precipitates?
- How does the temperature affect the deposit formation regarding morphology, amount, and type?
- How does the use of a tilted apparatus affect the deposit formation regarding morphology, amount, and type?
- How does the deposit formation depend on the addition of fresh and used engine oil?

1.2 Delimitations

This study was delimited by some factors, which limited the amount of new information that could be obtained by the investigations. Firstly, the maximum setting temperature of the heating plate used in the modelled lab scale injector was 250℃ due to material aspects, which restricted the possible temperature range for investigation to 50-190℃. Moreover, a constant pressure of 1.7 bar was used in the TDT due to material aspects. The analyses were mostly performed by scanning electron microscope-energy dispersive X-Ray (SEM-EDX) and Fourier transform infrared microscopy-attenuated total reflectance (FTIR-ATR) because of time constraints. Lastly, it would have been of relevance to investigate a vertical rig but due to construction issues a maximum inclination of 30° degrees could be used.

2. Background

Here follows relevant background information to support the experiments made in this report. Topics covered are different types of fuels, engines, IDIDs, and analysis methods. The formation of IDIDs as well as effects and important parameters are covered. The utilised analysis methods in this investigation were SEM-EDX, FTIR-ATR, pyrolysis GC-MS, and ion milling, where relevant information about them are comprised.

2.1 Biofuels

According to Abas et al. [2], it has been shown that natural resources other than fossil fuels can meet the world's energy demand. Advantages of the use of biofuels include high power generation, low greenhouse gas emission, and high performance. However, there are also disadvantages such as high cost and energy requirement, low energy density, and high land area [10], [11]. Biofuels can be divided into four categories, namely first, second, third, and fourth generation depending on the source and production. The first generation is from edible biomass, the second from non-edible, the third from algae, and the fourth from microalgae. Large amounts of biofuels are from first generation, produced from sugar, starch, and oil-seed feedstocks, which is competing with food security [10]. The feedstock used for biofuels is dependent on the availability in different countries where, for example, rapeseed is used a lot in Europe, and soybeans in the US and Brazil [7].

Different types of biofuels include, for example, bioethanol, vegetable oil, and biodiesel. Bioethanol is an important biofuel for transportation and can be used in both conventional petrol vehicles, and flexi-fuel vehicles [10], [11]. According to Lamb et al. [8], it has become more common with ultra-low sulphur diesel (ULSD) and renewable fuel blends where HVO and biodiesel are used. Sulphur in fuels leads to the formation of particulates and soot, which contribute to air pollution. Moreover, even small amounts of sulphur in diesel fuels can poison catalysts and reduce the effectiveness of oxidation. Many countries have adopted environmental regulations to decrease the sulphur content in fuels to 10-15 ppm, leading to ULSD fuels [12].

HVOs are paraffinic non-polar hydrocarbons without aromatics and sulphur. The paraffinic content results in a high cetane number and low density. The cetane number affects the performance of the engine, and indicates the ignition delay time of the fuel during combustion [13]. A high cetane number has several benefits such as reduced ignition delay time, improved cold start ability, and reduced smoke, noise, and emissions. However, the low density implies a lower volumetric energy content than of conventional diesel and biodiesel, and thereby also a higher fuel consumption [7], [14]–[16]. HVO can be used by itself, or in blends with petroleum diesel or additives [16]. The HVOs can be produced from a variety of feedstocks such as vegetable oils, recycled oils, or animal fats, in which the properties remain the same regardless of the feedstock [14]–[16]. Advantages compared to biodiesel are decreased deposit formation, improved storage stability, and better cold properties [7], [14]. Moreover, the emissions of CO, HC, soot, NO_x and particulate matter are lower than for both biodiesel and petroleum diesel [15], [16]. However, the investment costs of HVO production are higher than those of FAME production [15].

HVOs are produced by a hydro processing technique in which a high temperature and pressure are used together with catalysts and excess of hydrogen. Two types of catalysts are used in the hydrotreating process, namely noble catalysts, and transition metals. Initially in the hydrotreating process, double bonds are saturated, and cracking occurs. Cracking is needed to obtain molecules with a chain length within the boiling point range of diesel. Oxygen also needs to be removed from the product to improve oxygen stability and the heating value [16].

On Scania CV AB biodiesel is used as biofuel, where the biodiesel can be added to petroleum diesel in different amounts such as 7% (B7), 20% (B20), and pure biodiesel (B100) [7]. Biodiesel is a renewable, biodegradable, and nontoxic fuel consisting of FAME (see Figure 1). Biodiesel can be produced from any feedstock containing fatty acids where the source depends on the region. Soybeans are common in the US while rapeseeds are more common in, for example, Germany [17], [18]. Other possible feedstocks are fish oil, microalgae, and rice, amongst others. The composition of fatty acids in the biodiesel depends on the source, with different chain lengths and degrees of saturation. The fatty acids affect both the chemical and physical properties of the fuel. Esters from long-chained and saturated fatty acids have higher cetane numbers and can cause clogging of the nozzle, while esters from unsaturated fatty acids have lower cetane numbers and are easily oxidised [18], [19]. Moreover, Hoekman et al. [19] showed that the degree of saturation of the FAME influences viscosity, specific gravity, and low temperature performance.

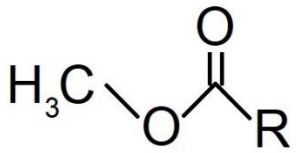

Figure 1: Chemical structure of a FAME molecule. R represents a hydrocarbon chain.

Schümann et al. [5] state that the addition of FAME into fossil diesel increases the polarity in the fuel due to the presence of oxygen atoms, which results in higher solubility. The polar end of the molecule can bind to other compounds with hydrogen bonds while the non-polar end is similar to fossil diesel, making it well-blended [20]. According to Scania CV AB, all molecules are not completely made into FAME molecules where some could have hydroxide groups instead of methyl groups (CH_3) in the ends (see Figure 1). Organic acids could then be formed, which increases the solubility further. Moreover, some molecules are cracked, forming shorter chains. These are more polar than long chains due to the short non-polar hydrocarbon tail. The more polar the molecules are, the more water can be absorbed by the fuel. The water could form micelles enclosing and protecting smaller polar compounds such as methanol and calcium [20]. Lamb et al. [8] argue that there is a connection between the FAME content and deposit formation. The esters may contribute to decomposing carboxylic acids due to the oxygen content, which could lead to the formation of metal carboxylate salts [8]. A good diesel fuel should consist of paraffines and not aromatics to be in liquid form and be able to be introduced into the engine [20].

Biodiesel can be produced in different ways, where the most common processes on large scale are the transesterification of vegetable oils and extraction from algae. Vegetable oils have high viscosity, which is a problem for the compression ignition. Therefore, the viscosity must be reduced, with the most dominant techniques being dilution, microemulsion, pyrolysis, and transesterification. Transesterification to produce biodiesel is a reaction between the oil and alcohols to form esters and glycerol, in which homogeneous or heterogeneous catalysts can be used (see Figure 2). Homogeneous catalysts can be both alkalis and acids where common alkalis include NaOH, CH_3ONa, and KOH, and common acids are H_2SO_4, HCl, BF_3, H_3PO_4, and organic sulfonic acids. However, homogeneous acid-catalysed reactions are much slower than base-catalysed, and therefore the base-catalysed ones are more common. There are some drawbacks with homogeneous catalysts such as high energy consumption and expensive separation of the catalyst and fuel. Heterogeneous catalysts offer an easier separation since solid catalysts are used [21].

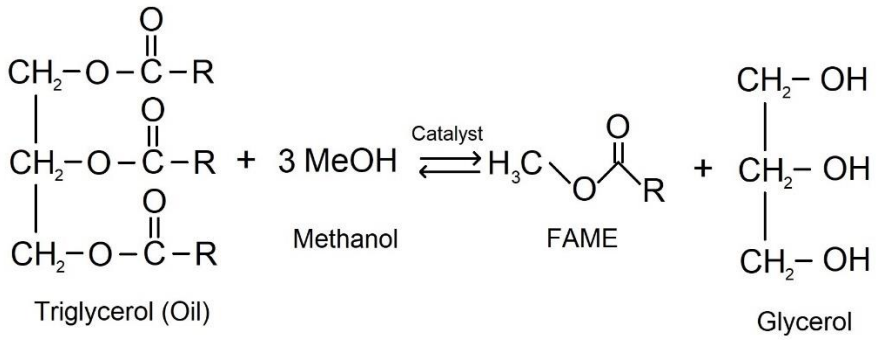

Figure 2: Production of biodiesel from oils through transesterification. R represents hydrocarbon chains.

Enzymes and supercritical or subcritical alcohol can be used in the transesterification additionally to catalysts. However, the use of enzymes may result in contaminations, and the apparatus for supercritical or subcritical alcohols are expensive due to high temperature and pressure. Nowadays, it is not common to use enzymes in the production, but it is possible to do in the future. Production of biodiesel from algae oil prevents competition with food security but 15-300 times more oil can be produced per area than with utilisation of traditional crops. However, the harvest and extraction include technical and cost difficulties where the processes for harvesting are expensive [21]. Different sources are used in different countries based on the availability. However, it does not matter what source that is used since it is only important that the biodiesel is similar to fossil diesel [20].

2.2 Engines

There are different types of engines, where two reciprocating engines used for biofuels are Otto engines and diesel engines [22]. The main difference between these is the ignition of fuel since Otto engines use spark ignition while diesel engines use compression ignition [23]. In this study, biodiesel fuels are used, which utilise the diesel engine. In the diesel engines, usually four strokes occur with two expansions and two compressions (see Figure 3) [24]. The pistons in the engine have at least two valves, one to take in air, and one to release exhaust gas after ignition. The valves open and exit in tandem with the piston movement [25].

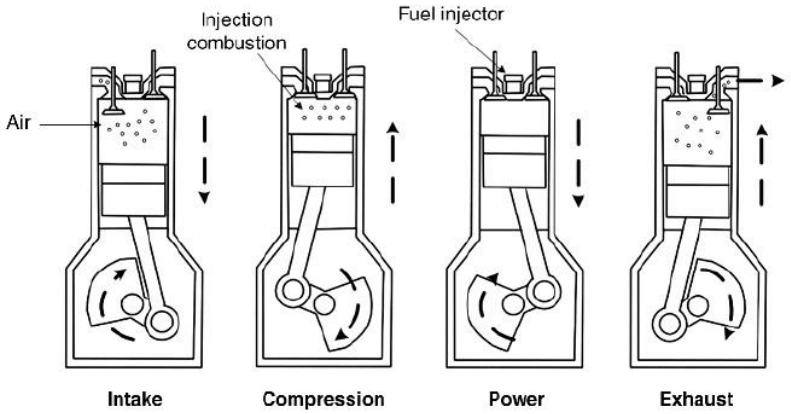

Figure 3: Schematic of the four strokes in the diesel engine [26].

The first stroke is the intake stroke where air is entering the chamber by the expansion of the piston. Thereafter, the compression stroke occurs by upwards movement of the piston. When the piston encounters the top of the chamber, the fuel is introduced by a separate nozzle, which produces a fuel spray of small droplets. To introduce the fuel, injectors are used, which need to accurately control the injected fuel amount since this amount determines the engine speed [25]. Due to no premixing of the fuel and air, rapid vaporisation in the engine is of significance, which relies on the mixing process between air and fuel. Therefore, the nozzle design is of high importance to ensure favourable characteristics of the fuel spray [27], [28]. During the compression stroke, the air is compressed to a high pressure that leads to a temperature above the ignition point of the fuel. Thereby, the fuel will spontaneously ignite when it enters the chamber [25]. This leads to the power stroke in which heat energy is released, leading to an increased pressure and forces the piston downwards. The force on the piston makes the crankshaft turn and rotary motion is generated. The last stroke is the exhaust stroke where the burned products are exiting the piston chamber through the exit valve [24].

The performance of the engine relies on the precise control of fuel injection, which infers that injection must occur at the correct piston position [27]. Due to the critical timing, diesel engines are sensitive to deposit formation since the deposits affect the movement of the injector [20]. An incorrect injection timing affects the combustion efficiency, which can influence the power output and increase fuel consumption. This could imply higher exhaust emissions of both particulate matter and gases [28]. Moreover, diesel engines operate at higher temperatures than Otto engines due to a smaller amount of air and a higher pressure. The higher temperature implies more emissions of NO_x [24]. Besides NO_x, diesel engines have higher emissions of particulate matter and odour [27]. Thereby, emission control systems are needed to follow air-quality regulations [24]. Deposit formation inside the injector will make the fuel spray less fine, and affect the movement of the injector, which may lead to more emissions and deteriorated drivability. Thereby, research regarding the deposit formation is of particular significance for diesel engines.

2.3 Internal Diesel Injector Deposits

IDIDs have been found at several locations inside of the injector in diesel engines, and they have different morphologies depending on the location in the injector, mainly due to the temperature differences. A schematic of an injector can be seen in Figure 4. IDIDs have been found in different locations inside the injector where Barker et al. [29] have investigated the nozzle of the injector, and Scania CV AB has also found deposits higher up in the injector [30]. At the upper parts of the injector, the temperature is lower, which give rise to stickier deposits. However, towards the nozzle, the temperature increases and give rise to more brittle and hard deposits, which cause nozzle fouling, and nozzle coking [30].

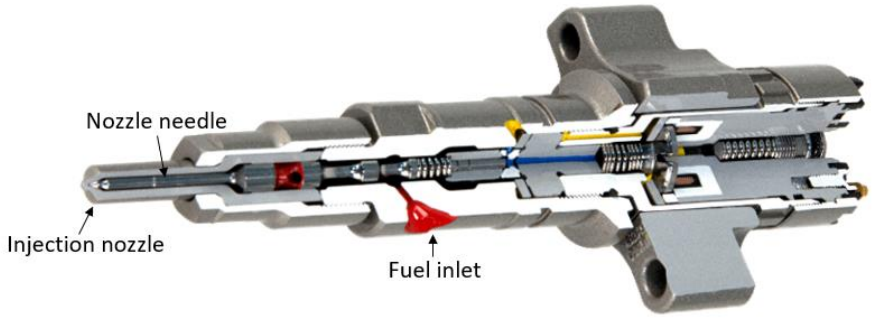

Figure 4: Schematic of an injector.

There are different types of IDIDs, divided into carbonaceous, inorganic salts, amides, aged fuel deposits, lacquer-based deposits, and carboxylate salts. They all have in common that they are coarse, porous, heterogeneous, and consist of different layers [8], [31]. Scania CV AB investigated IDIDs from field injectors where they could identify two layers with SEM-EDX. The bottom layer consisted of $CaSO_4$ crystals, and the top layer consisted of mainly organic materials, but also small amounts of inorganic elements such as calcium and sulphur [32]. Lamb et al. [8] have also identified different layers with a top layer consisting of carbon, nitrogen, and oxygen, a middle layer with salts and a bottom amorphous organic layer with majorly carbon [8]. Moreover, Barker et al. [33] have found a layer structure with a bottom layer of ordered carbon, a middle layer of carbon, nitrogen, chloride, sulphur, and fluorine, and a top layer of sodium hydroxide, sodium sulphate, calcium, and potassium [33]. However, the piston in the injector usually has a coating consisting of graphite and diamond, and this could therefore be the layer of ordered carbon that Barker et al. found [7].

Scania CV AB has performed lab experiments with a TDT explained under 4.2 Investigation of Deposit Formation in the TDT. Large amounts of carbon and oxygen were identified but also sodium, aluminium, and calcium. At some locations on the deposits, they could also identify magnesium, silica, sulphur, chloride, and iron [34]. Barker et al. [29] performed experiments in a jet fuel thermal oxidation tester (JFTOT) described under 2.4 Instrumental Setups, and found different types of deposits at different sections of the tube. One end had many carbonaceous deposits with short hydrocarbons, inorganic metal ions, sulphates, and phosphates. The other end had more silicones and hydrocarbons. They concluded that ageing of the fuel had occurred along the rod, which resulted in different types of deposits. Moreover, they found oxygenated species and fatty acid

methyl esters [29]. Scania CV AB has also found different types of deposits at different locations within the injector. They argue that the deposits turn firmer at higher temperatures due to evaporation of fuel, methanol, and water [7].

One deposit type of interest in the injector is metal carboxylate salts, called metal soaps, such as sodium soaps and calcium soaps where Reid et al. [35] found that interactions between monoacid lubricity additives and sodium precursors resulted in injector sticking. The soap is formed by a reaction between, for example, metal compounds and carboxylic acids. Factors that affect soap formation are ligand coordination, competing metals, solubility factors, acids and metals from impurities, temperature, and pressure [35]. Scania CV AB has also seen formation of soaps with sodium or calcium, which they state are sticky and insoluble [7]. The main component of the soap is degraded and oxidised fuel as well as organic acids and polar fuel contaminants such as glycerine, methanol, sterols, and water [30], [36].

The formation of IDIDs can have several causes depending on the fuel components and additive factors, which differ for different types of deposits [9]. Moreover, different mechanisms have been proposed for the deposit formation. The deposit formation has severe effects on the drivability of the vehicle, and for the environment, and air quality. Furthermore, different parameters affect the deposit formation such as temperature, engine oil, fuel type, and additives, where more information follows below.

2.3.1 Causes of the Formation of IDIDs

The IDIDs can consist of, for example, organic polymers, amid based polymers, and metal soaps. Organic polymers can be formed from, for example, oxidative products, hydrocarbons, and fatty acids while amid-based polymers are majorly formed from the carboxylic acids in the biodiesel. The soaps are metal carboxylate salts affected by different metal sources as well as carboxylic acids [9], [37]. Additives are added to the fuels when used in modern engines with fuel-lubricated injection systems. The additives contribute to the formation of all types of IDIDs [5], [9]. The additive polyisobutylene succinimide (PIBSI) can react with alkali metals and form amid deposits as well as metal soaps. Corrosion inhibitor fuel additives have also been seen in the IDIDs, such as C16/C18 fatty acids [31]. Processes that affect the deposit formation are fuel oxidation, decomposition, surface effects, micelle formation, and additive interactions [9]. According to Schümann et al. [5], IDIDs are favoured by aromatic components in diesel fuel FAME blends. When these components are oxygenated they form poorly soluble products, which end up on the hot injector surface [5].

Lamb et al. [8] state a variety of origins of deposits depending on the deposit type. They argue that salt material can originate from storage tank bottoms, lubricant oil contamination, or biodiesel with poor quality. Calcium has been shown to come from lubricating oil due to its presence together with sulphates and phosphates. Moreover, alkylbenzene sulfonates (ABS) have been found in the IDIDs, which substantiates that lubricant additives could be an origin of deposits. It has also been shown that zinc is a constituent of the IDIDs, which

could enter as an impurity from tanks, zinc-coatings, or the zinc dialkyldithiophosphates (ZDDP) additive in lubricant oil [8].

Edney et al. [31] also state different possible causes of the formation of IDIDs, as for example contamination, operating conditions and fuel composition. They argue that fuels with low thermal stability often form deposits where degradation of the fuel can arise from pyrolysis or polymerization, which could lead to formation of polynuclear aromatic hydrocarbons and alkyl radicals. The alkyl radicals can form hydro-peroxides, which can attach to the injector surface and initiate the formation of deposits [31]. Moreover, Edney et al. [31] express that carbonaceous deposits can be formed from the degradation of organic compounds in the fuel. They also state that alkali metals contribute to the formation of inorganic deposits and metal soaps. The metals could originate from water bottoms, as for example fuel storage tanks [31].

Barker et al. [29] state that high pressure common rail systems can affect the deposit formation since it involves high temperatures. High pressure common rail systems are closed-loop systems with high pressures, and shall lead to better performance, higher energy efficiency, and reduction of emissions [29]. However, they are more sensitive to IDIDs since the timing of fuel addition and movement inside the engine is more precise. Therefore, deposits easier interfere with the timing and can cause malfunction [7]. Edney et al. [31] state that biodiesel blends have been shown to contribute to deposit formation due to unsaturated long-chain molecules with high reactivity to oxygen. Moreover, FAME and rapeseed based methyl esters in biodiesel have been seen as unstable during long-term storage and found as a possible source of deposits [31]. Scania CV AB argues that the deposits are formed from soft particles, which are insoluble compounds that easily stick to each other [36]. These are usually a micron in size and are formed from degraded fuel and contaminants [30]. The combination of more advanced engine systems and higher usage of biodiesel results in more deposit formation [7].

2.3.2 Mechanisms behind the Formation of IDIDs

In injectors from Scania CV AB, it has previously been seen that the IDIDs consist of two layers, a bottom layer of calcium sulphate ($CaSO_4$) crystals and a top layer of soft particles, in which the main components are metal soaps and PIBSI. The mechanism for this deposit structure could be that $CaSO_4$ is transferred to the injector from other parts of the process, where it precipitates and forms a crystal layer. Eventually, soft particles are attached to the crystal layer to form a second layer of deposits. The layer gets thicker with time and some deposits are transferred higher up in the injector through vibrations, contact with the plunger, or squeezing. It will then enter the guidance where it is spread out. The smear in the guidance affects the plunger movement because of its high viscosity. With time, the smear and crystals will be washed off since the smear is not hardly attached, and the crystals are removed by shearing forces [7].

There are several theories behind the transfer of $CaSO_4$ to the injector. The most probable one is that $CaSO_4$ is formed in engine oil and then leaked through the high-pressure pump to the fuel. This is supported by the detection of PIBSI in the deposit, which is an additive used in lubricating oils. The $CaSO_4$ may be soluble in

engine oil but when entering the fuel the solubility may decrease, which makes the solution oversaturated and crystals are formed [7]. The higher oversaturation, the more formation of crystals [30]. The reason behind decreased solubility of $CaSO_4$ could be an increased temperature since it generally has lower solubility at higher temperatures. Furthermore, it has been seen that the most IDIDs appear on the nozzle of the injectors from Scania CV AB, which is the warmest part. The solubility could also depend on the environment, fuel type, additives, and oxidation [7], [30]. Moreover, the $CaSO_4$ could be complex bounded to for example fatty acids in the engine oil and this could make it soluble. When entering the diesel, the complexes could fall apart due to the different environment, which would make the solution oversaturated and deposits could be formed [7].

The theory that $CaSO_4$ is dissolved in the engine oil, and then transferred to the fuel system is supported by the behaviour of metal-based detergents in the engine oil. Metal-based detergents are added to engine oil to neutralise contaminations of acidic substances since the acids accelerate degradation of the oil, which leads to agglomeration of soot. The detergents consist of carboxylates, sulfonates, phenolates, or carbonates of metals such as calcium and magnesium. These metals are dispersed in forms of salts within the oil. It is also shown that the dispersion of $CaSO_4$ containing water in the oil is improved by the addition of additives for diesel engines. Moreover, it has been found that $CaSO_4$ absorbs water and sticks to parts of the piston, showing that it could be dissolved in the engine oil and then precipitate [38].

Another theory behind the formation of $CaSO_4$ crystals is Ostwald ripening, based on that larger crystals are thermodynamically favoured over small crystals [7], [20]. Small crystals of $CaSO_4$ could be dissolved in the fuel, and then deposit over time as larger crystals. Larger particles have a lower surface per volume unit, which makes them energetically favourable, and their solubility would be lower than the solubility of small particles [39]. The lower solubility of larger crystals could promote the precipitation of them.

2.3.3 Effects of the Formation of IDIDs

When IDIDs are formed they damage movable parts, such as the injector. The deposits make it narrow inside the injector, which restricts the free movement of it [7]. This could make the injector needle getting stuck and replacement could be needed. Moreover, the deposit formation results in a less fine fuel spray, leading to poor mixing of air and fuel as well as the formation of a fuel-film, which may result in increased emissions of soot, unburned hydrocarbons, carbon monoxide, nitrogen oxides, and particulate matter. In the end, this leads to poor air quality and global warming [31]. The deposit formation also affects the drivability with issues such as power loss and high fuel consumption [9], [31]. A reason for the higher fuel consumption could be that the IDIDs cause bad timing between the movable parts in the injector and the fuel injection. This leads to injection of fuel at the wrong time point, which could make the needle stop moving, and consequently, fuel combustion is higher [7]. IDIDs also damage the function of the engine with failures and rough idling [8], [35]. Furthermore, difficulties with starting, and a decrease in engine efficiency have been noticed [29], [31].

2.3.4 Important Parameters on the Formation of IDIDs

Several parameters could affect the formation of IDIDs, which have been investigated in several studies [5], [7]–[9], [20], [29], [37]. Commonly investigated parameters with the reason for investigation can be seen in Table 1.

Table 1: Most investigated parameters in the studies of deposit formation in the injectors.

Parameter	Reason	Reference
Temperature	Different deposits can be found at different temperatures.	[7], [9], [29]
	The temperature within the engine varies.	
Tilted apparatus	Horizontal mode can lead to the formation of lumps.	[7]
Addition of engine oil	The hypothesis is that the $CaSO_4$ is dissolved in the engine oil and transferred to the fuel.	[5], [7]–[9], [37]
	Constituents could affect the fuel stability.	
Ca^{2+} content in the test fuel	Calcium has been found in the formed deposit.	[7], [8]
Fuel type	The content of the fuel has been shown to affect the deposit formation.	[5], [8], [9]
Preparation of test fuel	Can affect the content of the fuel.	[7], [9]
	Has noticed lumps on the substrate.	
Additives or other components	Have been shown to affect deposit formation.	[5], [8], [9], [20], [37]
Water content	Can form micelles.	[20]
Sodium content	Has been shown to interact with acids in the fuel and form deposits.	[35]

As mentioned, studies have been performed on most of these parameters in which a variety of results has been gathered, following below.

2.3.4.1 Influence of Temperature on the Formation of IDIDs

Deposit formation has been shown to depend on the temperature since different types of deposits are formed in different temperature ranges [5], [9]. Initially, a small portion of the deposits consist of contaminants such as glycerine, sterols, and methanol. When the temperature increases, fuel is combusted and a larger portion will be contaminants [7]. The deposits also have different morphologies at different temperatures. At lower temperatures, they are slimier, leading to filter blocking. In the injector, the temperature is higher, which makes the deposits stickier [30]. At even higher temperatures closer to the injector tip, they become firmer and more brittle due to the low content of water, fuel, and methanol. This type of deposits can cause nozzle fouling and nozzle cooking [7], [30]. Berndt et al. [9] state that within the range of 100-250°C, several types of deposits can be formed. At lower temperatures salting reactions occur and precipitation of sodium carboxylate soaps. At higher temperatures, above 200°C, amide-type and autoxidative deposits were shown to be formed [9].

Berndt et al. [9] have performed experiments to investigate the deposit formation in a laboratory test method in which a modelled injector was used. In the article, they investigated deposit formation at a set point temperature of 240°C, leading to a temperature gradient within the modelled injector. It could be seen that the largest number of deposits was formed at the highest temperatures. Moreover, it was stated that in the range of 180-240°C, fuel oxidation or additive decomposition begins while deposits at the nozzle tip of the injector are formed at temperatures higher than 240°C [9].

2.3.4.2 Influence of Engine oil on the Formation of IDIDs

According to Lamb et al. [8], it has been shown that contamination of engine oil in the fuel, from for example lubricated pumps, contributes to deposit formation. It has been argued that $CaSO_4$ is a constituent of the formed deposits where both calcium and sulphate can originate from the engine oil. Calcium acts as a counter-ion to the detergent molecule ABS, which is a lubricant additive. When the engine oil degrades with time, more $CaSO_4$ could be formed [7]. Moreover, oil consists of nitrogen-containing compounds and oxygenates, which could affect the fuel stability and decomposition of the fuel, leading to formation of IDIDs [8].

Schümann et al. [40] investigated the effect of engine oil as a contaminant in JFTOT tests by the addition of engine oil to B7. They investigated both fresh and used Shell Rimula R4 L engine oil. The tested concentrations were 0.1%, 0.5%, and 1%, which here was assumed to be wt% since it was not stated in their article. The engine oil consisted of 1730 calcium mg/kg, 327 magnesium mg/kg, and 1060 zinc mg/kg, which all can cause soap formation. The results showed that the thickness was highest for B7 with 0.5% and 1% fresh lubricating oil, where it was about 90 nm. B7 with 0.5% and 1% used lubricating oil resulted in deposits with a thickness of about 70 nm. The lowest thickness was obtained for fuels without the addition of oil, in which it was only about 5 nm [40]. Scania CV AB performed an experiment with addition of aged engine oil (Scania LDF-4) where they achieved deposits with a thickness of about 20 nm [7], which correlates with the studies of Schümann et al. [40].

2.3.4.3 Influence of Calcium Content on the Formation of IDIDs

$CaSO_4$ has been found inside the IDIDs and is therefore argued to have an impact on the deposit formation [8]. Scania CV AB has performed experiments with the JFTOT setup on two test fuels with different concentrations of calcium. In the first fuel, they had a concentration of 1 ppm of calcium, and in the second fuel 3 ppm. They noticed that when the concentration was increased from 1 ppm to 3 ppm, the thickness of the deposits went from 6 nm to 30 nm [7].

2.3.4.4 Influence of Fuel Type on the Formation of IDIDs

It has been argued that the deposit formation is affected by the content of the fuel including for example FAME and oxygenates where FAME is the major constituent in biodiesel [8]. According to Lamb et al. [8], there is a connection between the FAME content and the deposits since the FAMEs can decompose to carboxylic acids and form soaps [8]. Other characteristics of fuels that could have an impact on deposit formation are oxidation stability, acid number, and additives [9]. One study that investigated different fuel types was performed by Schümann et al. [5] who investigated different types of biodiesel blends in a diesel deposit formation test (DDFT) in which the maximum deposit thickness was measured. They noticed that the FAME component seemed to decrease the height of deposits where it was 9 nm for B7 and 5 nm for B100 at temperatures in the range of 180-220°C. At temperatures below 180°C no deposits were observed for pure FAME or FAME blend fuels. It was shown that deposit formation depends on the type of diesel fuel blends where different types of FAME resulted in different deposit thicknesses. For example, soy oil methyl esters gave a thickness of 15 nm at temperatures below 180°C while rape seed oil methyl ester gave a thickness of 4 nm [5].

2.3.4.5 Influence of the Preparation of the Test Fuel on the Formation of IDIDs

When experiments are performed in lab environments, a test fuel can be prepared to mimic the fuel with contaminants from the field, and to ensure that the desired deposits can be formed. The preparation of the test fuel could have an impact on the deposit formation since it influences the type of particles and substances present in the sample. Berndt et al. [9] investigated the effect of filtration of the fuel on the deposit formation. They noted that without filtration, the repeatability of the experiments was poor. When they filtered the sample with a pore size of 4-12 µm, variations of repetitions of the experiments were significantly smaller. Moreover, the deposit thickness of soaps was much higher for unfiltered samples [9].

2.3.4.6 Influence of Additives and other Components on the Formation of IDIDs

To improve the performance of fuels and engine oils, additives are added, where some are specific for engine oils and others are specific for fuels. These could surround molecules by complex bonding to protect them from reacting, which could help them stay dissolved instead of precipitate. However, some additives may only work in engine oil and when entering the fuel, the protected molecule could precipitate. PIBSI is an example of an additive used in engine oil, which has been found in the deposits [20]. Moreover, dodecenylsuccinic acid (DDSA) has been connected to IDIDs since it reacts with sodium and forms deposits [8].

Studies have been conducted to examine the effect of additives and other substances on the deposit formation. Examples include antioxidants, PIBSI, 2-ethylhexyl nitrate (2-EHN), DDSA, and deposit control additives [5], [8], [9], [37]. Schümann et al. [5] have shown that antioxidants help to decrease the deposit thickness. An addition of 200 ppm antioxidants resulted in a deposit thickness of 1046 nm at a temperature above 180°C while an addition of 1500 ppm led to a thickness of only 16 nm [5].

Berndt et al. [37] investigated the addition of soap forming components to a reference diesel fuel in a JFTOT test. In the experiments, they increased the concentration of sodium and DDSA. They could see that a higher addition resulted in more deposits where a sodium concentration of 3 ppm and DDSA concentration of 20 ppm resulted in a deposit thickness of roughly 190 nm compared to roughly 62 nm without addition [37]. Moreover, Berndt et al. [9] investigated short-chained PIBSI and 2-EHN. It could be seen that the addition of both short-chained PIBSI and 2-EHN resulted in the highest deposit thickness of 1079 nm at temperatures above 180°C. They concluded that the addition of 2-EHN to a reference fuel containing polyamide-forming substances resulted in more deposits. Moreover, they state that the concentration of PIBSI affects deposit formation. They also investigated the addition of 150 ppm of a detergent to reference fuel with 0.5 ppm sodium and 10 ppm DDSA showing a small increase of deposits [9].

2.3.4.7 Influence of Water Content on the Formation of IDIDs

Water from the air could be absorbed by the fuel due to polarities. Thereafter, the water could contribute to the formation of IDIDs by forming micelles that surround other molecules as for example $CaSO_4$, acetic acid, and methanol. These molecules could then form colonies. At higher temperatures, the micelle could rupture and release the content, which could lead to deposit formation. Water could leak into the process at several locations, surround $CaSO_4$ from the engine oil, and transfer it to the injector. In the injector, it is warmer and the water may evaporate, which could release the $CaSO_4$ and deposits could be formed [20].

2.3.4.8 Influence of Sodium Content on the Formation of IDIDs

It has been shown that sodium contributes to IDIDs where it interacts with acids in the fuel. For example, lubricity improvers and corrosion inhibitors contain sodium salts, and can contribute to the formation of IDIDs. Sodium hydroxide can form deposits together with DDSA, while sodium 2-ethylhexanoate could form sodium carboxylates together with a lubricity improver and di-acid DDSA [35]. Reid et al. [35], performed tests in an 1997 cm^3 engine in which a lubricity improver and sodium sulphate solution were added to RF-06-03 base fuel. The results showed that IDIDs were not formed. They also tested the addition of a deposit control additive, together with sodium 2-ethylhexanoate and DDSA, to the fuel, which did not result in any IDIDs. From this, they concluded that deposit control additives help to avoid sodium based injector deposits [35].

Reid et al. [35] also performed laboratory bench tests based on the JFTOT procedure in which they added sodium salts to the fuel both with and without presence of acids. Sodium naphthenate resulted in carboxylate salt deposits both with and without acids. Sodium 2-ethylhexanoate resulted in more deposits when the fuel

contained di-acids. Sodium hydroxide and sodium chloride did not result in any deposits [35]. Reid et al. [35] performed experiments in which DDSA was added to fuel containing soluble sodium and could see that DDSA affected the deposit type and location on the JFTOT tube. However, a mono-acid lubricity improver did not have the same effect, which was explained by that DDSA is a stronger acid and therefore exchanged more with sodium [35].

2.4 Instrumental Setups

There are several studies conducted on deposit formation where one commonly used method on lab scale is JFTOT, which has been developed to assess the oxidation of jet fuels [29]. However, the method can also be used to investigate the fuel's oxidative thermal stability, and deposit formation [29], [41]. The thermal degradation of the fuel is either measured by discoloration of a heated tube or by filter pressure drop. When a heated tube is used, the fuel flows over an aluminium tube for 2.5 hours at a fuel rate of 3 mL/min and a setting temperature of 260°C. Thereafter, the tube is visually examined in a visual tube rater in which a colour appears and can be compared with a colour chart. Based on the colour, it can be determined if the fuel has passed its breakpoint for degradation. If the fuel is examined by filter pressure drop, particulates from the fuel degradation will lead to a higher filter drop, and if the pressure drop is higher than 25 mmHg, the breakpoint for degradation is reached. To pass the JFTOT test, the fuel must meet both the criteria of tube colour and pressure drop [41].

The JFTOT test allows for direct analysis of the deposits with different analysis techniques in which there is no need for washing or scraping off the deposit [29]. Barker et al. [29] utilised this method to investigate deposit formation from diesel fuels. They used a fuel rate of 3 mL/min and the fuel passed through a filter with a pore size of 4 μm. It was flown over a metal piece of stainless steel at a temperature of 260°C for 2.5 hours. Thereafter, the stainless steel piece was cleaned with toluene and acetone [29]. Several authors have performed experiments based on the JFTOT setup. One example is Berndt et al. [9] who performed experiments on deposit formation with a setup they called DDFT. The fuel was flown over aluminium heater tubes where deposits were formed on the surface and were assessed visually and by optical measurement of the layer thickness. The fuel was first flown through dried air for 6 minutes and then over the aluminium tube where it was heated in a temperature gradient. The system pressure was 34.5 bar, the fuel flow rate was 3 mL/min, the setting temperature was 240°C, and the test duration was 2.5 hours. The layer thickness was examined with an ellipsometer based on changes in the polarisation state of laser light [9].

2.5 Analysis Techniques

In this study, SEM-EDX were used on all samples from the TDT to evaluate the deposit formation in different regions of the aluminium foil substrate. The advantage of SEM-EDX was that both the overview and a closer view of the deposits could be investigated by changing the magnification. Furthermore, no sample preparation was needed, and the sample was not destroyed and could be analysed after with FTIR-ATR. However, there were also a limitation in the size of the sample since it must fit into the microscope chamber, which required

that it was cut into two pieces [42]. After the SEM-EDX analysis, all samples were analysed with FTIR-ATR to identify characteristic bonds in the compounds present in the sample. The analysis was fast and offered quantitative as well as kinetic information [43], [44]. Moreover, it offered effectiveness, reliability, and easy sample preparation [31], [43], [45].

Pyrolysis GC-MS was also used on one sample to gain more insight into the constituents of the deposits. It offered a sensitive analysis with high resolution, selectivity, and sensitivity. Moreover, minimal sample preparation was needed, and the analysis only required micrograms of the sample. However, the sample was destroyed [46], [47]. Lastly, broad ion milling was performed on two samples to investigate the cross-section of the deposits. This offered a large and distortion-free cross-section of the sample for SEM analysis [48].

2.5.1 SEM-EDX

SEM utilises beams of electrons in the range of 100-30 000 eV to generate signals on the surface of solid samples. From the signals, information about morphology, chemical composition and structure can be obtained. The analysis instrument is connected to a software, which shows a two-dimensional image of the sample. The magnification of the image can be 20-30 000 X, or even 1 000 000 X in some modern models. The image can be improved by adjusting the brightness, contrast, and intensity [42], [49].

The signals from the sample include secondary electrons, backscattered electrons, diffracted backscattered electrons, photons, visible light, and heat. The secondary electrons (SE) give rise to the images, the diffracted backscattered electrons show crystal structures, and the photons give elemental analysis by X-rays [42]. The received information depends on the voltage used, where more details of the surface can be identified with voltages below 5 kV. However, high voltages of 15-30 kV can penetrate deeper into the sample and give information underneath the top surface [49]. SEM can be used together with EDX to achieve qualitative and semi-quantitative information on chemical composition as well as the distribution and concentration of elements [42], [50]. The EDX detector measures the X-rays omitted from the sample [50].

Different studies have utilised SEM to analyse deposit formation whereas Edney et al. [31] have gathered results. According to them, the severity of deposit formation and loss of fuel flow rates have been related with help of SEM. Moreover, the degradation of micelles has been connected to insoluble soap formation. Fouling has also been visualised, where the growth of deposits has been connected to degradation of lubricating oil. Furthermore, analyses with SEM-EDX have been performed in which elements from lubricating oil have been found in the IDIDs such as sulphur, calcium, and phosphorus. Other elements that have been identified are sodium and zinc [31].

2.5.2 FTIR

FTIR can be used to identify organic, inorganic, and polymeric materials by using infrared light [29], [51]. Moreover, contaminants, additives, oxidation, and decomposition can be detected [51]. When the sample is radiated with infrared light, some light is absorbed and some transmitted where both absorption and transmission spectra can be obtained [43]. Molecular groups have characteristic bands in the spectrum corresponding to molecular vibrations [52]. Therefore, chemical structures have characteristic spectral fingerprints [43]. The detector identifies changes in dipole moments within the bonds when exposed to infrared light. Therefore, symmetric vibrations in molecules are usually not detected. Molecular groups with polar bonds result in strong IR absorption bands [52].

To achieve a spectrum, the transmission, attenuated total reflection (ATR), diffuse reflectance, and true specular reflectance absorption could be used. In this study ATR was used, in which the beam is radiated at a certain angle on a crystal with a high refractive index such as diamond. This gives rise to internal reflectance, which creates a temporary wave. When the wave encounters the sample, some energy is absorbed, and the remaining beam is going to the detector. ATR is appropriate for several sample types such as plastics, natural powder, and liquids [44].

The spectrum from FTIR is in the range of 666-4000 cm^{-1} where different types of bonds appear in different regions of the spectrum. Single bonds of for example O-H, C-H, and N-H can be identified at wavenumbers of 2500-4000 cm^{-1}, triple bonds are found at 2000-2500 cm^{-1}, and double bonds at 1500-2000 cm^{-1}. There is also a fingerprint region at 650-1500 cm^{-1}, which is the vibration of the molecule as a whole and characteristic of different molecules [44]. The wavenumbers at which the bonds appear differ depending on the type of vibration such as stretching vibration and bending vibration [52]. For example, the C-H bond can be found even at lower wavenumbers where CH_2 and CH_3 bend in alkanes are detected at about 1450 cm^{-1}. Moreover, C-O bonds in for example alcohols, esters and carboxylic acids, as well as C-N bonds in amines, can be identified at 1000-1300 cm^{-1} [44].

FTIR is appropriate for analysis of car components such as oil coatings, fuel, and exhaust gas emissions [53]. The sensitivity is high, making it useful for advanced applications [44], [52]. FTIR has been used in several studies of IDIDs, where Edney et al. [31] have compiled results. Several types of bonds have been identified such as aromatic bonding, C-O stretches characteristic of carboxylate salts, and peptide bonds. Moreover, PIBSI molecules and sulphonate species have been observed [31]. Shameer and Nishath [45] used FTIR to investigate biodiesel by a PerkinElmer spectrum instrument. They identified peaks of O-H at 3500 cm^{-1}, C-H at 2700-3000 cm^{-1}, C=O at 1700 cm^{-1}, and C-O at 600-1500 cm^{-1}. It is argued that the C-O and C=O bonds show the presence of ester or ether groups in the sample [45].

2.5.3 Pyrolysis GC-MS

A variety of information can be obtained from GC when coupled with MS such as thermal stability, composition, and decomposition mechanisms [54]. The mobile phase in GC is a gas while the stationary phase could be either a solid or a liquid [46]. The stationary phase governs the selectivity and separation of different components in the sample based on the affinity to individual compounds [47]. The mobile phase should be inert and act as a transport medium. Due to the inertness, the mobile phase does not affect the selectivity but has an impact on the efficiency depending on the solute diffusion rate. Common mobile phases are nitrogen, helium and hydrogen where nitrogen is frequently used due to its low cost and high safety [46].

The sample for GC-MS could be a solid, liquid, or gas, and should be thermally stable and able to vaporise but not decompose. When the sample has been injected, it is transferred by the mobile phase to the column for separation [46]. The temperature within the column must be controlled since it affects the amount of compounds in the vapour phase [55]. After the column, the components in the sample are eluted at characteristic time points depending on the affinity to the stationary phase. The components are analysed by a detector, in which the signal intensity is proportional to the amount of the component. Characterisation can be made from the characteristic retention times for different compounds [46].

GC-MS cannot be applied on non-volatile, insoluble, and complex samples, which emphasizes the importance of pyrolysis GC-MS. In pyrolysis GC-MS the sample is pyrolyzed in a vacuum or inert atmosphere before the injection into the column. A temperature is chosen to allow the thermal decomposition of the sample into its components [46], [47], [54]. The temperature within the pyrolizer is 400-1500°C to break molecular bonds. This leads to a free radical formation where the radicals react by elimination, recombination, or rearrangement. However, methylation of the radicals can be used to prevent further reactions. The duration of the heating can be controlled to achieve a characteristic degradation with smaller volatile molecules to produce a characteristic chromatogram [46].

Analyses with GC-MS on the deposit formation have been performed in several reports where Edney et al. [31] have gathered results. However, they did only comply results from GC-MS without pyrolysis. Identification of aldehydes, ketones, and alkyl-hydroperoxides in IDIDs has been made, which showed the oxidative degradation mechanism in the deposit formation. Moreover, polycyclic aromatic hydrocarbons, C-16 and C-18 have been identified, which probably originate from carboxylic acids. Other compounds that have been detected are acid derived backbones and high mass sulphurous compounds. The sulphurous compounds are argued to originate from reactions between aromatics, olefins, and benzothiophene [31].

2.5.4 Ion Beam Milling

Radiation of ion beams on a solid sample leads to atom sputtering, electron emission, induction of chemical reactions, displacement of atoms, and alteration of properties [56]. Material is removed from the sample through atomic collisions, which can be controlled by adjustment of the beam current and voltage [57]. Ion beam milling can be used for, for example, reparation of photomasks, transmission electron microscopy (TEM) sample preparation, and production of cross-sections [56], [58]. The cross-sections can thereafter be analysed by for example SEM [59]. There are two types of ion beams, namely focused ion beams (FIB) and broad ion beams (BIB), where FIB usually uses 30 kV gallium and BIB 2-10 kV argon. A difference between FIB and BIB is that FIB uses beam-side milling while BIB uses beam-front milling where only beam-side milling has a positioning ability. This means that only FIB can produce cross-sections at specific positions [58]. However, according to Hatano et al. [48], cross-sections from BIB are less damaged.

An advantage of BIB is that the setting of the sample into the system is simple. However, the major disadvantage is that the cross-section cannot be precisely positioned, as mentioned before [48]. In a FIB system, the column consists of several optical lenses to focus the ions onto the sample [58]. To achieve a cross-section perpendicular to the surface with FIB, the sample must be tilted since the ion beams are entering with an angle [58]. The major advantage of FIB is the accurate beam position to produce uniform cross-sections. Moreover, the production is rapid [60]. However, FIB could lead to induced artifacts and can only handle small areas whereas BIB is useful to process larger areas [48], [60].

3. Methodology

The experimental part was divided into two parts to be able to answer all four research questions. First, two hypotheses were examined to investigate whether it is reasonable that soluble $CaSO_4$ is transferred from the engine oil to the fuel system and then precipitates. Thereby, the solubilities of $CaSO_4$ in engine oil and B7 were investigated. Moreover, it was examined if the deposit formation could be caused by Ostwald ripening where larger crystals are thermodynamically favoured over smaller crystals. The investigation of the solubility of $CaSO_4$ was performed by examining the solubility in fresh engine oil, used engine oil, and B7. Experiments were conducted of both $CaSO_4$ anhydrous and $CaSO_4$ dihydrate. Moreover, the solubility in the oils were investigated at both room temperature and 100°C, and the solubility in B7 at room temperature and 120°C to see how the temperature affects the solubility. The investigations of Ostwald ripening were performed by adding $CaSO_4$ to B7, and leave it for 9 days at 120°C. In this way, it could be examined whether small crystals were dissolved, and with time precipitated as larger crystals.

The second part of the experimental part was to study the deposit formation in the TDT as a function of temperature, rig inclination, and engine oil addition to examine how these parameters affect the deposit formation. Thereby, the temperature range 50-190°C was investigated by using the setting temperatures 120°C and 250°C on the heating plate. Moreover, the rig was tilted to 30° in some experiments to see how

sedimentation could affect the deposit formation. Lastly, both fresh and used engine oils were added to the test fuel to investigate if there were any differences of the deposit formation. All experiments were performed with at least three replicates to ensure repeatability and increase the reliability of the results.

The samples from all experiments were analysed in SEM-EDX with a ZEISS GeminiSEM apparatus to investigate the morphology and composition at different positions on the substrate. Thereafter, all samples were analysed with FTIR-ATR with an apparatus from PerkinElmer to identify present compounds and reactions. One sample was also analysed with pyrolysis GC-MS to gain more insight into the type of the deposits. Lastly, two samples were analysed in a broad ion milling Hitachi Arblade 5000 apparatus to examine the cross-sectional area of the deposit formation. The samples were then analysed in SEM-EDX in which layer characteristics and deposit height could be observed.

4. Experimental Setup

Different experimental setups were used for the $CaSO_4$ solubility experiments, Ostwald ripening, and the experiments in the TDT, which follows below. Firstly, an explanation of the investigations of the solubility of the $CaSO_4$ and Ostwald ripening will be given. Thereafter, the execution of the TDT experiments will be comprised.

4.1 Investigation of Hypotheses

Here follows the experimental setup of the investigations of the two hypotheses mentioned above. The most believed one is that $CaSO_4$ enters the fuel through engine oil contamination from the oil-lubricated high-pressure pump. However, Ostwald ripening could also be the cause of the crystal formation in the deposits.

4.1.1 Investigation of the Solubility of Calcium Sulphate

An investigation was made to examine the solubility of $CaSO_4$ dihydrate and $CaSO_4$ anhydrous in the engine oil and B7 to support the hypothesis that soluble $CaSO_4$ is transferred from the engine oil to the fuel where it precipitates. B7 was used as fuel since it is the standard fuel for diesel trucks and cars in Europe according to EN590 [61]. Two types of $CaSO_4$ were examined since it is not known which type that has been found in the deposits. Experiments were conducted at both room temperature and 100°C to investigate the influence of temperature on the solubility.

First, the solubility in engine oil was investigated in which two types of fresh engine oil and one type of used engine oil were examined. 0.2-0.5 g of the $CaSO_4$ was added to 30 g of fresh engine oil A, fresh engine oil B or used engine oil in a beaker containing a magnet. The beaker was placed on a stirring plate and stirred at 300 rpm for 24 hours. For the elevated temperature, the mixture was heated up to 100°C by using a heating plate. The mixture was then separated by filtration except for in the first trial of $CaSO_4$ dihydrate, in which centrifugation was used. For filtration, a 15 µm 520 B Rundfilter filter paper from Schleicher & Shuell MicroScience was used, and for centrifugation, 2500 rpm for 2.5 minutes was used. At the elevated temperature,

the filter funnel and filter paper were heated up to 100°C in an oven 1 hour before the filtration to prevent precipitation in the filter funnel. After the separation, the precipitate was washed with heptane. It was then dried and weighed to compare the weight of $CaSO_4$ before and after it was added to the engine oil. The specifications of the trials can be seen in Table 2.

Table 2: Specifications of the trials in the investigation of the solubility of $CaSO_4$ in the engine oil. The trials with 'di' represents $CaSO_4$ dihydrate the trials with 'an' represents $CaSO_4$ anhydrous.

Trial	Amount of $CaSO_4$ [g]	Amount of oil [g]	Stirring rate [rpm]	Duration [h:min]	Temperature [°C]	Type of engine oil	Type of $CaSO_4$
1di	0.48	31.84	560	24:16	Room temperature	Fresh engine oil A	Dihydrate
2di	0.48	30.03	300	23:50	Room temperature	Fresh engine oil B	Dihydrate
3di	0.53	32.04	300	24:16	100	Fresh engine oil A	Dihydrate
4di	0.5	34.7	300	23:55	100	Fresh engine oil A	Dihydrate
5di	0.21	30	300	24:00	100	Fresh engine oil B	Dihydrate
6di	0.48	28.6	300	24:00	Room temperature	Used engine oil	Dihydrate
7di	0.52	30.6	300	24:29	Room temperature	Used engine oil	Dihydrate
8di	0.66	29.82	300	23:53	100	Used engine oil	Dihydrate
9di	0.46	29.25	300	24:00	100	Used engine oil	Dihydrate
1an	0.51	30.48	300	23:35	Room temperature	Fresh engine oil B	Anhydrous
2an	0.52	29.72	300	23:41	Room temperature	Fresh engine oil B	Anhydrous
3an	0.49	30.02	300	23:43	100	Fresh engine oil B	Anhydrous
4an	0.55	29.48	300	24:40	100	Fresh engine oil B	Anhydrous
5an	0.55	31.98	300	23:51	Room temperature	Used engine oil	Anhydrous
6an	0.5	32.49	300	23:55	Room temperature	Used engine oil	Anhydrous
7an	0.59	30.9	300	23:50	100	Used engine oil	Anhydrous
8an	0.55	30.69	300	23:57	100	Used engine oil	Anhydrous

When investigations of the solubility of the $CaSO_4$ in engine oil had been performed, the solubility in filtered fresh B7 was examined. As in the case with engine oil, it was done both at room temperature and elevated temperature (120°C). The weight of $CaSO_4$ was 0.5 g, and the weight of the B7 was the same as the weight of

the engine oil. The methodology was identical to the one on engine oil in which filtration was used as separation technique. The specification of the trials can be seen in Table 3.

Table 3: Specifications of the trials in the investigation of the solubility of $CaSO_4$ in the B7.

Trial	Amount of $CaSO_4$ [g]	Amount of fuel [g]	Stirring rate [rpm]	Duration [h:min]	Temperature [°C]	Type of $CaSO_4$
1	0.48	31.06	300	23:37	Room temperature	Dihydrate
2	0.46	29.85	300	24:15	120	Dihydrate
3	0.6	30.43	300	24:12	120	Dihydrate
4	0.58	31.53	300	23:43	120	Anhydrous
5	0.46	29.21	300	24:07	120	Anhydrous
6	0.5	29.97	300	24:01	Room temperature	Anhydrous
7	0.56	30.53	300	24:38	Room temperature	Anhydrous
8	0.68	31.48	300	24:02	Room temperature	Anhydrous

4.1.2 Investigation of Ostwald Ripening

Two experiments were performed to investigate whether Ostwald ripening could be the cause of the deposit formation. The goal was to leave $CaSO_4$ powder in B7 for a defined time duration, and then see if the smaller crystals were dissolved to form larger crystals with time. One experiment was conducted with an oxygen atmosphere and one with a nitrogen atmosphere since an oxygen atmosphere could result in oxidation of the fuel. Moreover, a nitrogen atmosphere is more similar to the field since oxygen is absent in the fuel system [62]. In the oxygen atmosphere, about 1 g of the $CaSO_4$ anhydrous was added at a marked point to a beaker with fuel and was left at 120°C for 9 days. In the nitrogen atmosphere, the fuel and $CaSO_4$ were added to a round flask with three openings, in which the openings were sealed with vaseline to avoid that oxygen entered the flask. A thermometer was injected, nitrogen gas was bubbled into the system and the last opening was connected to a washing flask with distilled water. The washing flask was used to collect nitrogen gas and evaporation products. Thereafter, the gas was released to the air. The experiment was left for 9 days at 120°C. When the experiments were terminated, it was investigated whether the small crystals had been dissolved and larger crystals were formed. The setup of the experiment with a nitrogen atmosphere can be seen in Figure 5.

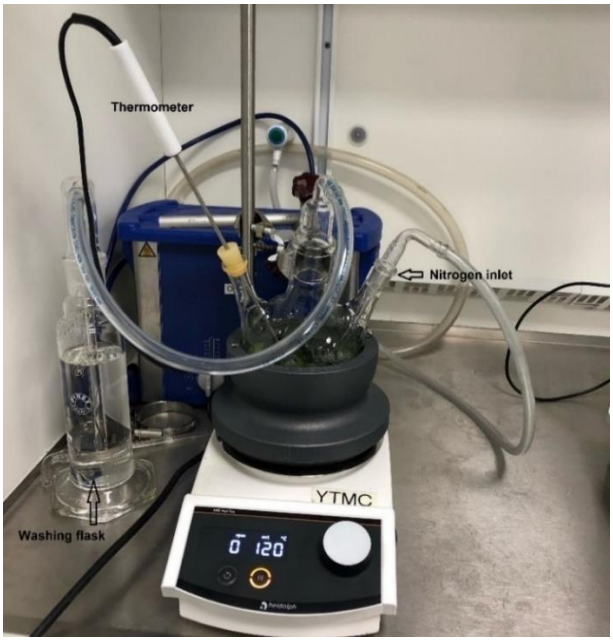

Figure 5: Setup of the Ostwald ripening experiment with a nitrogen atmosphere.

4.2 Investigation of Deposit Formation in the TDT

A new laboratory test setup with inspiration from JFTOT was used for the investigation of the deposit formation. The setup was called TDT and allowed for easier analysis compared to JFTOT since the fuel passed over a removable aluminium foil instead of an aluminium tube. The setup consisted of a feed unit, process unit, and cooling circuit (see Figure 6).

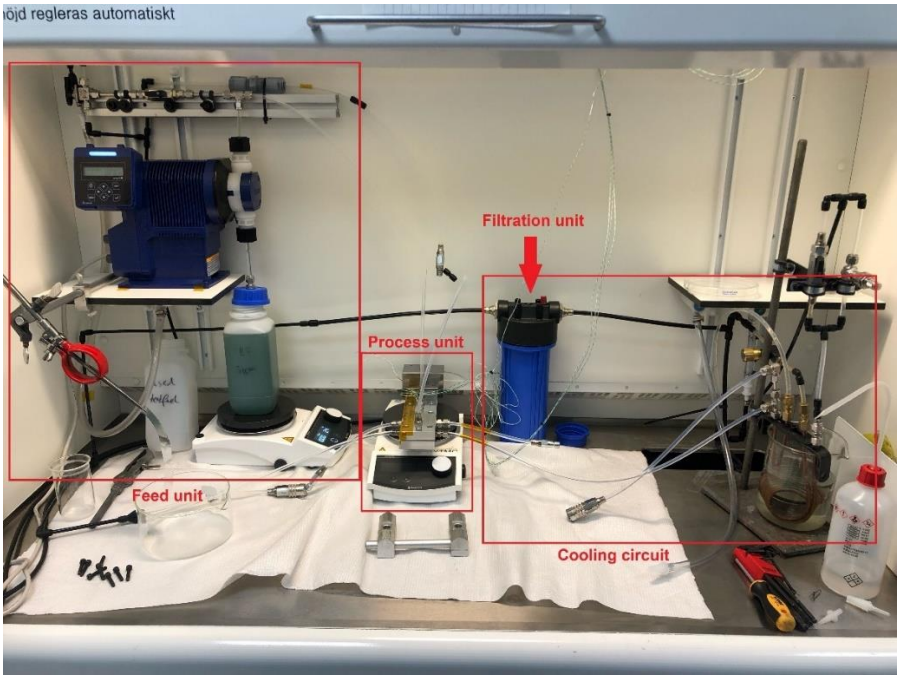

Figure 6: The total setup of the TDT.

The feed unit consisted of a pump, valves, a test fuel tank including a magnet, a stirrer, and a fuel waste tank (see Figure 7). The test fuel consisted of B7 and a concentrate including sodium hydroxide, calcium oxide,

distilled water, and aged B100. The calcium and sodium concentrate was added to B7 to allow formation of metal soaps since they are formed from carboxylic acids in the fuel and metal compounds. The N_2/bleed selector valve in Figure 7 was used to determine whether nitrogen gas should be flushed through the system or bleeding should be performed. Nitrogen was used after the experiment to spill out remaining fuel. Bleeding means that air was emptied from the system, and the pressure was released. It was done both before and after the experiment. The bleed valve was used to open the system for either N_2 or fuel where it was closed when fuel was pumped through the system, and opened if the system was flushed with nitrogen. The back pressure valve ensured that the pressure of 1.7 bar was kept through the system.

Figure 7: The feed unit of the process setup.

The process unit consisted of the modelled injector (rig) made of aluminium, which was placed on a heating plate (see Figure 8). One end was supplied with cooling channels while the other was placed on a heating block to obtain a temperature gradient within the rig (see Appendix A: Temperature Profile inside the Rig). The fuel entered in the cold end, was heated inside the rig, and exited from the hot end. Thermocouples were connected to the rig to be able to measure the temperature inside. Inside the rig, a gasket, consisting of fluorine kautschuk material (FKM), was placed on top of the substrate made of a sheet of aluminium foil. The gasket formed a split in which the fuel passed through. Moreover, the gasket helped to seal the rig, and to keep the upper part of the rig cool. In this way, deposits were only formed at the lower part on top of the aluminium foil.

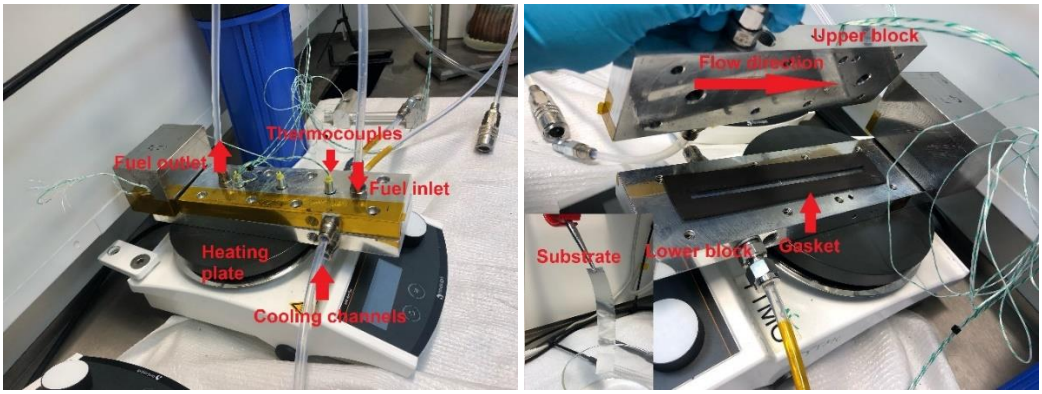

Figure 8: Components of the processing unit.

The cooling circuit consisted of a filtration unit, valves, and a beaker containing a heat exchanger and water (see Figure 6 and Figure 9). Cooling water was split with one part going to the system and the other to the heat exchanger. The water that went to the system was first purified in the filtration unit to reduce the hardness of the water and achieve a constant flow. Thereafter, the water was heated up in the rig and then cooled in the heat exchanger before exiting the system. It was cooled both for material and safety concerns. The valves could only handle a certain pressure, which was why the water needed to be cooled since a higher temperature meant a higher pressure. The heat exchanger valve adjusted the water flow in the heat exchanger, and the cooling bypass valve allowed for a higher flow of water through the system. During the experiment, the cooling regulating valve adjusted the cooling flow of water through the system. After the experiment, the substrate could be removed from the lower part of the rig. It was then washed with heptane and dried. Thereafter, it could be analysed in SEM-EDX, FTIR-ATR, ion milling and pyrolysis GC-MS.

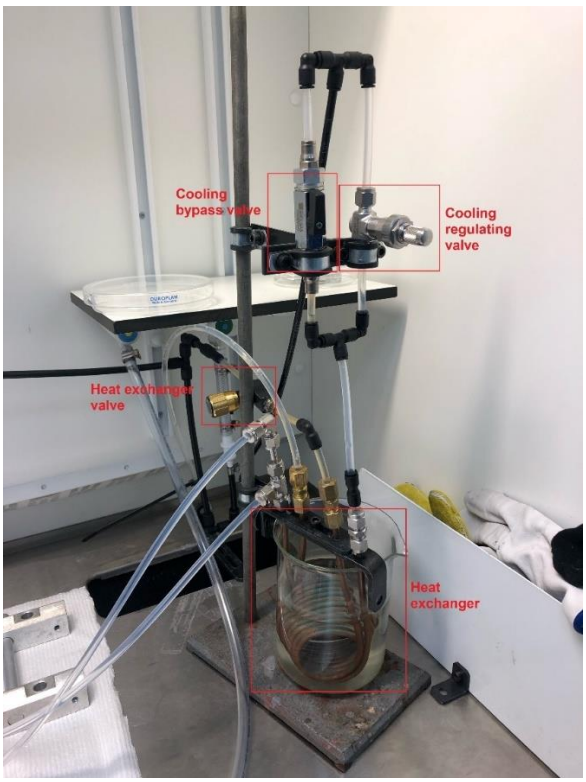

Figure 9: The cooling circuit of the process setup.

4.2.1 Preparation before the Experiments

Before the experiments in the TDT, some preparations were made. First, the substrate was prepared where a 160 mm long and 30 mm wide piece of aluminium foil was cut. Moreover, the test fuel was made 24 h prior to the experiment. The test fuel consisted of B7, and 15 ppm of concentrate to be able to form soap deposits. The concentrate was prepared by first adding 0.25 g of CaO, 1 g of NaOH, and 25 g of distilled water to a bottle. This mixture was stirred on a stirring plate for 5 minutes at 650 rpm to prevent formation of lumps. Thereafter, 220 g of B100 that had been aged for 66 h was added and the mixture was put in a homogenizer for 5 minutes at 7000 rpm. Lastly, the concentrate was left on a stirring plate at 650 rpm for 24 h. This resulted in a concentration of 0.1 wt% calcium and 0.4 wt% sodium.

To achieve a concentration of 15 ppm of the calcium and sodium concentrate in the test fuel, 1.8 g of the concentrate was added to 580 g of the B7 for the investigations on temperature, and 2.5 g of the concentrate was added to 830 g of the B7 for the investigations on engine oil. This was done in two rounds where firstly half of each amount was added and then stirred in a shaking machine for 45 seconds. Thereafter, the remaining amount was added, and the test fuel was stirred again for 45 seconds. The test fuel was then left for 24 h at a stirring plate at 750 rpm prior to the experiment. Moreover, in the investigations on engine oil, 8.4 g of the engine oil was added to the test fuel right before the experiment to achieve 1 wt% of the engine oil in the test fuel. Experiments were also performed on engine oil without addition of calcium and sodium concentrate. In these test fuels, 6.3 g of the engine oil was added to 620 g of the B7 right before the experiment to achieve 1 wt% of the engine oil in the test fuel.

Before any experiment was initiated, the surfaces of the heating block, gasket, and substrate were cleaned with heptane. Thereafter, the substrate was placed on the lower heating block with the gasket on top of it. The start, stop, and flow directions were marked on the substrate to facilitate the analysis. Lastly, the upper heating block was placed on top of the gasket and fastened with screws.

4.2.2 General Procedure of the TDT

To initiate the experiment, all fuel and cooling lines were connected, and the suction line was inserted into the test fuel tank (see Figure 7). Firstly, bleeding was performed to get rid of air bubbles and old fuel from earlier experiments. The N_2/bleed selector valve was opened for bleeding, which allowed fuel to enter the waste fuel tank. Then the bleed valve was opened, and the pump ran at a high flow rate until no air bubbles could be seen. Thereafter, the bleed valve was closed. Then the pump was run at high flow rate again to remove air from the complete system.

The next step was to initiate the cooling. Firstly, the cooling bypass valve and water tab were opened with water running at full speed for roughly one minute to exchange the water in the filter (see Figure 9). Thereafter, the cooling bypass valve was closed and desired water flows through the heat exchanger and the system were set by the heat exchanger valve and the cooling regulating valve. The flow rate was confirmed by weighing the

amount of water that passed through the system per minute. The pump and heating plate were then turned on and a metal sheet was placed in front of the process unit to prevent cooling of the system.

After the desired time duration, the experiment was terminated by turning off the heating plate and the pump. The heating blocks were placed on a spacer, which removed the contact between the heating blocks and the heating plate. Moreover, the cooling bypass valve was opened to allow rapid cooling of the heating blocks (see Figure 9). N_2 was then flown through the system to remove the remaining fuel. When the heating blocks were cold, the substrate was removed. Firstly, the water tab was closed, and the bleed valve was opened to release pressure from the system. The substrate could then be removed and was cleaned with 4 mL of heptane on each side. When dry, it was cut into two pieces to facilitate the analysis. Lastly, the gasket and heating block were cleaned with heptane, and the waste tank was emptied.

4.2.3 Reference Level

The reference level of the temperature, fuel flow rate, and time duration was chosen based on the work of Barker et al. [29] and Berndt et al. [9]. Their parameters, as well as the parameters used in this study, can be seen in Table 4. These parameter values serve as the basis for the investigation and are used unless otherwise stated.

Table 4: Reference level in the TDT experiments.

Parameter	**TDT**	**Barker et al.** [29]	**Berndt et al.** [9]
Temperature [°C]	250	260	240
Fuel flow rate [mL/h]	180	180	180
Time duration [h]	2.5	2.5	2.5

4.2.4 Investigation of Temperature in the TDT

The use of cooling water and a heating plate created a temperature gradient in the process unit. The temperature profile for different temperatures and cooling flow rates can be seen in Appendix A: Temperature Profile inside the Rig. To obtain investigations over a wide temperature range, experiments were conducted with the heating plate setting temperatures of 120°C and 250°C at a constant cooling flow rate of 100 g/min. Three replicates were run at each temperature to ensure repeatability. The specifications of the trials can be seen in Table 5.

Table 5: Method specifications of the trials within the investigation of temperature.

Trial	**Time from preparation of test fuel to experiment [h:min]**	**Duration [h:min]**	**Setting temperature [°C]**	**Cooling flow [g/min]**	**Fuel flow [mL/h]**
1	24:08	2:28	250	100	180
2	23:41	2:29	250	100	180
3	24:25	2:29	250	100	180
4	24:18	2:30	120	100	180
5	24:00	2:26	120	100	180
6	24:03	2:30	120	100	180

The setting temperatures from Table 5 allowed for the investigation of deposit formation in a temperature range of 50-190°C. The procedure was as described in 4.2.2 General Procedure of the TDT in which the temperature was adjusted on the heating plate.

4.2.5 Investigation of Tilted Apparatus in the TDT

Experiments were conducted with the rig tilted to 30° to investigate whether sedimentation could affect the deposit formation (see Figure 10).

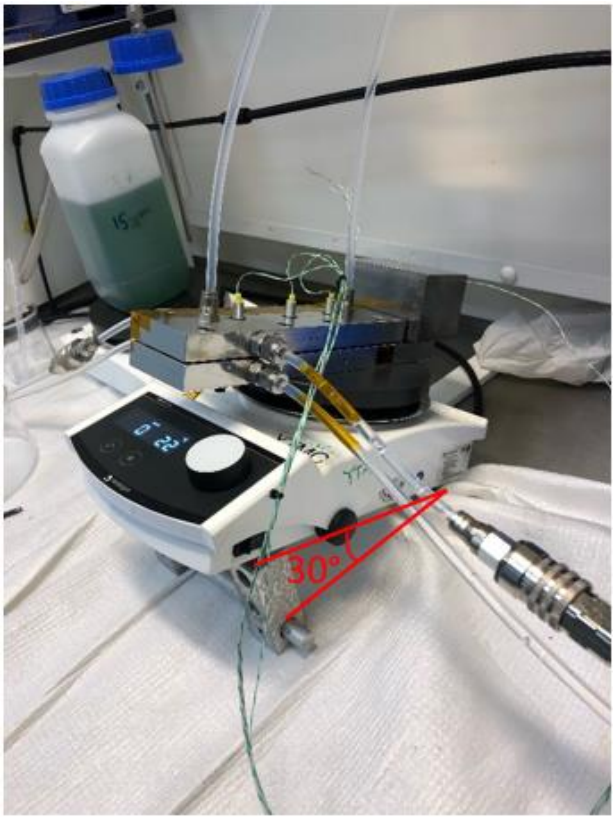

Figure 10: Setup of the tilted apparatus.

The parameters were set to the reference level (see Table 4). However, experiments were also performed at 120°C to investigate differences across the temperature range 50-190°C. Thereafter, the procedure was as described in 4.2.2 General Procedure of the TDT. As in the investigation of temperature, three replicates were performed on each condition to ensure repeatability. The specifications of the trials can be seen in Table 6.

Table 6: Method specifications of the trials within the investigation of a tilted rig.

Trial	Time from preparation of test fuel to experiment [h:min]	Duration [h:min]	Setting temperature [°C]	Cooling flow [g/min]	Fuel flow [mL/h]
1	24:05	2:35	250	100	180
2	24:03	2:30	250	100	180
3	24:35	2:30	250	100	180
4	23:55	2:30	120	100	180
5	24:13	2:30	120	100	180
6	23:23	2:30	120	100	180

4.2.6 Investigation of Engine Oil in the TDT

In the investigations of addition of engine oil into the test fuel, one fresh and one used engine oil were used. The composition of some of the elements in the engine oils can be seen in Table 7.

Table 7: Specifications of the two types of engine oil used in the TDT experiments with engine oil addition.

	Concentration [ppm]	
Elements	**Fresh engine oil B**	**Used engine oil**
Ca	1400	1610
Fe	n.d.	53.4
Mg	1000	1090
Na	n.d.	1.44
P	800	740
S	2100	n.d.
Si	30	6.62
Zn	900	920

4.2.6.1 Investigation of Fresh Engine Oil with Sulphuric Acid

The purpose of engine oil addition to the test fuel was to investigate whether crystals of $CaSO_4$ could be formed. However, sulphate was not present in the fresh engine oil B. Therefore, an addition of sulphate ions was needed before the initiation of the TDT. This was made by adding diluted sulphuric acid. Half of the hydroxide ions present in the oil were neutralised, where the total base number was 9.9 mg KOH/g oil. With an addition of 8.4 g of engine oil to the test fuel, the total moles of hydroxide ions were 0.0015 mol. The neutralisation of half of the moles of hydroxide ions represented an addition of 0.04 g of 95-95 wt% sulphuric acid to 8.4 g of engine oil (see Appendix B: Calculation on H_2SO_4 for the Fresh Engine Oil TDT Experiments). However, to simplify the additions, a mixture with a larger volume was prepared. In the first trial, 0.46 g of sulphuric acid was added to 1.8 g of distilled water to be diluted. This dilution was then transferred to 100 g of engine oil and stirred at 1000 rpm for 24 h. In the subsequent experiments, the additions were based on 50 g of engine oil. Therefore, 0.23 g of sulphuric acid was added to 0.46 g of distilled water for dilution. The mixture was then transferred to 50 g of engine oil and stirred at 1000 rpm for 24 h. Experiments were performed with oil at both room temperature and at 80°C.

The test fuel was prepared as described in 4.2.1 Preparation before the Experiments. When the experiment was to be initiated, 8.5 g of the engine oil and sulphuric acid mixture was transferred to the test fuel. Thereafter, the experiments were run as described in 4.2.2 General Procedure of the TDT. The specification of each trial can be seen in Table 8.

Table 8: Method specifications of the trials within the investigation of fresh engine oil with addition of concentrate.

Trial	Time from neutralisation to experiment [h:min]	Time from preparation of test fuel to experiment [h:min]	Duration [h:min]	Setting temperature [°C]	Cooling flow [g/min]	Fuel flow [mL/h]	Heating of oil before experiment
1	23:43	24:08	02:30	250	100	180	No
2	24:28	24:18	02:30	250	100	180	No
3	23:36	23:59	02:30	250	100	180	Yes
4	24:36	24:26	02:30	250	100	180	Yes
5	23:55	23:35	02:25	120	100	180	Yes
6	24:25	24:10	02:30	120	100	180	Yes
7	24:00	0:35	02:31	120	100	180	Yes

Experiments were also performed without addition of the calcium and sodium concentrate. In those experiments, the oil was neutralised as described in the first paragraph of this section. Moreover, 623 g of B7 was used instead of one litre of test fuel. When the experiment was to be initiated 6.4 g of the engine oil and sulphuric acid mixture was transferred to the B7. Thereafter, the experiments were run as described in 4.2.2 General Procedure of the TDT. The specifications of the trials within the experiments of fresh engine oil without addition of calcium and sodium concentrate can be seen in Table 9.

Table 9: Method specifications of the trials within the investigation of fresh engine oil without addition of concentrate.

Trial	Time from neutralisation to experiment [h:min]	Duration [h:min]	Setting temperature [°C]	Cooling flow [g/min]	Fuel flow [mL/h]
1	24:16	2:30	250	100	180
2	24:00	2:30	250	100	180
3	24:18	2:30	250	100	180

4.2.6.2 Investigation of Used Engine Oil

In the investigations of used engine oil, sulphate ions were supposed to be present. Therefore, no addition of sulphuric acid was needed. One litre of test fuel was prepared in the same manner as in the investigations for the fresh engine oil. When the experiment was to be initiated, 8.4 g of the used engine oil was added to the test fuel and the experiment was run as described in 4.2.2 General Procedure of the TDT. The specifications of the trials can be seen in Table 10.

Table 10: Method specifications of the trials within the investigation of used engine oil with addition of concentrate.

Trial	Time from preparation of test fuel to experiment [h:min]	Duration [h:min]	Setting temperature [°C]	Cooling flow [g/min]	Fuel flow [mL/h]
1	23:19	2:32	250	100	180
2	23:07	2:35	250	100	180
3	24:31	2:29	250	100	180
4	24:11	2:30	120	100	180
5	24:01	2:30	120	100	180
6	24:03	2:30	120	100	180

Experiments were also conducted without addition of the calcium and sodium concentrate in which 6.3 g of the used engine oil was transferred to 623 g of B7 when the experiment was to be initiated. The specification of each trial within the investigation of used engine oil without addition of calcium and sodium concentrate can be seen in Table 11.

Table 11: Method specifications of the trials within the investigation of used engine oil without addition of concentrate.

Trial	Duration [h:min]	Setting temperature [°C]	Cooling flow [g/min]	Fuel flow [mL/h]
1	02:30	250	100	180
2	02:30	250	100	180
3	02:30	250	100	180

4.2.7 Analysis of the Samples from the TDT

In the SEM-EDX analysis, type II secondary electrons (SE2) were utilised with an electron high tension (EHT) beam. The voltage used for the SEM images was 10 kV, and for the EDX analyses 16 kV. Moreover, the aperture size 30 µm was used for the SEM images but 60 µm for the EDX analyses. The working distance was changed in SEM to achieve good focus, but for the EDX analysis, 12 mm was used. In the FTIR-ATR, analysis absorption spectra were obtained and normalised to the hydrocarbon peak at 2928 cm^{-1} to be able to compare relative peak heights.

For the pyrolysis GC-MS analysis, an Agilent 8890 GC system was used with a HP-5ms Ultra Inert column. It is a crosslinked column made of (5%-phenyl)-methylpolysiloxane, and the used transport medium was helium. The sample was derivatised with tetramethylammonium hydroxide to stabilise the components for a better characterisation. In the BIB analysis, the cross-section area was produced in an argon environment where the samples were prepared in a glovebox and transferred to the ion milling apparatus in an airtight container. During the milling process, an acceleration voltage of 6 kV was used for a milling time of 30 minutes. Thereafter, a finer polishing was made with 4 kV for 30 minutes.

5. Results and Discussion

In this section, the results of all investigations and analyses will be presented and discussed.

5.1 Investigation of Hypotheses

Results from the investigation on the solubility of $CaSO_4$ and Ostwald ripening will be discussed in the following paragraphs.

5.1.1 Investigation of the Solubility of $CaSO_4$

From the investigations of the solubility of $CaSO_4$ in engine oil and B7, it could be discussed whether it is reasonable that dissolved $CaSO_4$ in the engine oil is transferred to the fuel system, and then precipitates. This is only possible if the solubility is significantly higher in the engine oil than in B7. The results of the trials on the solubility of the $CaSO_4$ dihydrate in the engine oils can be seen in Table 12 and Appendix C: Investigation of the Solubility of Calcium Sulphate Dihydrate in Engine Oil.

Table 12: Results of the investigation of the solubility of $CaSO_4$ dihydrate in the engine oils. A negative solubility represents an increase of powder.

Trial	Difference of $CaSO_4$ [mg]	Amount of engine oil [g]	Solubility [mg $CaSO_4$/g oil]	Type of engine oil	Temperature [°C]
1di	-40	32	1.3	Fresh engine oil A	Room temperature
2di	110	30	-3.7	Fresh engine oil B	Room temperature
3di	-130	32	4.1	Fresh engine oil A	100
4di	-100	35	2.9	Fresh engine oil A	100
5di	-80	30	2.7	Fresh engine oil B	100
6di	50	29	-1.7	Used engine oil	Room temperature
7di	50	31	-1.6	Used engine oil	Room temperature
8di	-130	30	4.4	Used engine oil	100
9di	-120	29	4.1	Used engine oil	100

The investigations of $CaSO_4$ dihydrate at room temperature indicated that it was not soluble in either the fresh or used engine oil since there generally was an increase in weight of powder. The increase in weight could indicate that the final powder included other components. Moreover, there could be oil residues on the filter paper. However, the first trial in the fresh engine oil showed a small decrease of the $CaSO_4$ powder but some powder was lost during the centrifugation and washing of the powder. Therefore, it was concluded that the difference was not significant. At 100°C, the $CaSO_4$ dihydrate was partially soluble in both oils. An average solubility was determined by calculating the mean value of the different trials for the same oil and temperature. The average solubilities at 100°C were 3.2 mg $CaSO_4$/g fresh engine oil, and 4.2 mg $CaSO_4$/g used engine oil.

It is reasonable that the solubility of $CaSO_4$ in the engine oil changes with temperature since the solubility in water changes with temperature [63]. Moreover, the increase in solubility of $CaSO_4$ dihydrate with temperature could be related to a decrease of the amount of water molecules since they could protect the crystals and prevent

dissolution. At 100°C, the water molecules may evaporate, which could facilitate the dissolution. Furthermore, the temperature dependence could indicate that an activation energy is required for the $CaSO_4$ dihydrate to dissolve [64]. The results of the trials on the solubility of the $CaSO_4$ anhydrous in the engine oil can be seen in Table 13 and Appendix D: Investigation of the Solubility of Calcium Sulphate Anhydrous in Engine Oil.

Table 13: Results of the investigation of the solubility of $CaSO_4$ anhydrous in the engine oils.

Trial	Difference of $CaSO_4$ [mg]	Amount of engine oil [g]	Solubility [mg $CaSO_4$/g oil]	Type of engine oil	Temperature [°C]
1an	-130	30	4.3	Fresh engine oil B	Room temperature
2an	-200	30	6.7	Fresh engine oil B	Room temperature
3an	-160	30	5.3	Fresh engine oil B	100
4an	-240	29	8.1	Fresh engine oil B	100
5an	-160	32	5.0	Used engine oil	Room temperature
6an	-260	32	8.0	Used engine oil	Room temperature
7an	-250	31	8.1	Used engine oil	100
8an	-200	31	6.5	Used engine oil	100

The investigations of the $CaSO_4$ anhydrous indicated that it is partially soluble in both the fresh and used engine oil at both temperatures. An average solubility was determined by calculating the mean value of the different trials for the same oil and temperature. The average solubility at room temperature was about 6.5 mg $CaSO_4$/g used oil and 5.5 mg $CaSO_4$/g fresh oil. At the elevated temperature, the solubility increased slightly to 7.3 mg $CaSO_4$/g used oil and 6.7 mg $CaSO_4$/g fresh oil.

The solubility of $CaSO_4$ dihydrate showed to depend more on the temperature than the solubility of $CaSO_4$ anhydrous. The reason for this could be that the $CaSO_4$ anhydrous does not contain any water molecules that could affect the solubility. Moreover, it is reasonable that the solubility of $CaSO_4$ dihydrate and $CaSO_4$ anhydrous in the engine oils differs since they have different solubility in water. At room temperature, the $CaSO_4$ anhydrous has higher solubility in water than the $CaSO_4$ dihydrate [63], which is in line with the results of this study. However, according to the literature, the solubility of $CaSO_4$ anhydrous in water decreases with temperature, and becomes lower than the solubility of $CaSO_4$ dihydrate at 100°C [63]. This is not consistent with the results of this study because the solubility of $CaSO_4$ anhydrous increased slightly with temperature and was higher than the solubility of $CaSO_4$ dihydrate. Anyhow, the constituents of water and oil differ significantly, which could be the reason for the different trends in solubility. The solubility of both $CaSO_4$ dihydrate and anhydrous differed between the fresh and the used engine oil where it was higher in the used engine oil. This is reasonable since the components of the oils are different. In the used oil, degradation has occurred, in which organic acids have been formed. The acids can form complexes with the $CaSO_4$, which may facilitate dissolution.

In most experiments, the oil was diluted with heptane to facilitate the filtration. It is important to consider that this may affect the solubility since the environment is altered. Moreover, losses occurred in the filter funnel and beaker in all experiments, which could have reduced the weight of the powder, and this can have resulted in a

higher solubility. However, in all experiments, oil residues were observed on the filter paper, which could have resulted in an increase in weight. With all this in mind, the calculated solubilities may not be fully accurate, but rather an estimation. However, since the same error sources were present in all the experiments, they can still be compared to each other.

The results of the trials on the solubility of $CaSO_4$ dihydrate and anhydrous in the B7 can be seen in Table 14 and Appendix E: Investigation of the Solubility of Calcium Sulphate in B7.

Table 14: Results of the investigation of the solubility of $CaSO_4$ in the B7. A negative solubility represents an increase of powder.

Trial	Difference of $CaSO_4$ [mg]	Amount of engine oil [g]	Solubility [mg $CaSO_4$/g oil]	Type of $CaSO_4$	Temperature [°C]
1	40	31	-1.3	Dihydrate	Room temperature
2	-60	30	2.0	Dihydrate	120
3	-150	30	4.9	Dihydrate	120
4	-390	30	13	Anhydrous	Room temperature
5	-70	31	2.3	Anhydrous	Room temperature
6	-30	31	1.0	Anhydrous	Room temperature
7	-100	32	3.2	Anhydrous	120
8	30	29	-1.0	Anhydrous	120

The investigations of the solubility of the $CaSO_4$ dihydrate indicated that the $CaSO_4$ dihydrate was not soluble in the B7 at room temperature. However, at the elevated temperature, it seemed as the $CaSO_4$ dihydrate was partially soluble. An average solubility was determined by calculating the mean value of the different trials. The average solubility at 120°C was 3.5 mg/g fuel. The solubilities in the engine oils at 100°C were 3.2 mg/g fresh oil and 4.2 mg/g used oil. Thereby, the $CaSO_4$ dihydrate has similar solubilities in the B7, the fresh engine oil, and the used engine oil at elevated temperature. However, the loss of weight for the $CaSO_4$ dihydrate may be related to the release of its water molecules, indicating that it is indeed insoluble. Anyhow, this was not investigated due to time constraints.

The investigations of the solubility of $CaSO_4$ anhydrous in the B7 indicated that it has low solubility at both temperatures. At room temperature, trial 4 showed a large decrease of powder while the other two showed a smaller decrease. Therefore, the first trial was considered an outlier and was disregarded, and the average solubility was calculated as the mean of trial 5 and 6. Consequently, the average solubility of $CaSO_4$ anhydrous at room temperature was 1.6 mg/g fuel. The solubilities of the $CaSO_4$ anhydrous in the oils at room temperature were 5.5 mg/g fresh oil and 6.5 mg/g used oil. This resulted in a 70-75% lower solubility in the B7 compared to the engine oil. At 120°C, there was a decrease in trial 8 and an increase in trial 7. The average solubility was calculated by taking the mean of trial 7 and 8, leading to an average solubility of 1.1 mg/g fuel. In the engine oils, the solubilities at elevated temperature were 6.7 mg/g fresh oil and 7.3 mg/g used oil. Thereby, the solubility was about 85% lower in the B7 compared to the oils. The significantly lower solubility of the $CaSO_4$ anhydrous in the B7 indicates that engine oil contamination could be the reason for the crystal formation in the IDIDs if the $CaSO_4$ crystals consist of $CaSO_4$ anhydrous.

5.1.2 Investigation of Ostwald Ripening

Investigations of Ostwald ripening were performed to examine whether it could be a reason for the crystal formation. It can only indicate that it could be a reason if the powder of $CaSO_4$ dissolves in the fuel, to then precipitate with time as larger crystals. In the experiment of Ostwald ripening with an oxygen atmosphere, only the original $CaSO_4$ powder could be seen but no larger crystals (see Figure 11). However, the B7 changed colour from green to orange, and sticky and slimy deposits could be seen on the wall of the beaker and in the edges of the bottom of the beaker. The identification of sticky and slimy deposits is consistent with the literature, as more slimy deposits has been seen at lower temperatures and the temperature was 120°C [7]. The reason for not forming crystals could be that the time duration was too short or that too much powder may have been added. Another reason for no formation of larger crystals may be that oxidation occurred due to the oxygen atmosphere, which also could explain the change of colour.

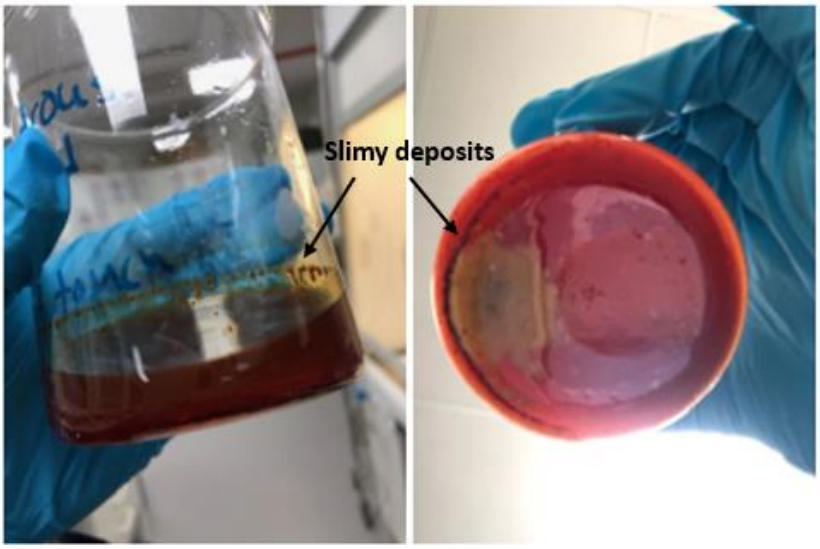

Figure 11: Results of the investigation of Ostwald ripening with an oxygen atmosphere.

The result of the investigation with a nitrogen atmosphere can be seen in Figure 12. The colour did not change to the same extent as in the experiment with an oxygen atmosphere since it was still green, which may indicate that the oxidation process was prevented. Moreover, no deposits could be seen, which also could be due to that the oxidation process was avoided. The original $CaSO_4$ powder could be seen but no larger crystals.

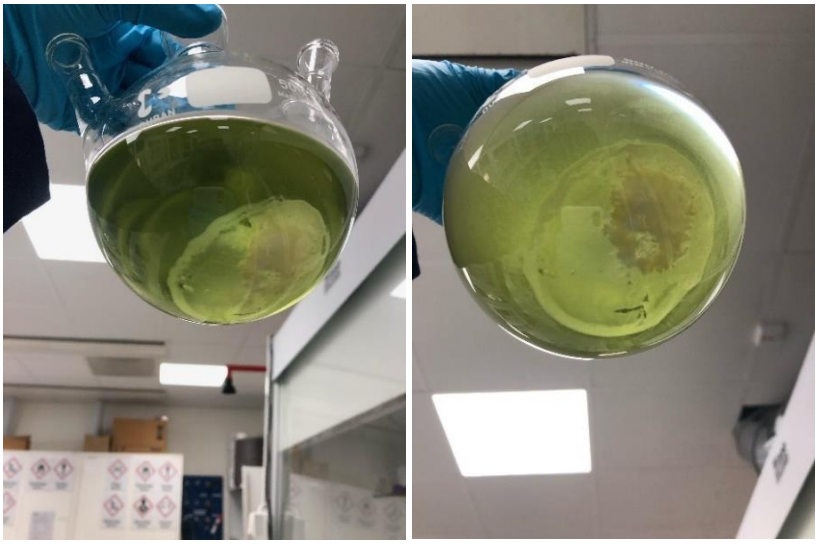

Figure 12: Results of the investigation of Ostwald ripening with a nitrogen atmosphere.

Only the original $CaSO_4$ powder without formation of larger crystals could be seen in both experiments regardless of the atmosphere. Thereby, Ostwald ripening may not be the reason for the crystal formation in the IDIDs. However, it is important to keep in mind that the fuel system differs from the round flask used in this experiment. In the fuel system, there is more components that could affect the process such as contaminants, temperature, pressure, size, and time duration.

5.2 Investigation of Deposit Formation in the TDT

Three parameters from Table 1 were chosen to be investigated further to be able to answer the research questions of the study. Temperature was first investigated since it has been shown to influence the deposit formation, and with this newly designed rig it is possible to analyse the deposit formation more thoroughly over a temperature gradient. The setting temperatures 120℃ and 250℃ were used on the heating plate to achieve a temperature range of 50-190℃ within the rig. Moreover, a tilted apparatus was investigated since the deposit formation could be affected by sedimentation. Out in the field, sedimentation does not occur since the injector is vertical. However, in this study the rig was usually used horizontal. Thereby, it was of interest to exclude that sedimentation influences the results. Lastly, engine oil was chosen because the most believed hypothesis is that $CaSO_4$ from the engine oil has an influence on the deposit formation. Moreover, other components in the engine oil could affect the deposit formation. The deposit formation was investigated visually, with SEM-EDX and with FTIR-ATR. Moreover, some samples were analysed by ion milling and pyrolysis GC-MS.

5.2.1 Investigation of Temperature in the TDT

Visually, the deposits differed between the trials and the location on the foil. Generally, brown deposits could be seen on the substrate, but the number of brown deposits was larger at lower temperatures. Moreover, the deposits were stickier at lower temperatures. This is consistent with what have been seen previously since deposits formed at lower temperatures usually are more sticky compared to at the higher temperatures [30].

The amount and size of the deposits seen in SEM differed between the trials for both setting temperatures. At a setting temperature of 250°C, more and larger deposits were seen in the first trial. The difference could be related to the preparation of the test fuel. It could also be related to the stirring speed of the test fuel since a lower stirring speed was used in the first trial. Moreover, it was noted that air entered the process in the end of the experiment, which could affect the deposit formation. At a setting temperature of 120°C, all trials yielded different trends in size and amount, which indicates that the repeatability may be worse at lower temperatures. However, common for all trials was that a large amount and size could be seen when the temperature reached 90°C. The results also indicated that the number of deposits was lower at the lower temperatures. This was also seen in the investigations at the setting temperature of 250°C since the number of deposits was highest at the highest temperature (see Figure 13). In the figure, there is a larger number of dots in the right picture, which shows the larger number of deposits. This could be related to the evaporation of liquids such as fuel and water at high temperatures, which could make the deposits smaller and more brittle. It could also be related to reactions that may occur at certain temperatures [64].

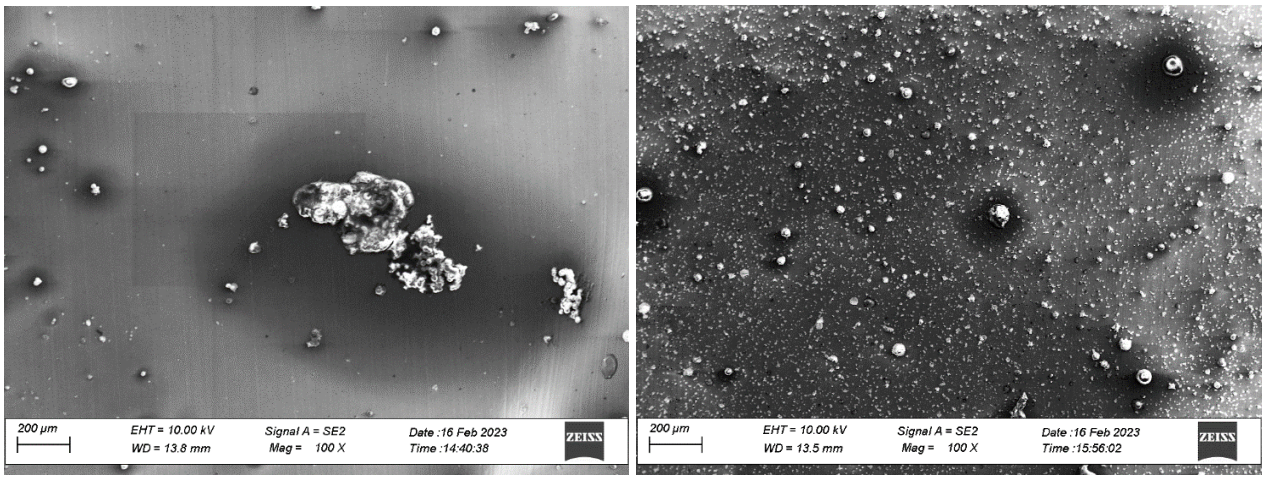

Figure 13: Comparison of the deposit size at 95°C (left) and 185°C (right) in trial 1 at the setting temperature 250°C. The deposits are the dots seen in the images.

The size at the end of the foil at a setting temperature of 120°C was compared to the size at the beginning of the foil at the setting temperature of 250°C to examine if the position on the foil affects the deposit formation (see Figure 14).

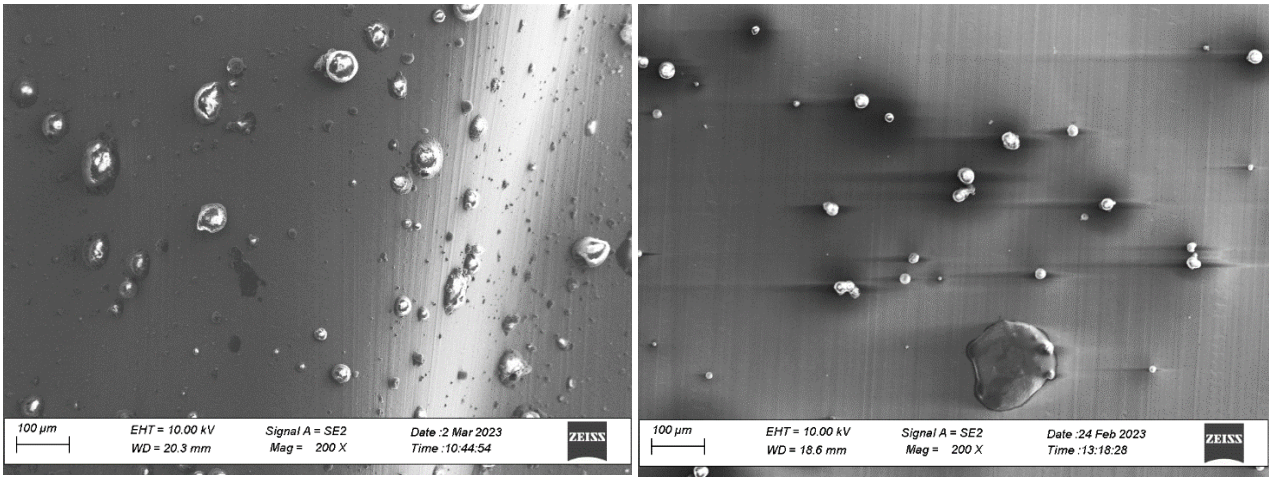

Figure 14: Comparison of the deposits at 90°C in trial 2 at a setting temperature of 120°C and the deposits at 95°C in trial 3 at a setting temperature of 250°C.

In Figure 14, it could be seen that the distribution and morphology were similar since the shape, size and number of deposits look similar in both images. This suggests that the morphology may be more related to the temperature than the travelling distance. The results from the investigations at both the setting temperature 120°C and 250°C indicated that, in general, there was a peak of size of the deposits at the temperature of 80-90°C and the amount and size seemed to thereafter change until 190°C where the amount was high, but the size was small. This is consistent with Berndt et al. [9] who argue that the greatest amount of deposits is formed at higher temperatures. However, due material limitations, it was not possible to investigate temperatures above 190°C. From the SEM analysis it could also be seen that in several locations on the foil, less deposits were formed in the middle of the substrate compared to the edges. This could be related to the fuel flow rate, which is highest in the middle, making it more difficult for the deposits to adhere to the surface. This is in accordance with Edney et al. [31], who state that the severity of deposit formation can be related to the loss of flow rate.

In the SEM-EDX analysis, the composition at different positions on the substrate could be evaluated. Figure 15 shows the average composition of the different trials in which the composition was normalised to exclude aluminium to be able to investigate the deposits, and not the aluminium foil.

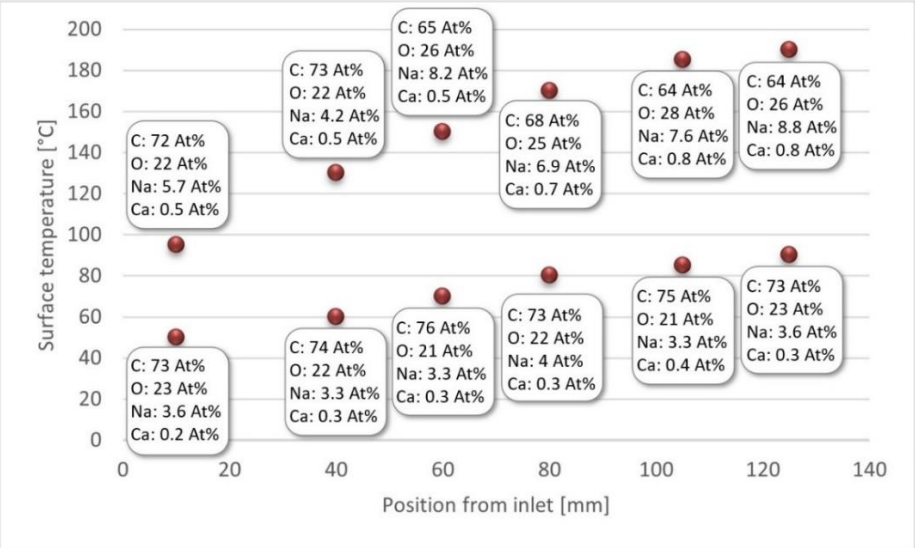

Figure 15: Average composition of the deposits at different positions and temperatures. The upper points in the figure belong to a setting temperature on the heating plate of 250°C and the lower points to 120°C.

From Figure 15, the composition at the same position from the inlet at the two different temperatures could be compared. It could be seen that the composition of the elements generally differed between the temperatures at the same position from the inlet. Thereby, the position from the inlet may not affect the type of deposit. However, it could be seen that the composition for all elements changed with the temperature. This can be seen more clearly in Figure 16 and Appendix F: Comparison of Composition with Temperature for each Element.

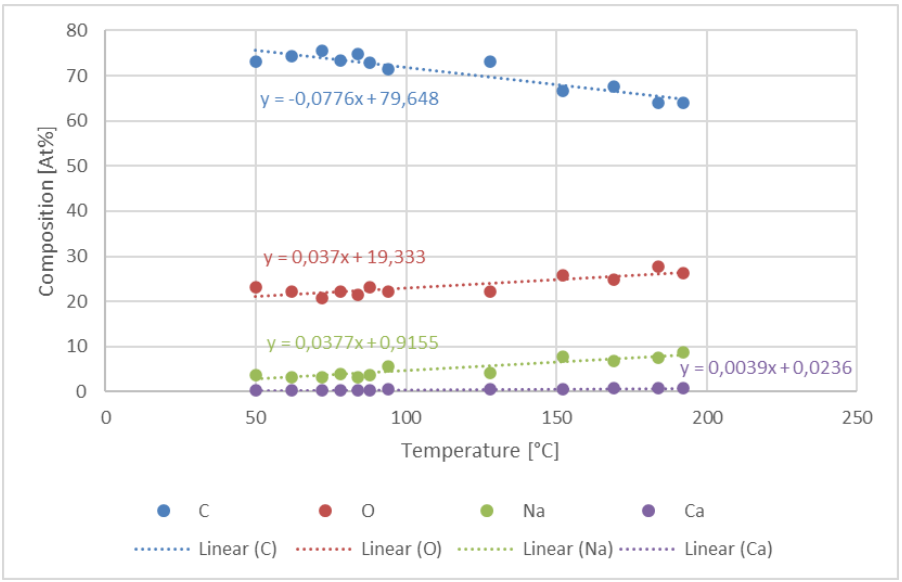

Figure 16: Comparison of composition of deposits formed at different temperatures for the four main elements.

It could be seen that the largest change in composition starts at 80-90°C. The largest deposits were also found in SEM at this temperature, which could indicate that a reaction occurred that both affected the size, and the composition of the deposits. The identification of the mentioned elements correlates with the literature where Scania CV AB previously identified all of these elements [34]. Moreover, Barker et al. [29] have identified hydrocarbons and metal ions. However, Scania CV AB have also identified magnesium and sulphur, and Barker

et al. sulphates and phosphates [29], [34]. The reason for not identifying these compounds could be that the test fuel consisted of fresh fuel and an artificial calcium and sodium concentrate, while the fuel out in the field becomes aged with time and may therefore consist of other contaminants.

The spectra from the FTIR-ATR analysis at a setting temperature of 250°C showed peaks at 1060 cm^{-1}, 1199 cm^{-1}, 1417 cm^{-1}, 1565 cm^{-1}, 1738 cm^{-1}, 2856 cm^{-1}, 2925 cm^{-1} and 3000-3500 cm^{-1} (see Figure 17). Moreover, trial 2 and 3 showed a peak at 955 cm^{-1}. However, a comparison with the spectra from the aluminium foil indicated that this peak belongs to the foil.

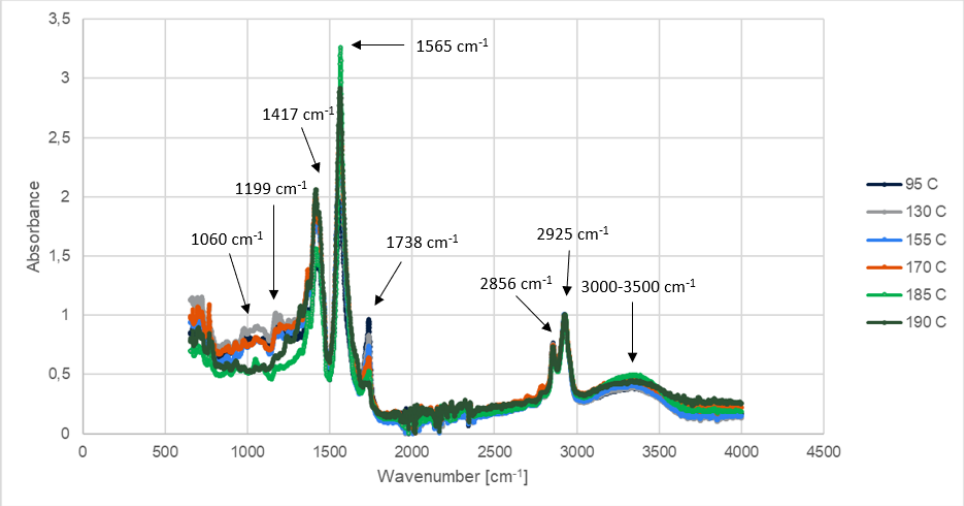

Figure 17: FTIR spectra from trial 1 at a setting temperature of 250°C. The intensity has been normalised to the peak at 2828 cm^{-1}.

The peaks at 1060 cm^{-1} and 1199 cm^{-1} could belong to alcohols, carboxylic acids or esters according to Sigma Aldrich [65], Mohamed et al. [48] and Shameer and Nishath [50]. According to Sigma Aldrich [65], the peak at 1417 cm^{-1} could belong to alcohols or carboxylic acids. The strong peak at 1565 cm^{-1} could be related to metal carboxylates in soap formation [66]. The peak at 1738 cm^{-1} is most likely a C=O stretching of aldehydes, ketones or carboxylates, according to Sigma Aldrich [65] and Berndt et al. [9]. The peaks at 2856 cm^{-1} and 2915 cm^{-1} have previously been identified as C-H bonds in alkanes by Shameer and Nishath [45]. The last broad peak at 3000-3500 cm^{-1} does probable belong to OH stretching of alcohols or water [65]. In the FTIR-ATR analysis of the deposits at a setting temperature 250°C, it could be observed that the peaks at 1060 cm^{-1}, 1199 cm^{-1} and 1738 cm^{-1} seemed to decrease at higher temperatures while the peaks at 1417 cm^{-1} and 1565 cm^{-1} seemed to increase (see Figure 18).

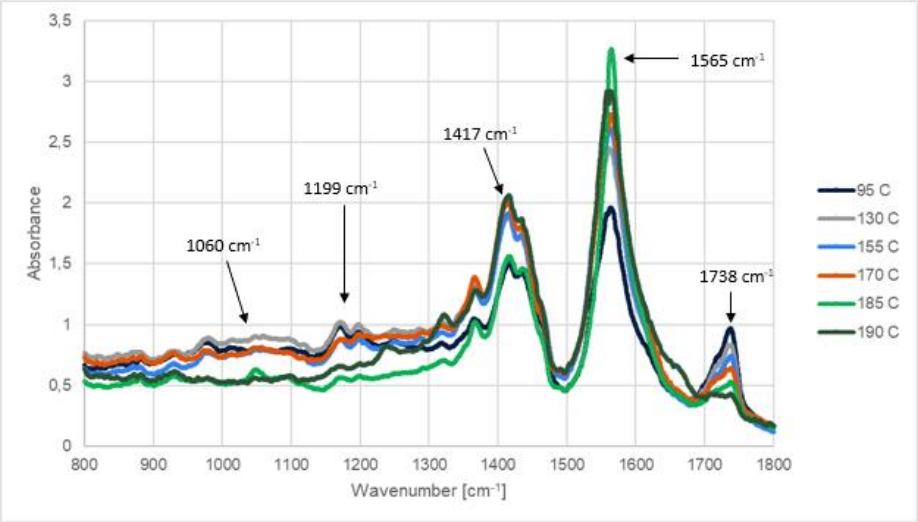

Figure 18: Closer view of the peak increase and decrease in trial 1 at a setting temperature of 250°C. The intensity has been normalised to the peak at 2928 cm^{-1}.

The decrease of three peaks and increase of two peaks indicate that some reaction occurs, which correlates with the SEM-EDX results since both the morphology and composition of the deposits differed along the foil. Moreover, it could indicate evaporation of fuel components, making other compounds more concentrated. The FTIR-ATR spectrum was compared to the spectrum of the test fuel, B7 and B100 (see Figure 19).

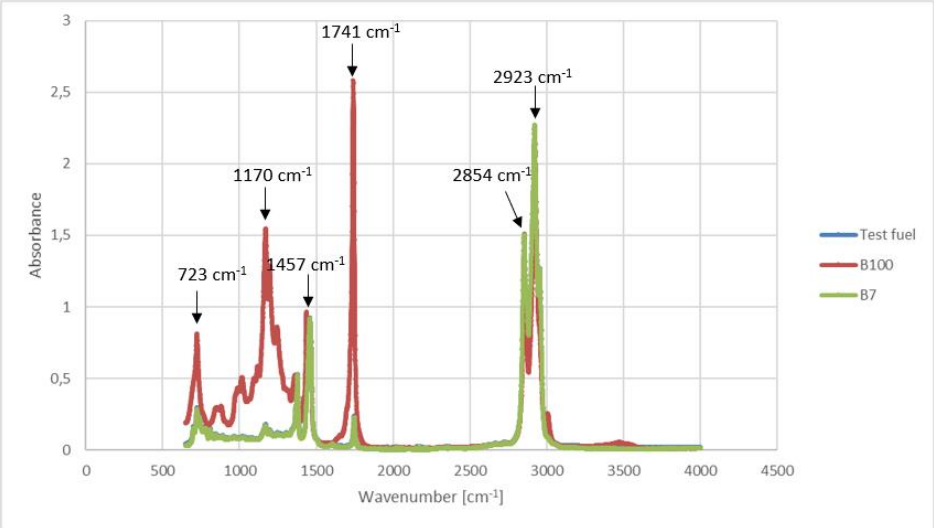

Figure 19: FTIR spectra of the test fuel, B100 and B7. The intensity has been normalised to the peak at 2858 cm^{-1}.

It can be seen that peaks were found at similar wavenumbers in Figure 19 as the decreasing and increasing peaks in Figure 18, except the peak at 1565 cm^{-1}, which was absent in the fuels. The spectra of B7 and the test fuel were identical, which is why the test fuel spectrum is not visible in the figure. However, it is reasonable since a major part of the test fuel is B7 while a minor part is the calcium and sodium concentrate. The decreasing peaks in the spectra from the samples had high intensities in B100, which indicates that it could be related to the FAME content. At higher temperatures, the fuel content may decrease, which in turn decreases the FAME content. Therefore, the difference in peak heights could appear. Moreover, the ester content may decrease due to reactions to form metal carboxylates [8]. According to Shameer and Nishath [45], peaks around wavenumbers

of 1000-1300 cm^{-1} and 1738 cm^{-1} indicate presence of ester or ether groups, which strengthens the claim that these peaks are related to the FAME content. The peak at 1457 cm^{-1} in Figure 19 had the same intensity in all fuel types, which indicates that the peak around 1419 cm^{-1} in the spectra from the samples may not be related to the FAME content. Therefore, it could be other components of the fuel such as hydrocarbons or alcohols. The increasing peak at 1565 cm^{-1} may be absent in the fuels since it, as mentioned, could be related to soap formation, which correlates with the results of the SEM-EDX analysis since the content of calcium, sodium and oxygen increased with temperature.

In the FTIR-ATR analysis of the deposits at the setting temperature 120°C, peaks were found at the same wavenumber as at the setting temperature 250°C. However, there were no clear trends of increasing and decreasing peaks (see Figure 20). This may indicate that a reaction is occurring when the temperature reaches 100°C, which could be related to evaporation of fuel or breakage of ester, ether, or carboxylic bonds. This is in accordance with the results of the SEM-EDX analysis in which the size and amount started to alter after 90°C. Moreover, the largest change of composition in the SEM-EDX analysis were between 90°C and 150°C (see Figure 16). The change in composition at a higher temperature indicates that an activation energy is needed for the reactions to occur [64].

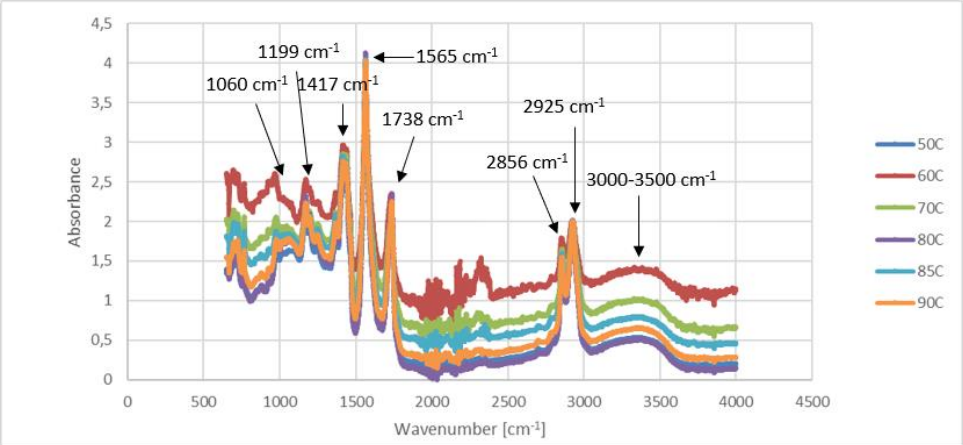

Figure 20: FTIR spectra from trial 1 at a setting temperature of 120°C. The peaks have been normalised to the peak at 2858 cm^{-1}.

Ion milling was performed on trial 1 from the investigations at the setting temperature 250°C. However, no layer structures could be seen. This is not consistent with the literature since several layers have been found in the field [7], [8], [31]. However, the cross-section area was made at a temperature of 110°C where a smaller number of deposits could be found, which may have affected the possibility of layer structures. In the SEM analysis of the cross-section, the height of the deposit could be estimated (see Figure 21). It could be seen that the maximum thickness at a temperature of 110°C was 3 µm. This is a higher thickness than the literature suggests since deposits with a thickness in nanometre size have been found [5], [7], [40]. The reason for the difference in thickness could be that different types of test fuels were used. Moreover, different conditions might have been used in the experiments. Anyhow, a major part of the deposits was generally much smaller at 110°C in this study.

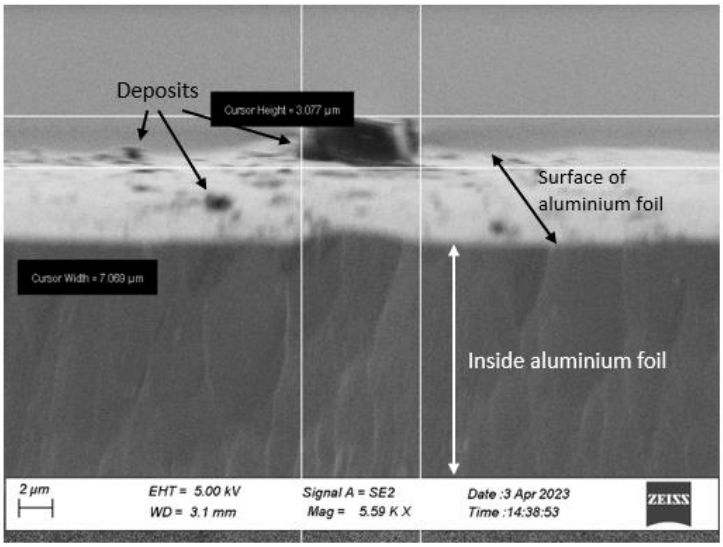

Figure 21: Estimation of the height of the deposit at a temperature of 110°C in the investigations on a setting temperature of 250°C.

The sample from trial 2 in the investigations of temperature at a setting temperature of 120°C was analysed with pyrolysis GC-MS (see Figure 22). However, the analysis could not be performed at a specific location on the aluminium foil due to a low number of deposits. Anyhow, the FTIR spectra showed the same peaks at all temperatures in which only the peak heights differed with temperature (see Figure 17). This suggests that the present peaks in the GC-MS spectrum should not be affected by at which location on the aluminium foil the analysis was performed. In the spectrum, several peaks connected to the degradation of the fuel and soap formation could be seen, which was as expected from the FTIR and SEM-EDX analyses. Different types of acids could be seen, which are components of metal soaps, and are formed when the fuel degrades. Moreover, the observed compounds were methylated due to the use of methylation to protect reactive ends of the molecules.

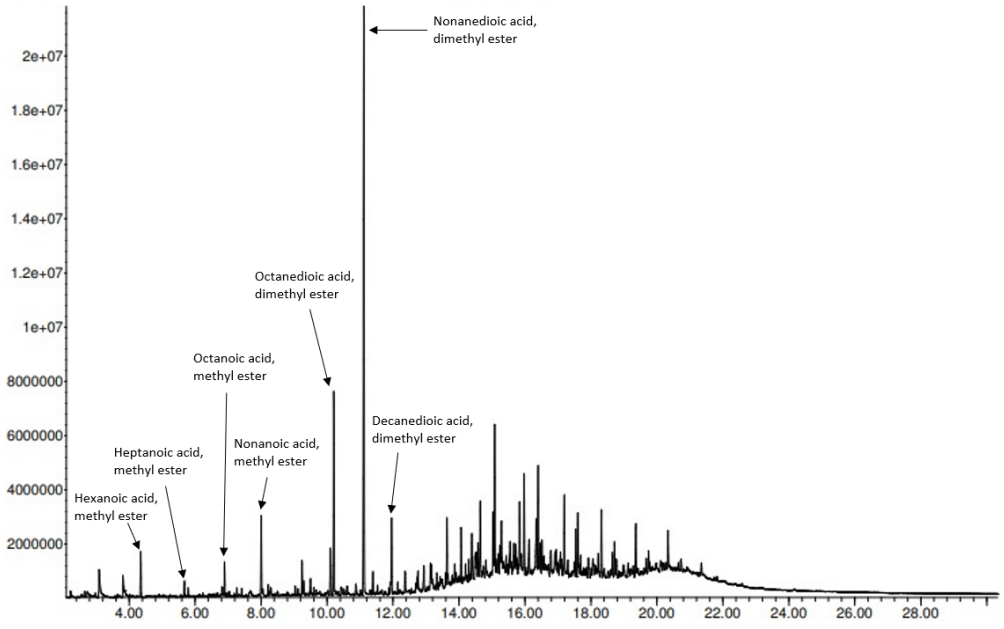

Figure 22: Spectrum from pyrolysis GC-MS at a setting temperature of 120°C. The unit of the time is minutes.

The results from the investigations of the influence of temperature on the deposit formation showed that the formation is temperature dependent in terms of morphology, composition, and reactions. This could be concluded since the size and number of deposits seen in SEM changed with temperature. Moreover, the SEM-EDX analysis showed that the composition of the elements changed when the temperature increased. The largest change of composition was shown to be when the temperature exceeded 90°C. Similarly, the peak heights started to change at this temperature, which indicated that reactions occurred when the temperature reached 100°C.

5.2.2 Investigation of Tilted Apparatus in the TDT

Visually, some deposits could be seen but not to the same extent as in the horizontal rig. This was also confirmed by the SEM analysis since less deposits were seen in general especially at higher temperatures (see Figure 23). However, similar trends as in the horizontal rig could be observed. The size of deposits increased up to a temperature of 80-90°C. Thereafter, the size decreased with temperature while the quantity increased. Moreover, in some locations larger deposits than usual could be found, possibly because of agglomeration. There was also more deposit formation along the sides than in the middle, as in the previous experiments. It is reasonable that the number of deposits was lower in general in the tilted rig since sedimentation was prevented. If sedimentation occurs, it may promote the deposits formation, and lead to a higher number of deposits. However, since the same trends could be seen with both a horizontal and a tilted rig, the trends in size and amount are rather connected to the temperature than the inclination of the rig.

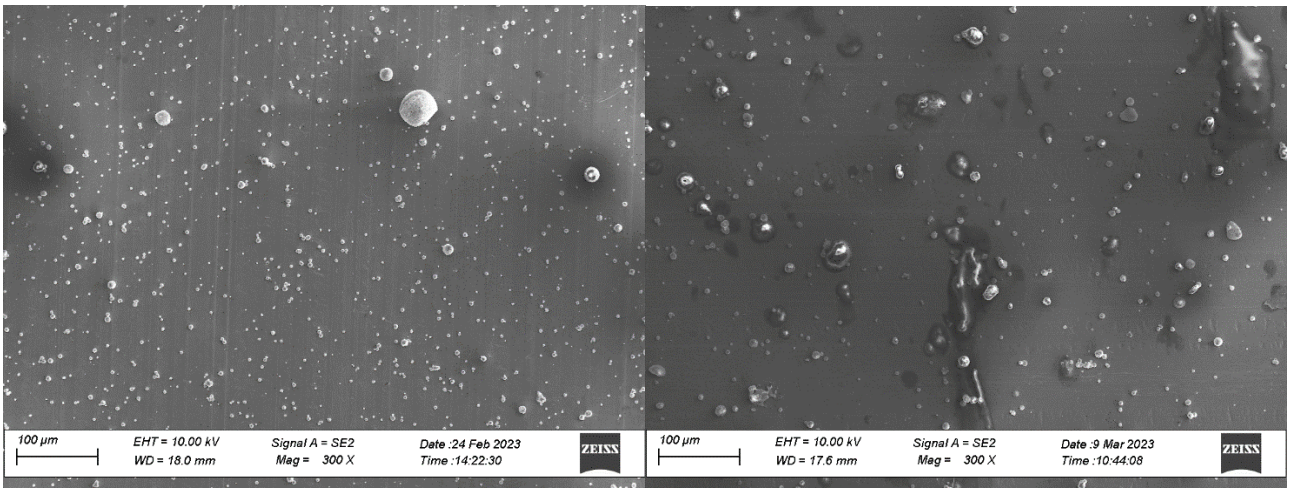

Figure 23: Comparison of the deposits in the horizontal (left) and tilted (right) rig at a temperature of 190°C.

In the SEM-EDX analysis, the same elements were observed as in the horizontal rig, namely carbon, oxygen, calcium, and sodium. The results of the different trials differed slightly, especially in the end of the rig. The deviating results could be related to the preparation of the test fuel, the stirring speed, or that air entered the process. When comparing the average composition from all trials with the results in the horizontal rig, the trend was similar up to 150°C to thereafter deviate and be reverse (see Appendix G: Comparison of Composition between Tilted and Non-tilted). The reason for the deviating results could be that the inorganic soap deposits have difficulties sticking to the surface at the higher temperatures when the rig is tilted, which could explain

that the compositions of sodium, oxygen and calcium decrease at the higher temperatures. Moreover, in the end of the rig, the fuel is sucked out of the rig instead of pushed through. Therefore, the deviating trend could be connected to issues with the extraction of fuel. Additionally, most of the points on the foil had a large content of aluminium, which indicates that the deposits have a lower thickness than in the horizontal rig. The lower thickness could make the results of composition less reliable.

From the SEM-EDX analysis, the composition at different positions on the substrate could be evaluated (see Figure 24). The composition was normalised without inclusion of aluminium to be able to investigate only the deposit, and not the aluminium foil.

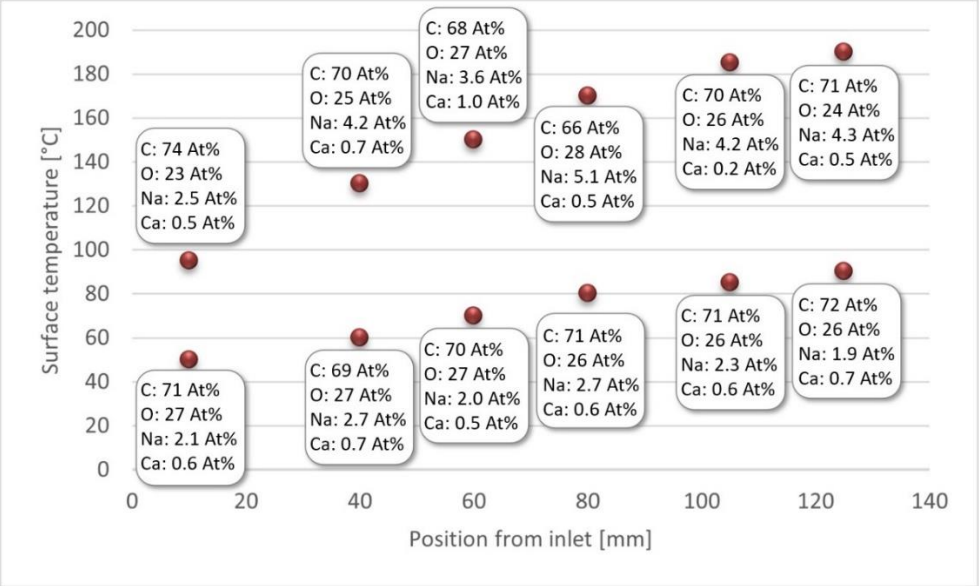

Figure 24: Average composition of the deposits at different positions and temperatures in the tilted rig. The upper points in the figure belong to the setting temperature 250°C and the lower points belong to 120°C.

When comparing the composition in terms of position from the inlet in Figure 24, it was seen that the composition differs between the temperatures at the same position, which indicates that the position does not affect the composition. However, the temperature affects the composition, which can be seen better in Figure 25 and Appendix G: Comparison of Composition between Tilted and Non-tilted. When the total average composition from all trials was determined, the trend was similar to the results from the horizontal rig for all elements except calcium since the composition of calcium increased in the horizontal rig but decreased in the tilted (see Figure 16, Figure 25, and Appendix G: Comparison of Composition between Tilted and Non-tilted).

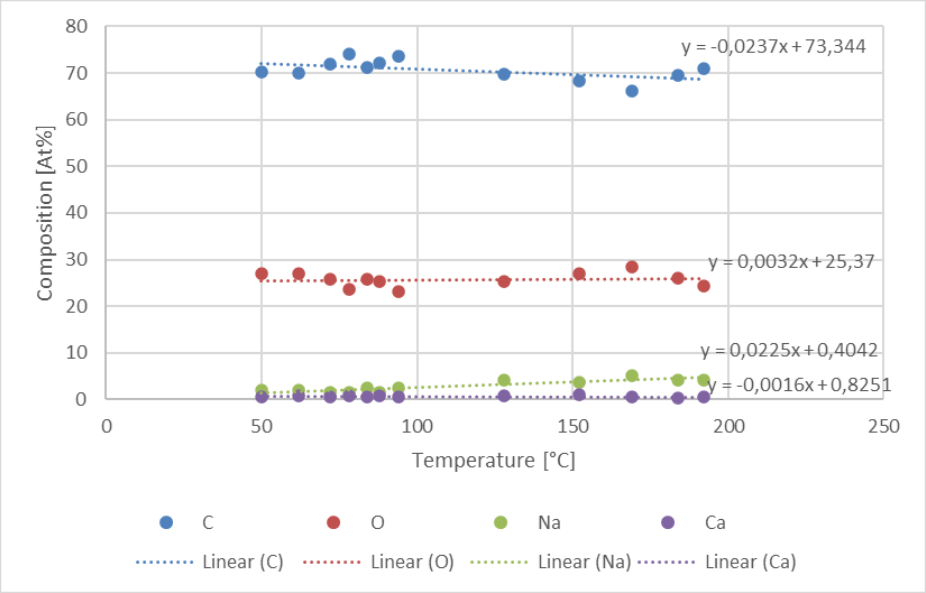

Figure 25: Comparison of composition at different temperatures for the four main elements when the rig was tilted.

The largest change of composition was in the range of 90-150°C, similarly to the results in the horizontal rig. The changes are smaller than the changes in the horizontal rig for all elements except oxygen. The different results could, as mentioned, be related to that the elements have difficulty adhering to the surface when the rig is tilted. Moreover, the reason for the different trend of calcium could be that calcium is added in a low amount into the test fuel, which could make it more sensitive to noise in the measurement especially when fewer deposits are formed.

The FTIR-ATR analysis of the deposits at a setting temperature of 250°C in the tilted rig showed similar trends as the experiments in the horizontal rig, with peaks at the same wavenumbers, and three decreasing and two increasing peaks (see Figure 26). However, the peak at 1565 cm^{-1} was highest at a temperature of 170°C inside the rig but at least higher at the higher temperatures. The similar trends indicate that the same elements and reactions occur regardless of whether the rig is tilted or not, which implies that the reactions are connected to the temperature. It could also have been that some elements were present in lower amounts or that new elements appeared due to different possibilities to adhere to the surface in a tilted rig. However, since the same peaks and trends were seen it could be concluded that sedimentation does not affect the present compounds, only the total number of deposits.

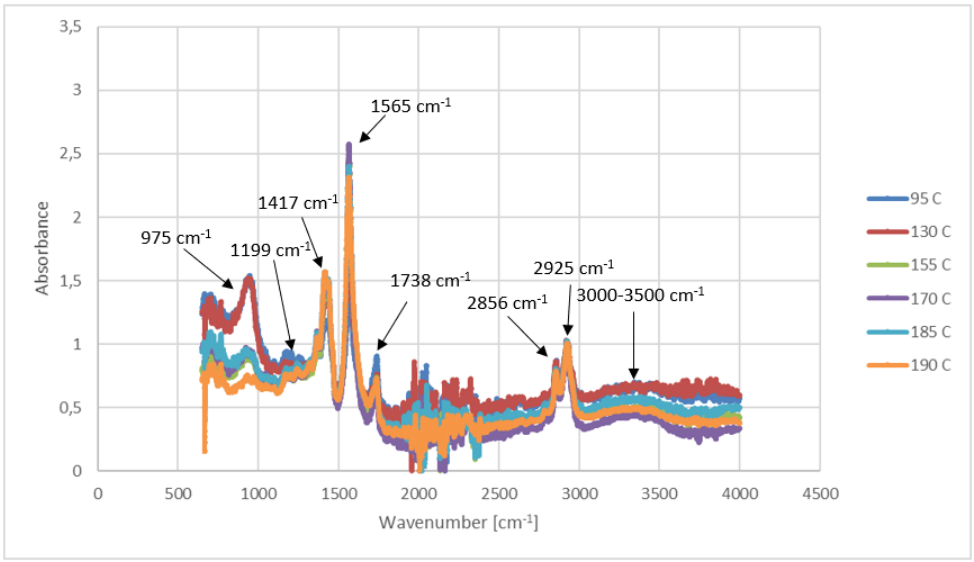

Figure 26: FTIR spectra from trial 1 in the tilted rig at a setting temperature of 250°C. The peaks have been normalised to the peak at 2858 cm^{-1}.

At a setting temperature of 120°C, no clear trends could be seen (see Figure 27), which is consistent with the results in the horizontal rig. As mentioned before, this indicates that the trend of reactions was the same regardless of if the rig was tilted or not since the change in peak heights occurred when the temperature reached 100°C. At both temperatures, a clear peak could be discerned at 975 cm^{-1}. This peak was also found in some trials in the horizontal rig and is connected to the aluminium foil. The identification of the aluminium foil indicates that less deposits were formed, which was consistent with the SEM analysis.

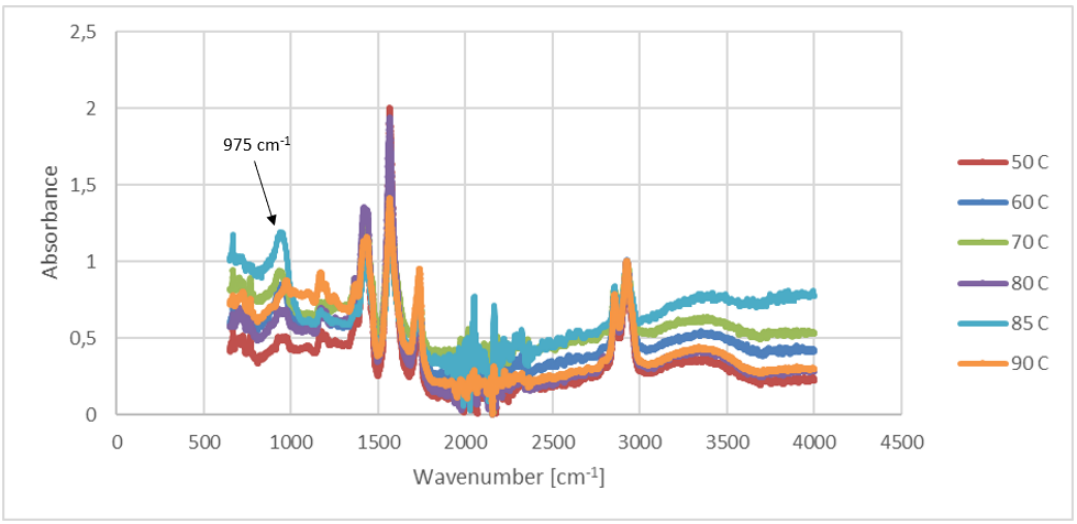

Figure 27: FTIR spectra from trial 3 in the tilted rig at a setting temperature of 120°C. The peaks have been normalised to the peak at 2858 cm^{-1}.

The results of the investigations with a tilted rig showed that sedimentation does not affect the trends of the deposit formation regarding size, composition, and reactions. However, the number of deposits were reduced, and deviations were seen in the end of the rig possibly connected to difficulties for soap deposits to adhere to the surface.

5.2.3 Investigation of Engine Oil in the TDT

To answer the research question of how engine oil affects the deposit formation, experiments were conducted with addition of fresh and used engine oil to the test fuel. It made it possible to see if any crystals could be formed, and if there were any changes in morphology and reactions when either fresh or used engine oil was added. Experiments were made both with and without addition of calcium and sodium concentrate to see if it had an influence on the formed deposits.

5.2.3.1 Investigation of Fresh Engine Oil with Sulphuric Acid and Addition of Concentrate

Visually, the number of deposits varied between the different trials and positions on the aluminium foil with more deposits at some locations but without a clear trend of the number of deposits. Moreover, the results from the SEM analysis differed between the trials. At the setting temperature 120°C, experiments were only performed with preheated oil. However, at the setting temperature 250°C, two experiments were also performed with unheated oil. The number of deposits was not consistent between the trials of the preheated oil. For example, many deposits were only observed at 50°C in one of the trials, and small at 85°C in one other trial. However, all trials of the preheated oil showed relatively many deposits at 190°C, which was in line with the results without oil addition. No clear trend could be seen regarding size, since the trials showed large deposits at different temperatures. However, it seemed like larger deposits could be seen at higher temperatures (see Figure 28).

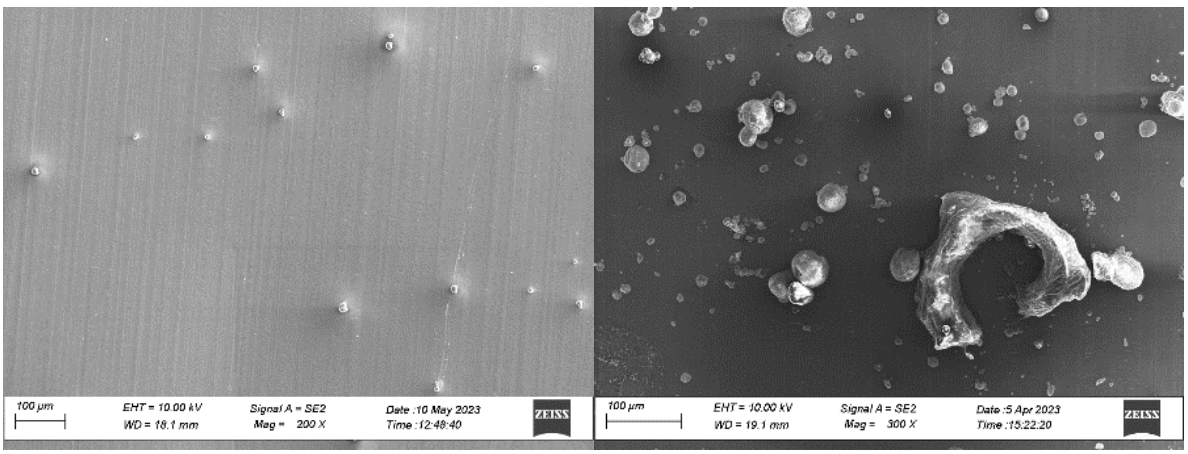

Figure 28: Comparison of size in the investigation of preheated fresh oil addition with sulphuric acid at a setting temperature of 250°C. The left image is at the temperature 50°C and the right at the temperature 190°C.

The trials with unheated oil showed more deposits in general compared to the preheated oil (see Figure 29). This could be due to that the neutralisation of the oil at room temperature might have led to larger crystals, which may ease the sticking of soft particles and lead to more deposits. Smaller crystals may be formed at a higher temperature since the higher temperature could lead to destruction of the crystals. Trends could not be seen either in size or amount with the unheated oil.

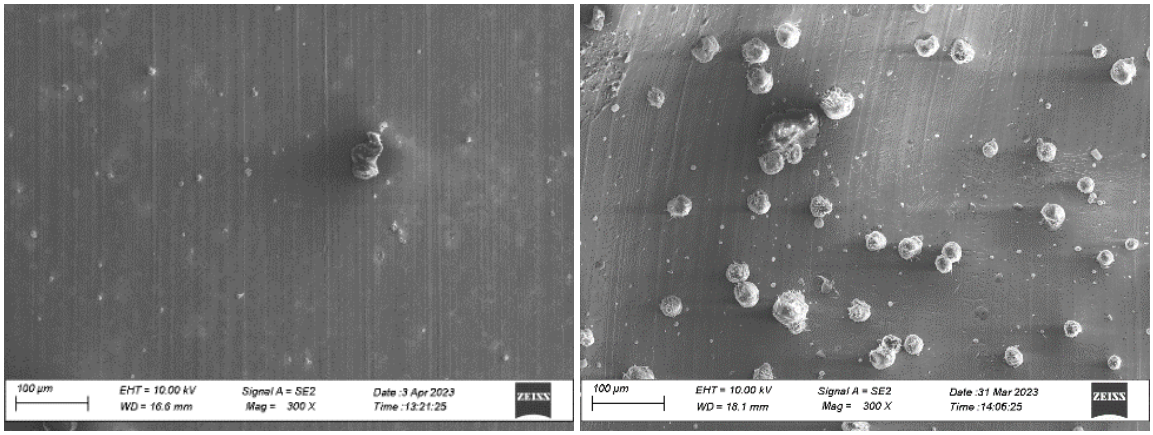

Figure 29: Comparison of the deposits between the preheated and unheated fresh engine oil at a temperature of 150°C. The left image is the unheated oil, and the right is the preheated oil.

When the results were compared with the investigation without oil addition, it could be seen that the trends of size and number of deposits differed, which is reasonable since crystals were formed when the oil was added. However, in general, the number of deposits was larger at higher temperatures both with and without oil addition. Regarding size of the deposits, no trial in the investigations of oil addition followed the same trend as without oil addition, which could be due to the formation of crystals. The crystals may promote the deposit formation, which could lead to more and larger deposits.

The results of the SEM-EDX analysis differed between the trials (see Appendix H: Comparison of Composition in the Trials on Fresh Oil Addition). However, the same elements could be identified in all trials, namely carbon, oxygen, sodium, calcium, and sulphur. Moreover, zinc was found at some locations, especially at the setting temperature 120°C. The identification of these elements are in line with the literature since the elements have been identified by Edney et al. [31], Scania CV AB [34], and Barker et al. [29]. At the setting temperature 250°C in the investigation with addition of fresh engine oil, the trends of composition were similar in trial 1, 2, and 3 (see Appendix H: Comparison of Composition in the Trials on Fresh Oil Addition). In general, the carbon content seemed to be higher at 90°C to then decrease and be quite constant. Moreover, calcium, oxygen and sulphur increased while sodium had a peak around 150°C. Thereby, calcium, oxygen and sulphur followed the same increasing trend, which suggests that the amount of $CaSO_4$ crystals increased. This is reasonable since most $CaSO_4$ crystals have been found at the warmest part of the injector out in the field [7].

In the SEM-analysis, a large size could be seen at 150°C, at which temperature the sodium content also was high (see Appendix H: Comparison of Composition in the Trials on Fresh Oil Addition). This could be related to that more soap deposits were formed since they consist of carboxylates and metals, such as sodium or calcium. Moreover, the size was large at the higher temperatures, which could be due to a higher amount of $CaSO_4$ crystals. At the setting temperature 120°C, the results from the SEM-EDX analysis were more similar between the trials except from calcium (see Appendix H: Comparison of Composition in the Trials on Fresh Oil Addition). Carbon and oxygen showed reverse trends in which oxygen was higher when carbon was lower. This is reasonable since carbon indicates more organic deposits while oxygen represents more inorganic. Sulphur

and zinc were generally low but higher at some locations. The trends of zinc and sulphur were similar at the lower temperatures, indicating that zinc sulphate ($ZnSO_4$) might have been formed. Sodium and calcium were generally higher at the higher temperatures.

Since trial 4 at the setting temperature 250°C showed deviating results, it was excluded from the calculation of the average compositions. When comparing the average composition of the different elements at different temperatures, trends could be seen more clearly (see Figure 30 and Appendix I: Comparison of Composition with and without Oil Addition). Oxygen and carbon were generally constant but varied more at lower temperatures, sodium had a peak concentration at 150°C, and sulphur and zinc varied at the temperatures below 90°C. Thereafter, sulphur increased while zinc was almost absent. Calcium was increasing in the entire temperature interval but more when the temperature exceeded 100°C. These results indicate that at the lower temperatures there might be more $ZnSO_4$ but at the higher temperatures, $CaSO_4$ is more prominent. This is consistent with the field since more $CaSO_4$ has been found at the injector tip where the temperature is higher [62]. However, $ZnSO_4$ has not been seen before, and could be a result of contaminations.

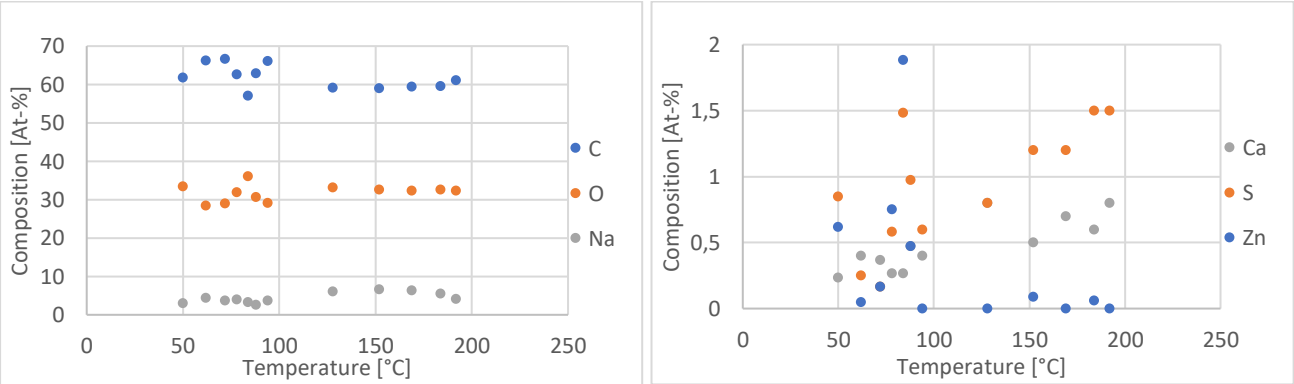

Figure 30: Comparison of composition at different temperatures for the main elements in the experiments regarding fresh oil addition. The second trial was disregarded due to deviating results.

The composition of the major elements in the investigations regarding fresh oil addition was compared to the composition in the investigations with no oil addition (see Appendix I: Comparison of Composition with and without Oil Addition). It could be seen that carbon and oxygen was quite constant at lower temperatures in both experiments. However, when the temperature increased, carbon decreased continuously without oil addition but decreased slightly up to 130°C to then be quite constant with fresh oil addition. Similar but reverse trends could be seen for oxygen. Moreover, the composition of oxygen was generally higher in the fresh oil experiments while the composition of carbon was generally lower. This indicates that more inorganic deposits are formed when oil is added to the test fuel, which is reasonable since more inorganic substances are present.

Calcium showed similar trends with and without oil addition where it increased, especially at higher temperatures (see Appendix I: Comparison of Composition with and without Oil Addition). However, sodium followed the same trend up to 150°C both with and without oil addition after which it continued to increase without oil addition but decreased when fresh oil was added. The reason for the different trend of sodium could be that less soaps were formed at the higher temperatures when the fresh oil was added due to the formation of

$CaSO_4$ crystals. The formation of crystals could lead to a competition between soap formation and crystal formation since they could compete for the space on the aluminium foil. Therefore, less soaps may be formed. Another reason for the decrease in sodium at the end could be that the oil may have acted as a detergent and washed away the sodium soaps [62].

In the FTIR-ATR analysis at both setting temperatures, same peaks as in previous experiments were seen in all trials except in trial 3 at a setting temperature of 250°C in which the soap peak was almost absent. Moreover, another peak was found at 1154 cm^{-1} in all trials, while the peak at 1199 cm^{-1} was missing (see Figure 31).

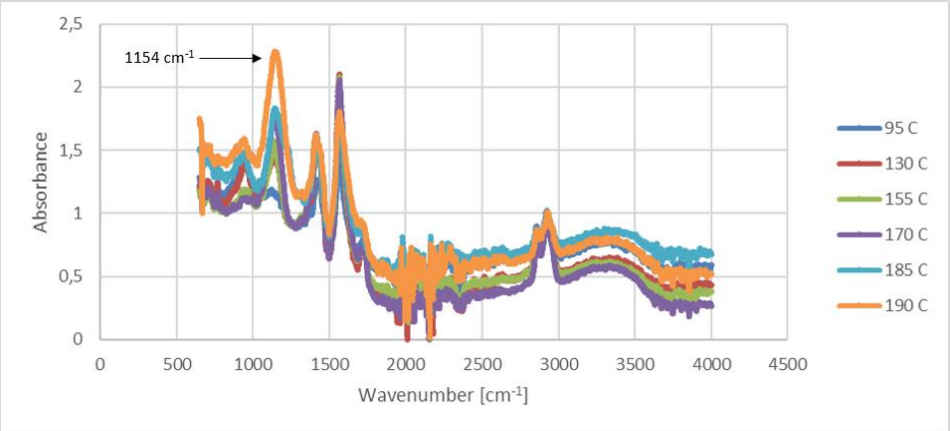

Figure 31: FTIR spectra from trial 1 in the experiments with fresh oil addition at room temperature at a setting temperature of 250°C. The peaks have been normalised to the peak at 2858 cm^{-1}.

According to Sigma Aldrich [65], a peak at 1154 cm^{-1} could belong to C-N bonds in amines, C-O bonds in alcohols or S=O bonds. Since sulphuric acid was added in these experiments, it could be related to $CaSO_4$ crystals. The spectrum was compared with the spectra of $CaSO_4$ anhydrous and $CaSO_4$ dihydrate where a peak at 1095 cm^{-1} was found in both spectra (see Figure 32). Therefore, it is reasonable that a peak at 1154 cm^{-1} is related to $CaSO_4$. However, at some temperatures the peak was shifted to about 1166 cm^{-1}, which could indicate that some other sulphate compound was formed, such as $ZnSO_4$. This would also be consistent with the SEM-EDX analysis since zinc was identified at some locations. Anyhow, no analysis was performed to confirm this.

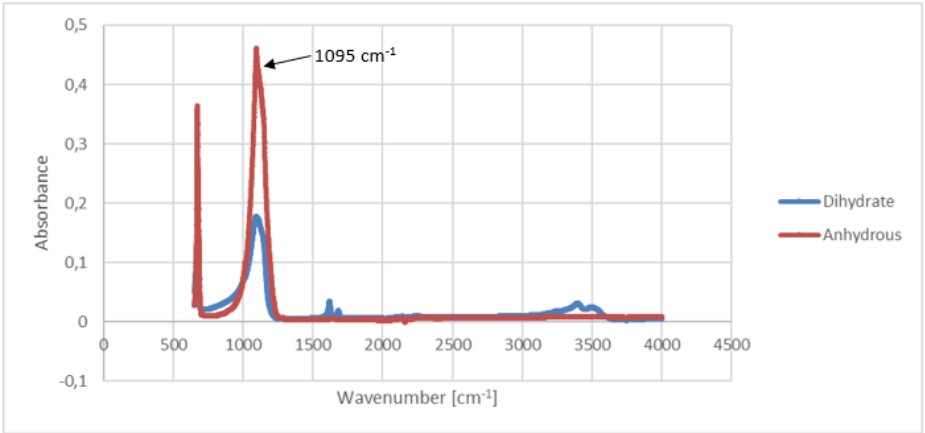

Figure 32: FTIR spectra of the $CaSO_4$ dihydrate and $CaSO_4$ anhydrous.

Trends of peak increase and decrease were not consistent among the trials. In trial 1 at the setting temperature 250°C, the peak at 1154 cm^{-1} increased with temperature (see Figure 31). However, it seemed to decrease in trial 3 (see Figure 33). Moreover, no clear trend could be seen in trial 2 and 4. Anyhow, the peak was often high at 190°C, which might indicate that more $CaSO_4$ crystals are formed at higher temperatures, which would be consistent with the results of SEM-EDX and the literature [62]. The soap peak at 1565 cm^{-1} seemed to be highest around 130-170°C, which is consistent with SEM-EDX since sodium had a peak around this temperature. The results of more $CaSO_4$ and less soap at higher temperatures are consistent with the phenomenon seen in the field. Soap deposits has been observed in the upper part of the injector where the temperature is lower while $CaSO_4$ mainly has been found in the tip where the temperature is higher [62].

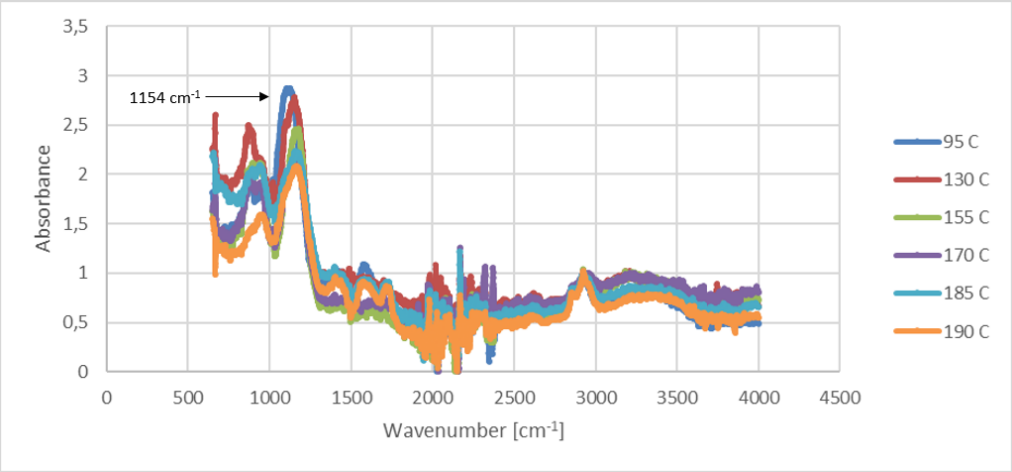

Figure 33: FTIR spectra from trial 3 in the experiments with fresh oil addition at 80°C at a setting temperature of 250°C. The peaks have been normalised to the peak at 2858 cm^{-1}.

At the setting temperature 120°C, the peak at 1154 cm^{-1} increased with the temperature in trial 1 and 2. However, in trial 3, it was only present at 85°C. The soap peak showed different trends in the different trials. However, in general, it seemed like the soap peak was lower when the sulphate peak was higher, which is reasonable since there might be competition between formation of crystals and formation of soaps.

The results from the investigations with fresh engine oil addition with sulphuric acid, and calcium and sodium concentrate showed that the engine oil addition affected the deposit formation. Crystals could be seen, which was consistent with the literature. Moreover, the trends of the soap formation differed possibly due to the formation of crystals.

5.2.3.2 Investigation of Fresh Engine Oil with Sulphuric Acid without Addition of Concentrate

When experiments were conducted on fresh engine oil addition without addition of calcium and sodium concentrate, a significantly smaller number of deposits were formed. This is reasonable since no additional sodium and calcium were added, which are constituents of soap deposits. It indicates that addition of both calcium and sodium concentrate, and engine oil facilitates the deposit formation possibly because the soft particles formed from the concentrate makes it easier for the $CaSO_4$ to stick. Thereafter, more deposits could

attach to the surface due to impurities. However, in the real injectors, the $CaSO_4$ has been found in the bottom layer, and not inside of the soft particles. The reason for this could be that the surface in the injector is rougher, which eases the formation of crystals since the nucleation commonly initiates on surface irregularities [7].

The size of the deposits differed between the trials, but all trials seemed to have a larger size at 90°C and smaller at 190°C (see Figure 34), which is consistent with the results of the investigations without oil addition. The deposits were smaller and less crystals could be seen when the calcium and sodium concentrate was absent compared to the investigation of fresh oil addition with concentrate. The number of deposits was also different in the different trials but generally the amount was largest at 90°C and 190°C. This is in line with the results from the investigations with addition of calcium and sodium concentrate. Crystals were only seen on a few locations, especially at the higher temperatures in trial 1.

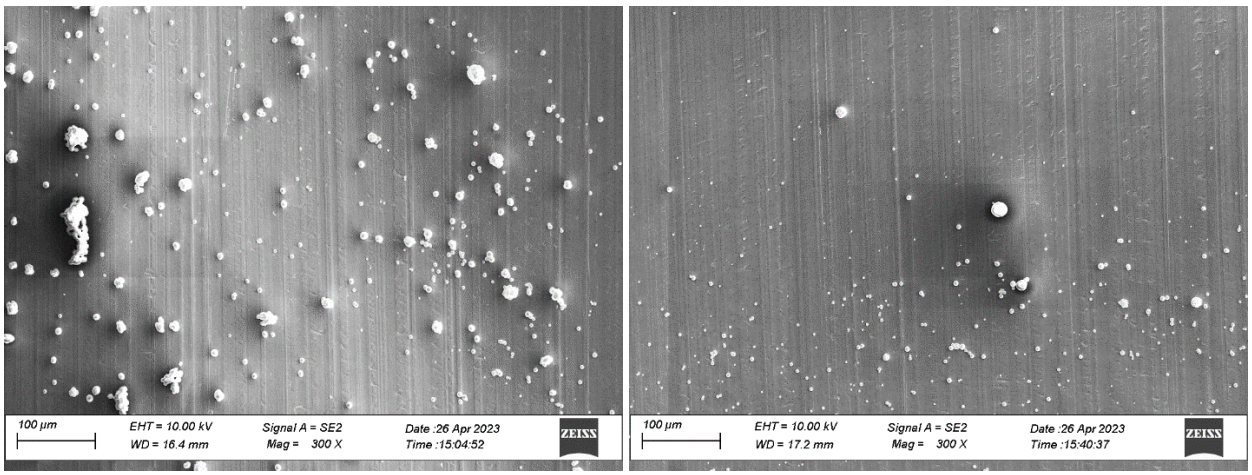

Figure 34: Comparison of size between 90°C and 190°C in trial 3 in the investigations regarding addition of fresh engine oil with sulphuric acid but without addition of concentrate.

In the SEM-EDX analysis, more elements were identified in comparison with the investigations on the fresh engine oil with addition of calcium and sodium concentrate, and the investigations without addition of fresh engine oil. The presence of more elements could be due to that the contents of sodium and calcium were lower, which could make other elements visible since the composition shows the atomic percentage of different elements. The identified elements were sodium, sulphur, calcium, zinc, oxygen, carbon, fluorine, iron, and silicon. The identification of these elements are in line with the literature since all have been found except from iron, and fluorine [29], [31], [34]. The identification of iron and fluorine could be due to contaminations. Fluorine could for example originate from the FKM gasket since the gasket contains fluorine. Moreover, aluminium was present in high amounts, which could make the identification of the other elements less reliable. The results differed between the trials (see Appendix J: Comparison of Composition with Fresh Engine Oil without Concentrate). However, trial 2 and 3 showed more similar results than trial 1, which could be due to that the aluminium foil in trial 1 was damaged. The content of silicon, fluorine, and iron varied significantly, which could be due to inaccurate measurement because of the high aluminium content or that it is impurities at

some locations. The average compositions of the elements in all trials were compared despite the differing results (see Figure 35).

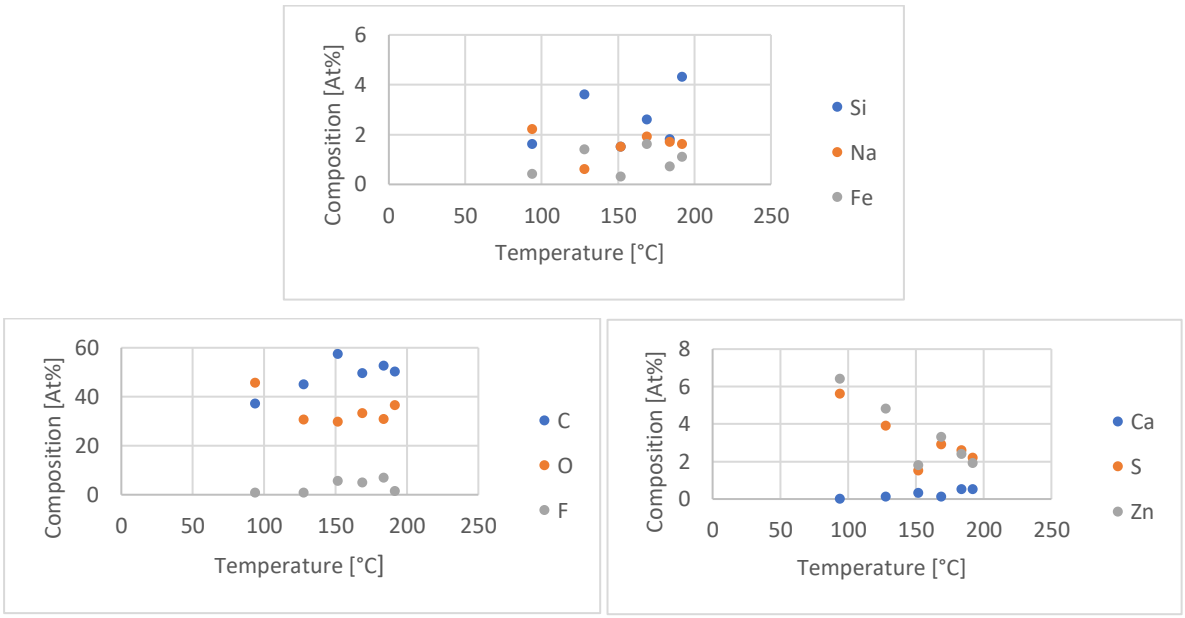

Figure 35: Comparison of composition at different temperatures for the main elements in the experiments regarding fresh oil addition without concentrate.

Zinc and sulphur were present in similar amounts and followed similar changes in composition. Therefore, it was concluded that $ZnSO_4$ was formed instead of $CaSO_4$, possibly due to the low available amount of calcium since no additional calcium was added. The only source of calcium could therefore be from the fuel or oil, which could lead to a higher amount of zinc than calcium. The higher amount of zinc could favour the formation of $ZnSO_4$ over $CaSO_4$. The elemental compositions were compared with the compositions in the investigations of fresh engine oil addition with addition of calcium and sodium concentrate (see Appendix K: Comparison of Composition with Fresh Engine Oil with and without Concentrate). Oxygen and calcium followed similar trends in both investigations. Moreover, the calcium and sodium contents were generally higher when the calcium and sodium concentrate was added, which is reasonable since the concentrate contains these two elements.

Silicon, fluorine, and iron were not present when the calcium and sodium concentrate was added (see Appendix K: Comparison of Composition with Fresh Engine Oil with and without Concentrate). The reason for the absence of these three elements when concentrate was added could be that the other elements were present in larger concentrations, which could mean that the atomic percentage of silicon, fluorine and iron may be too low to be visible. The contents of sulphur and zinc were higher in the investigations without calcium and sodium concentrate but seemed to decrease with temperature. This could indicate that $ZnSO_4$ was formed before the rig and then precipitated immediately when entering the aluminium foil. Zinc may originate from other parts of the system to then react with sulphate from the oil. However, since the composition was highest in the beginning of the foil and then decreased, it is more reasonable that $ZnSO_4$ was formed already in the oil.

The FTIR spectra differed significantly between the trials, which is consistent with the SEM-EDX results since they also differed. However, trial 1 and 3 seemed to have a slightly higher peak at 1170 cm^{-1} at higher temperatures (see Figure 36).

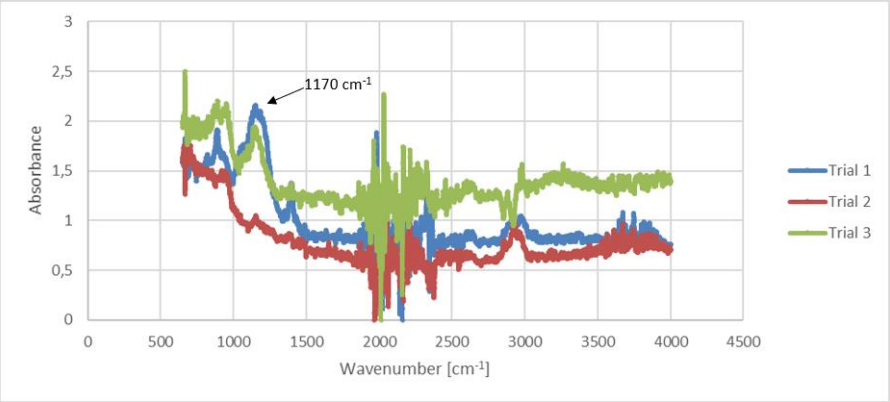

Figure 36: FTIR spectra at the temperature 190°C for the three trials at the setting temperature 250°C on fresh engine oil with sulphuric acid without addition of concentrate.

It could be seen that the peak at 1170 cm^{-1} was slightly shifted to the right compared to the experiments with addition of calcium and sodium concentrate (see Appendix L: Comparison of FTIR spectra with Addition of Fresh Engine Oil with and without Addition of Concentrate). This could be due to that $ZnSO_4$ was formed instead of $CaSO_4$, which would be consistent with the results of the SEM-EDX analysis. In general, the soap peak was not seen at any temperature. There was no trend in peak increase or decrease between the three trials. However, a sulphate peak seemed to be visible at 130°C, 185°C and 190°C. Therefore, it might be claimed that more $ZnSO_4$ is formed at higher temperatures. However, this is not consistent with the results from SEM-EDX since the zinc and sulphur contents decreased with the temperature. The calcium content did though increase with temperature, which might indicate that the peak is a mix of $CaSO_4$ and $ZnSO_4$. Moreover, trial 1 showed a large peak at 1150 cm^{-1} at 95°C. In the SEM-EDX analysis of trial 1 at this temperature, the content of zinc was very high, which indicates that it may be connected to $ZnSO_4$. This might imply that the peaks between 1150 cm^{-1} and 1170 cm^{-1} could belong either to $CaSO_4$ or $ZnSO_4$.

The results of the investigation of addition of fresh engine oil with sulphuric acid but without calcium and sodium concentrate showed different results compared to when the concentrate was added. Less deposits were formed, and the soap peak was generally absent. Moreover, $ZnSO_4$ was formed to a larger extent than $CaSO_4$. The results showed that the addition of both engine oil, and calcium and sodium concentrate promote the deposit formation.

5.2.3.3 Investigation of Used Engine Oil with Addition of Concentrate

Investigations were also made with addition used engine oil since the constituents differs from the fresh engine oil (see Table 7). When used engine oil, and calcium and sodium concentrate were added to the test fuel, more deposits were visible compared to both the investigations without oil addition and the investigations with fresh engine oil. The reason could be that the used engine oil contains more components than the fresh. Therefore,

the deposits could consist of, for example, different types of additives, which could contribute to the formation of more or larger deposits [62]. The number of deposits seemed to be small at the lower temperatures and then increase up to 90°C. At the higher temperatures the amount was generally relatively large, but highest at 190°C. The size of the deposits seemed to increase with temperature in general (see Figure 37).

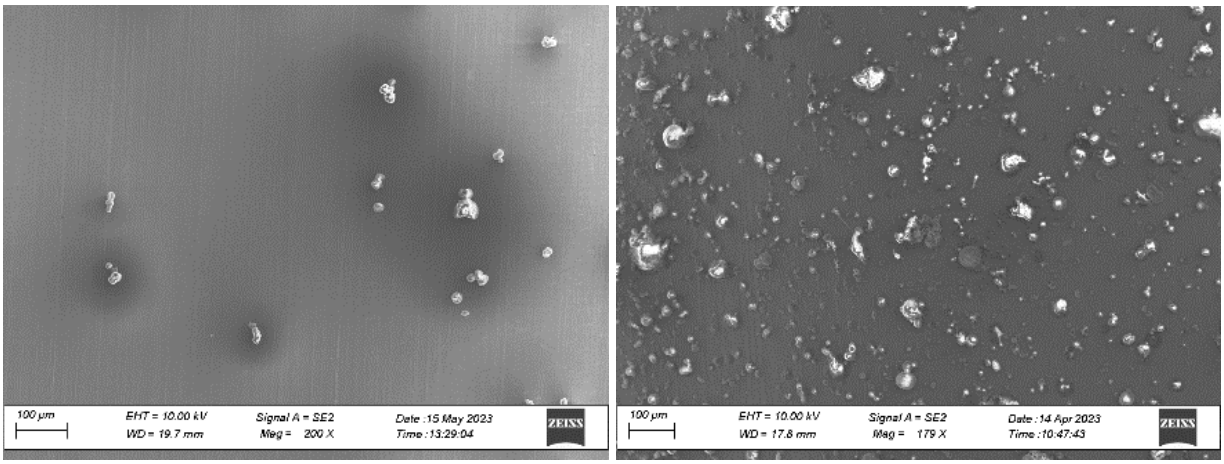

Figure 37: Comparison of size between 60°C (left) and 190°C (right) in the investigation of used engine oil.

As with the experiments on fresh engine oil with sulphuric acid, crystals were seen on some locations, which indicates that the oil addition facilitates formation of crystals. This is consistent with literature since Lamb et al. [8] argued that engine oil contributes to deposit formation and that both calcium and sulphate can originate from the oil. Fewer crystals were observed in the investigations of the used engine oil compared to the investigations of the fresh engine oil (see Figure 38). The reason for this could be that less sulphate was available for the reaction of sulphate crystals. In the fresh engine oil, sulphuric acid was added in a determined amount. However, in the used engine oil, present bases have reacted to form both sulphuric acid and carboxylic acids. Therefore, less sulphuric acid could be available for the formation of crystals [62].

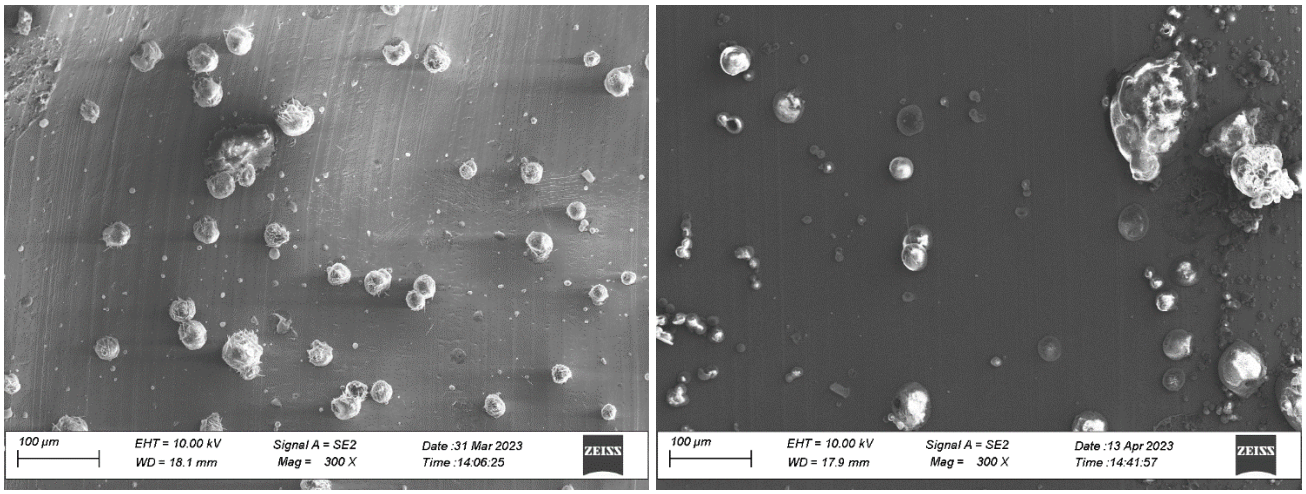

Figure 38: Comparison of formation of crystals between fresh oil with sulphuric acid (left) and used oil (right).

The identifications of crystals were not consistent between the trials. However, some similarities were identified including that crystals were commonly seen at 95°C and 190°C. Moreover, no crystals could be seen at the

temperatures below 90°C or between 150-170°C. The formation of more crystals at higher temperatures is in line with the field since more $CaSO_4$ has been found at the injector tip at which the temperature is higher [62]. The reason for absence of crystals between 150-170°C could be that more soaps might have been formed in this range, which could compete with the formation of crystals.

The main elements found in the SEM-EDX analysis were carbon, oxygen, calcium, sodium, zinc, and sulphur. Moreover, magnesium and phosphorus were found on some locations. Zinc could be a component of the ZDDP additive used in lubricating oils. However, it could also be an impurity from tanks, zinc coatings or lab equipment. The investigations at a setting temperature of 120°C showed consistent compositions for sodium, calcium, and carbon (see Appendix M: Comparison of Composition in the Trials on Used Oil Addition). For sulphur, zinc, and oxygen the trials yielded inconsistent results. At the setting temperature of 250°C, the composition of the elements deviated between the trials at the temperatures below 150°C (see Appendix M: Comparison of Composition in the Trials on Used Oil Addition). However, above 150°C, similar trends were seen for carbon, sulphur, oxygen, and calcium in all trials. Zinc was only found in a few locations, which could explain the deviating results. Calcium, sulphur, and oxygen followed similar trends, similarly to the experiments on the fresh engine oil with sulphuric acid. Thereby, it is indicated that $CaSO_4$ crystals might have been formed, which is consistent with the results from SEM.

The average composition of the different elements at different temperatures can be seen in Figure 39. The compositions of sodium, calcium, and sulphur increased while the composition of oxygen was constant, and the composition of carbon and zinc decreased if the last point for zinc was disregarded. The decreasing trend of carbon is consistent with the literature since more organic deposits have been observed at lower temperatures and more inorganic at higher [62]. Moreover, in the SEM analysis, more crystals could generally be seen at the higher temperatures, which could explain the increase of calcium, sulphur, and oxygen.

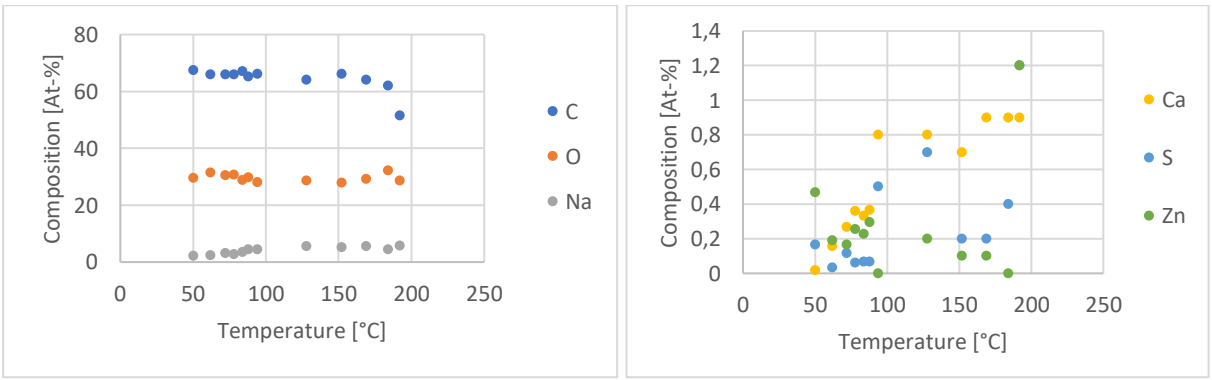

Figure 39: Comparison of composition at different temperatures for the main elements in the experiments regarding used oil addition.

The compositions of the major elements in the investigations of used oil addition were compared to the fresh oil addition and no oil addition (see Appendix I: Comparison of Composition with and without Oil Addition). The change in composition differed between the addition of fresh and used oil. This can be seen as all elements except oxygen had a greater change of composition in the investigations of used engine oil. No crystals were

seen at the low temperatures, which may lead to the large increase in the composition of calcium and sulphur. Carbon, calcium, and zinc followed similar trends in all investigations. Moreover, the sodium composition with used oil addition followed a similar trend as with no oil addition. However, the increase in composition at higher temperatures was not as high as without oil addition. As mentioned earlier, this could be due to the formation of crystals, which could compete with the formation of soap deposits. Moreover, the oil may have acted as a detergent and washed away some of the soap deposits. It was also observed that the sodium composition decreased more at higher temperatures in the investigation of fresh oil with sulphuric acid compared to the investigation of used oil. However, the sulphur composition also increased more. This could indicate that more crystals were formed with the fresh engine oil, resulting in less soap deposits, which also would be consistent with the SEM results since more crystals were seen in the investigations of fresh engine oil.

The FTIR spectra were similar for all trials at both setting temperatures except from trial 1 at the setting temperature 120°C in which the soap peak was absent below 80°C. Moreover, the sulphate peak was not seen at the setting temperature 120°C (see Figure 40). This is consistent with the SEM results since no crystals were observed.

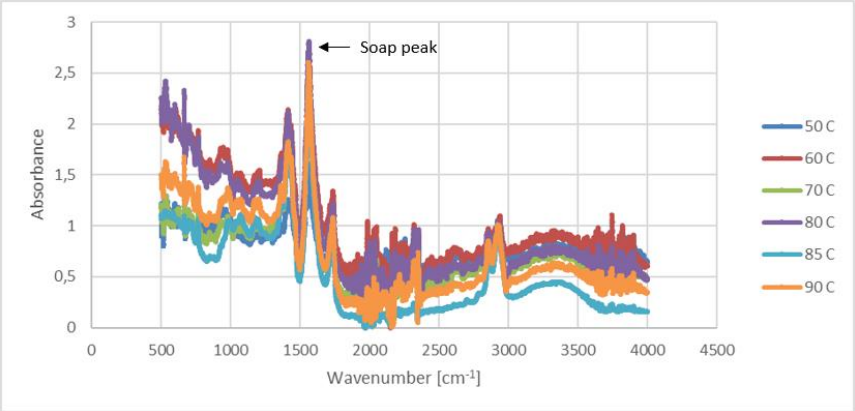

Figure 40: FTIR spectra at a setting temperature of 120°C in the experiments with used engine oil. The intensity has been normalised to the peak at 2828 cm^{-1}.

At the setting temperature 250°C, the sulphate peak was found at higher temperatures but also at 95°C in trial 1 (see Figure 41). The reason for a large amount of crystals at 95°C is not as expected since crystals are usually found in the warmest part of the injector [62]. However, one explanation could be that the crystals were formed already in the test fuel and then precipitated immediately when encountering the foil. Over time, more crystals may have been formed at the end of the foil as well. Generally, the same peaks as in the investigation of the fresh engine oil were seen, which is reasonable since the main elements were the same in the EDX analysis.

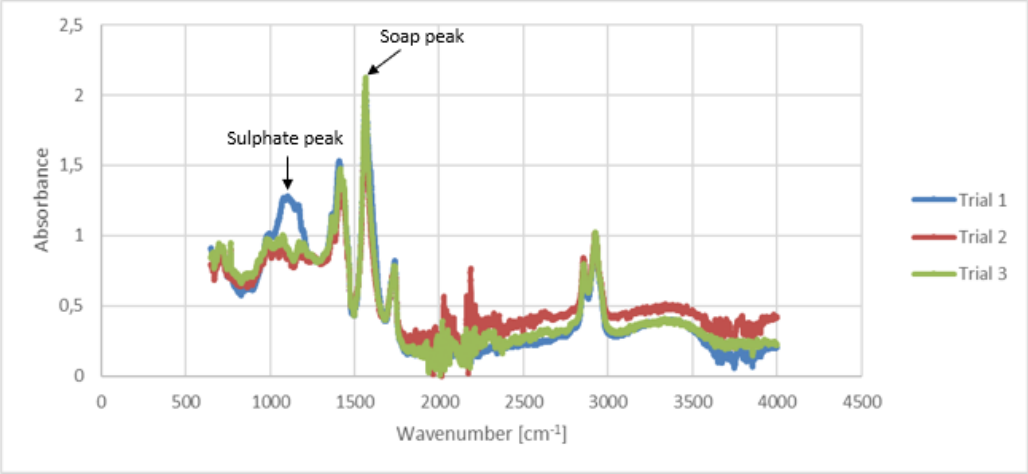

Figure 41: FTIR spectra at 95°C at a setting temperature of 250°C in the experiments with used engine oil. The intensity has been normalised to the peak at 2828 cm^{-1}.

The trends of increased and decreased peaks were examined similarly to the previous experiments (see Figure 40 and Figure 42). A similar trend regarding the $CaSO_4$ peak could be seen since it was high at 190°C and generally absent at the lower temperatures. In trial 2 and 3 at the setting temperature 250°C, small peaks could be seen at 1060 cm^{-1} and 1199 cm^{-1} at lower temperatures, which were present in the investigations without oil addition. Anyhow, no crystals could be found in this range, which could be the reason for the absence of the sulphate peak and the presence of the two peaks at 1060 cm^{-1} and 1199 cm^{-1}. The trend of the soap peak was not consistent between the trials at the setting temperature 120°C. However, the results without oil addition did not show any clear trend in peak increase or decrease in this temperature range either. The reason for similar results as without oil addition could be that few crystals were formed. At the setting temperature 250°C, the trends of peak alteration of the soap peak varied as well. However, in all trials it was high at 190°C similarly to the investigations without oil addition. The reason for the high soap peak at 190°C could be that crystals were formed in a smaller amount compared to the experiments with fresh engine oil.

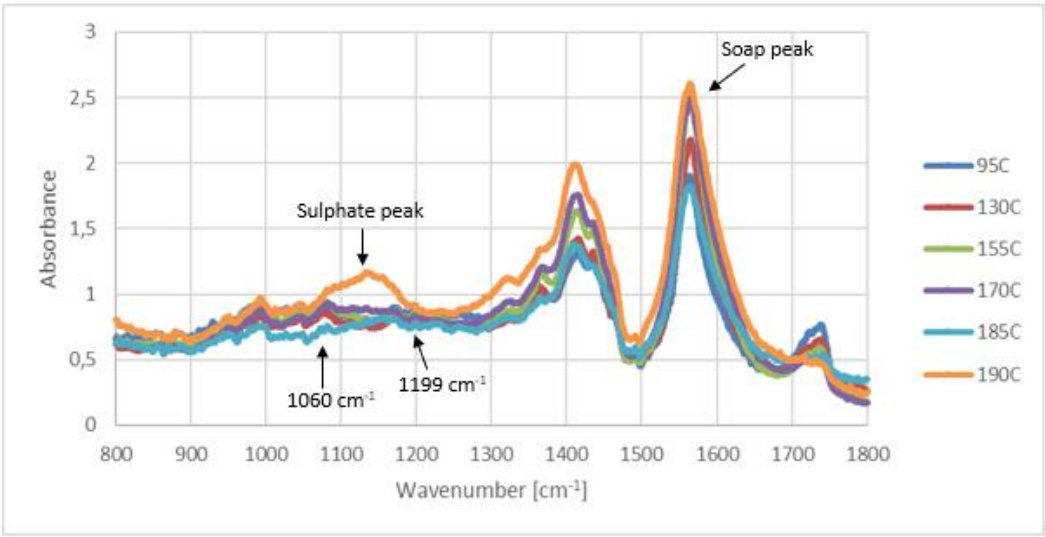

Figure 42: FTIR spectra from trial 2 in the experiments with used oil addition at a setting temperature of 250°C. The peaks have been normalised to the peak at 2858 cm^{-1}.

Ion milling followed by SEM-EDX was performed on the sample from trial 1 at a setting temperature of 250°C (see Figure 43). In the figure, the colours represent different elements. All elements except oxygen, aluminium, and carbon were identified all over the sample, which could indicate that the measurement was imprecise (see Appendix N: SEM-EDX Mapping of the Cross-sectional Area with Used Engine Oil with Concentrate). The measurement gives a relative estimation of the composition of different elements at different locations. Thus, the reason for the identification of sodium, zinc, and calcium over the whole sample may be that they were not found in a greater amount anywhere.

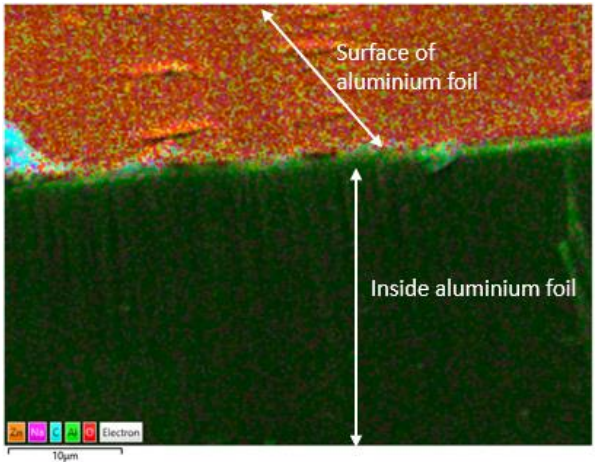

Figure 43: SEM-EDX mapping of the cross-sectional area of the sample from trial 1 at a setting temperature of 250°C. Ion milling was performed at the location with a temperature of 150°C.

In Figure 43 and Appendix N: SEM-EDX Mapping of the Cross-sectional Area with Used Engine Oil with Concentrate, it was seen that carbon appeared as a thin bottom layer all over the aluminium foil with lumps at some locations while oxygen was found majorly on the top surface. Thereby, the mechanism that a $CaSO_4$ layer is formed first to be followed by attachment of soft particles is not supported. However, as mentioned earlier, the surface may be too smooth for the crystals to attach, leading to formation of soft particles before the crystals could adhere to the surface. Barker et al. [33] found another layer structure in which carbon was found in the bottom layer and compounds with oxygen in the top layer. Moreover, Lamb et al. [8] identified a bottom layer of majorly carbon, a middle layer with salts, and a top layer of carbon, nitrogen, and oxygen. This is in line with the layer structure found in this study, which makes it consistent with the literature.

From the SEM-analysis on the cross-sectional area the height of the deposits could be estimated (see Figure 44). The height was estimated to 28 µm, which is 9 times higher than in the experiments without oil addition. However, this is consistent with the literature since a 14 times larger thickness have been found when used oil was added to the test fuel compared to no oil addition [40]. The thickness was 1000 times larger than a previous found thickness by Scania CV AB of 20 nm [7]. However, different oils were used, which could affect the deposit formation due to different properties. Furthermore, the test fuel could have had different concentrations of the calcium and sodium concentrate. Moreover, it could be seen that deposits were built up on top of each other and this increases the thickness.

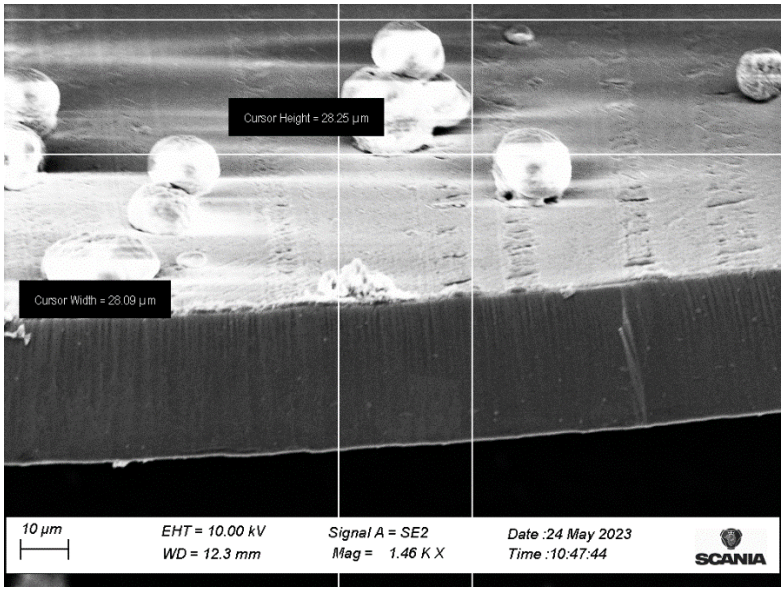

Figure 44: Estimation of the height of the deposits of trial 1 in the experiments with used engine oil and concentrate at a setting temperature of 250°C.

The results of the investigation of used engine oil with addition of calcium and sodium concentrate showed different results than with the fresh engine oil. More deposits could be seen in general but less crystals. Furthermore, a layer of carbon could be seen all over the aluminium foil, and the deposit height was higher compared to the investigations without addition of engine oil.

5.2.3.4 Investigation of Used Engine Oil without Addition of Concentrate

When the used engine oil was added without addition of calcium and sodium concentrate, a significantly lower number of deposits was observed (see Figure 45). This is reasonable since no additional sodium and calcium were added, which could make it more difficult to form soap deposits, similarly to the investigation with fresh engine oil without concentrate. The size and number of the deposits were much smaller in the entire temperature range compared to the investigations with addition of the calcium and sodium concentrate. Crystals were barely seen in any trial except from at a few locations, usually at higher temperatures.

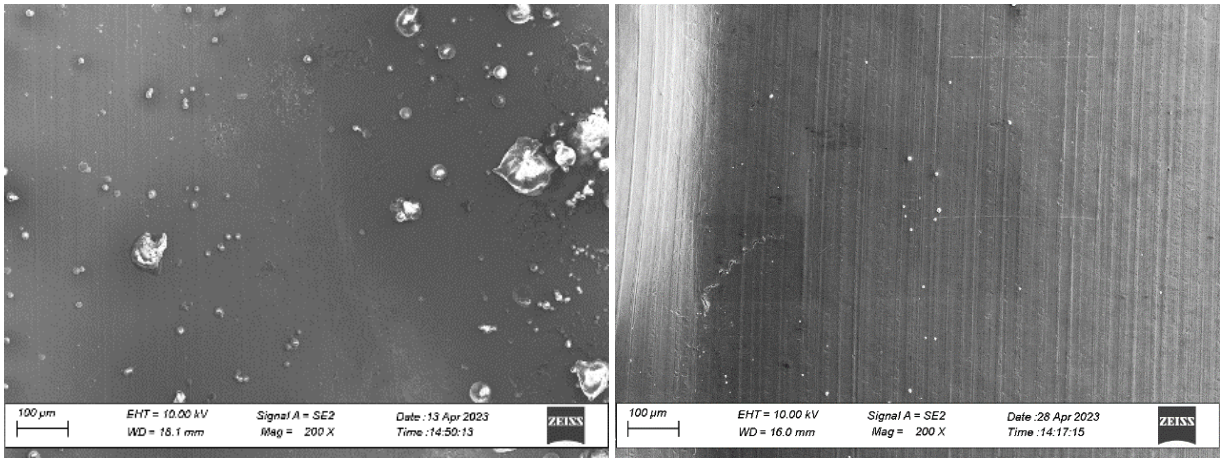

Figure 45: Comparison of the deposit formation in the investigations of used engine oil with (left) and without (right) concentrate at a temperature of 170°C.

The SEM-EDX analysis visualised the same elements as in the experiments on the fresh engine oil without calcium and sodium concentrate, namely sodium, sulphur, calcium, zinc, oxygen, carbon, fluorine, iron, and silicon. Moreover, magnesium was found at some locations. The results differed significantly between the trials and no clear trend could be seen (see Appendix O: Comparison of Composition with Used Engine Oil without Concentrate). The differing results are probably due to the low number of deposits, making the measurement less precise. Even though the composition differed significantly between the trials, an average composition of the different trials was calculated (see Figure 46). However, it cannot be claimed that the change in composition follows these trends since the trends were different in all the trials.

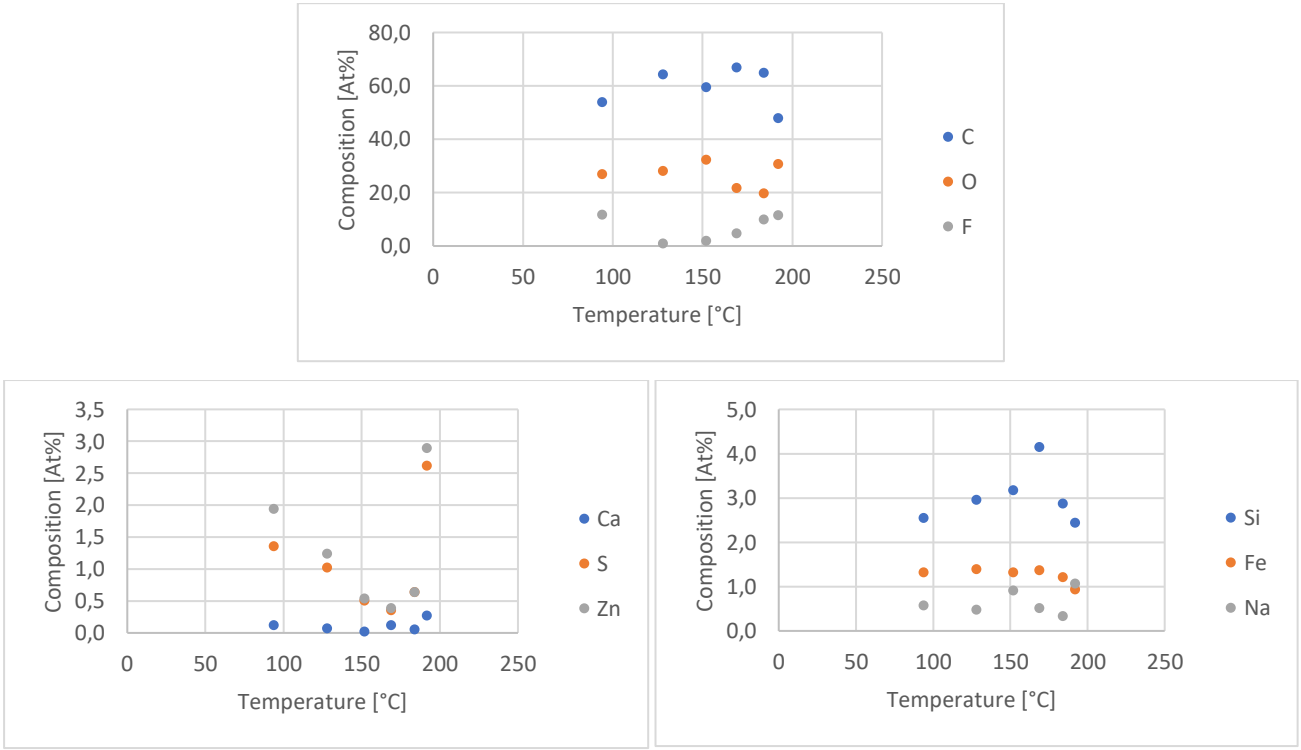

Figure 46: Comparison of composition at different temperatures for the main elements in the experiments regarding used oil addition without concentrate.

Carbon and oxygen were found in the highest amount while calcium and sodium were found in the lowest (see Figure 46). It is reasonable that calcium and sodium are present in low amounts since no calcium and sodium concentrate was added. Moreover, sulphur and zinc are present in similar amounts, which indicates that $ZnSO_4$ has been formed. It is reasonable that $CaSO_4$ is not formed to the same extent as in the experiments with calcium and sodium concentrate since there might not be enough calcium available. The identification of fluorine could, as mentioned before, be related to the FKM gasket. The reason why it is not visible in the analyses with addition of calcium and sodium concentrate could be that the other elements are present in higher amounts, which could make fluorine less visible.

The compositions of the elements were compared to the compositions in the investigations of used engine oil with addition of calcium and sodium concentrate (see Appendix P: Comparison of Composition with Used Engine Oil with and without Concentrate). It could be seen that the amounts of carbon and oxygen were similar,

which is reasonable since they probably originate from the fuel components. However, the amounts of sodium and calcium were lower at all temperatures while the amounts of the rest of the elements generally were higher. The lower amount of the remaining elements when calcium and sodium concentrate is added might be because sodium and calcium are present in higher amounts since the measurement is relative. As with the experiments with addition of calcium and sodium concentrate, the amounts of zinc and sulphate were relatively high already at 90°C, which again indicates that the $ZnSO_4$ wass formed before the rig. The $ZnSO_4$ is most probably formed already in the oil since no sulphuric acid was added for a reaction in the test fuel. However, this is not consistent with the SEM-analysis since no crystals could be seen except from at the higher temperatures. Anyhow, the crystals could be small and sit inside or under the soft particles, which could make them invisible in SEM.

As with the experiments on the fresh engine oil without calcium and sodium concentrate, the FTIR spectra differed significantly between the trials, which is consistent with the SEM-EDX analysis since those results also varied. An example of the differing spectra can be seen in Figure 47.

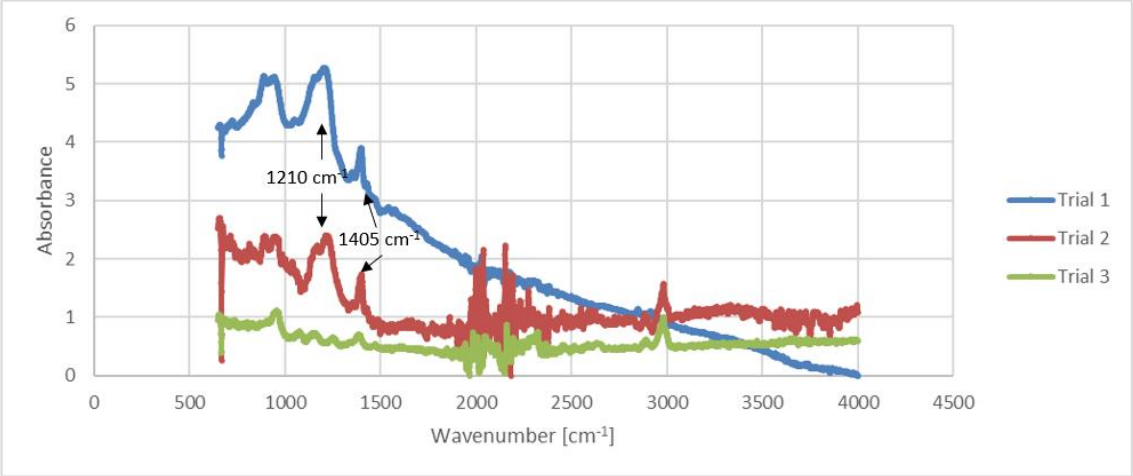

Figure 47: FTIR spectra at 190°C at a setting temperature of 250°C in the experiments with used engine oil without addition of concentrate. The intensity has been normalised to the peak at 2828 cm^{-1}.

It could be seen that trial 1 and 2 showed the peak of a sulphate compound at 1210 cm^{-1} as well as carboxylic acids or alcohols at 1405 cm^{-1}. However, at the lower temperatures, barely any peaks could be seen in trial 1 and 2, which is consistent with the SEM analysis in which a small number of deposits could be discerned. Trial 3 showed the same peaks at all temperatures (see Figure 48).

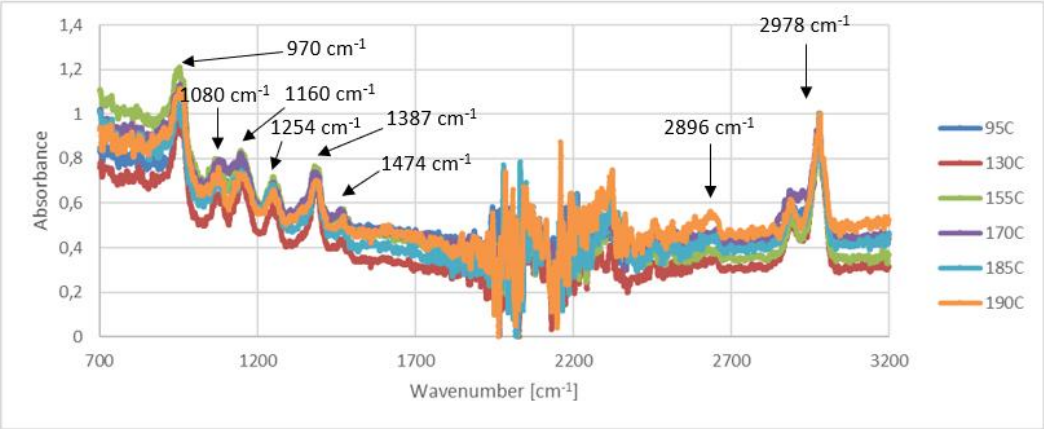

Figure 48: FTIR spectra from trial 3 in the experiments with used oil addition and concentrate at a setting temperature of 250°C. The peaks have been normalised to the peak at 2858 cm^{-1}.

The reason for the visualisation of these peaks could be due to the small number of deposits, wrong measurement location on the aluminium foil, or contaminations. A reason could be presence of fuel residues or impurities from the FKM gasket. An attempt to identify the peaks was made. By comparison with the previous investigations, it was concluded that the first peak is the aluminium foil. Moreover, the peak at 1080 cm^{-1} could be alcohols, carboxylic acids or esters, and the peak at 1160 cm^{-1} is probably related to a sulphate compound. The peaks around 2900 cm^{-1} are probably connected to alkanes.

The peaks at 1254 cm^{-1}, 1387 cm^{-1}, and 1474 cm^{-1} in Figure 48 have not been found in the previous investigations. In the previous investigations, carboxylic acids, alcohols, or esters have been observed at 1199 cm^{-1} and 1417 cm^{-1} while soaps have been identified at 1565 cm^{-1}. Therefore, the peaks in this investigation of used engine oil without calcium and sodium concentrate could be related to those compounds but might have been shifted due to contaminations or differences in nearby bonds. According Sigma Aldrich [65], the peak at 1254 cm^{-1} could also be related to C-O stretches in ethers. Moreover, the peak at 1387 cm^{-1} could belong to C-H bending, OH bending, or S=O stretching, and the peak at 1474 cm^{-1} to C-H bending. These peaks might therefore belong to fuel residues, sulphate compounds or alcohols residues but they have not generally been found in other studies, which might indicate that they are appearing from contaminations. No trial showed any trends in peak increase or decrease (see Figure 48 and Appendix Q: FTIR spectra from the investigations on Used Engine Oil without Concentrate). However, in trial 1 and 2, the sulphate peak was seen at the higher temperatures, which is consistent with the SEM-EDX analysis.

The results of the investigations of addition of used engine oil without addition of calcium and sodium concentrate indicated that the addition of the concentrate promotes the deposit formation. Very few deposits could be seen, which complicated both the SEM-EDX analysis, and the FTIR-analysis. However, it was concluded that $ZnSO_4$ was formed to a larger extent than $CaSO_4$, which is in accordance with the results of the fresh engine oil without addition of calcium and sodium concentrate.

5.3 Comparison with Field

The investigations of the deposit formation with the TDT offered many advantages since an easier analysis was possible compared to, for example, JFTOT. The use of a removable aluminium foil instead of a metal rod made it easier to insert the sample into different analysis instruments. The easier analysis possibilities resulted in that more information could be gained, which increased the possibility of understanding the deposit formation observed in the field. However, the modelled lab scale injector will not replace any runs out on the field.

To be able to apply the results from this study on the phenomenon observed in the field, it is important to consider that there are several differences between the setup in this study and the field. The material, angle, and size of the TDT are different from the engines used in the field. The angle of the injector is vertical out in the field while the rig is horizontal in this study. This could affect the deposit formation since the deposits have different capabilities of sticking to the surface depending on the angle. Moreover, the size of the rig was smaller than the engines in the field, which also could influence the deposit formation. This means that the results of this study cannot be fully applied in the field.

Another aspect to consider is the conditions under which the experiments were conducted. In this study, temperatures in the range of 50-190°C was investigated with a constant temperature at different locations on the foil. However, in engines, the temperature shifts depending on the speed, braking, and idling, resulting in a different temperature profile compared to the one in this study. Moreover, the pressure was set to 1.7 bar in this study, which is lower than the pressure in a real fuel system. Furthermore, the time duration in this study differed from the field since the engines are running for a longer time than the 2.5 h that was used in this study. Therefore, the deposits have more time to build up in the real fuel system, which could affect the extent of deposit formation and occurring reactions.

Finally, an artificial test fuel was used in this study, which differs from the reality. In the field, Scania CV AB injects B7 into the injector with the presence of other components due to contaminations. Contaminants can enter the fuel from, for example, engine oil or system components. However, in this study the test fuel consisted of B7 and an artificial concentrate of CaO, NaOH, distilled water, and B100. Therefore, the components were pre-determined, which affected the deposit formation since deposits could only be formed from these components. However, in the experiments on the oil addition, the present components may be more like the field since the used engine oil has been used inside the fuel system. Nevertheless, the components in the test fuel are not identical to the fuel in the field, which might have impacted the deposit formation.

6. Conclusions

This study aimed to investigate the mechanism behind internal injector deposits through experiments in a newly designed rig, and investigations of two possible hypotheses behind the deposit formation. The TDT experiments focused on examining temperature dependency, influence of the inclination of the rig, and the effect of engine oil addition to the test fuel. The investigated hypotheses behind the deposit formation were engine oil contamination, and Ostwald ripening where larger crystals are thermodynamically favoured over small crystals. The aim and research questions could successfully be answered where more information about the deposit formation was obtained. It was shown that a repeatable methodology had been implemented from the investigations of temperature and tilted apparatus. However, in the investigations of oil addition the trials differed more. Consequently, adjustments might be needed for further investigations on the oil addition. The results were in line with the phenomenon seen in the field, which validated the methodology.

To answer if it is reasonable that soluble $CaSO_4$ is transferred from the engine oil to the fuel system and then precipitates, investigations regarding the solubility of $CaSO_4$ anhydrous and $CaSO_4$ dihydrate were performed. It was shown that the hypothesis of engine oil contamination as a reason for the deposit formation could be possible since the $CaSO_4$ anhydrous had a significantly lower solubility in the B7 compared to the engine oils. However, error sources including losses and washing with heptane, made the results less reliable. The investigations on Ostwald ripening showed that this should not be the reason for the deposit formation since no larger crystals could be seen, making the hypothesis of engine oil contamination more probable.

The temperature dependency of the deposit formation was investigated in the temperature range 50-190°C by using the setting temperatures 120°C and 250°C on the heating plate. It was found that the temperature affected the size and number of deposits, and that reactions occurred, leading to different types of deposits in different temperature ranges. The size was smallest at the higher temperatures but largest around 90°C. Moreover, the number of deposits showed to increase with temperature. The major elements found in the deposits were the same at all temperatures, namely carbon, oxygen, sodium, and calcium. In SEM-EDX, the composition of the different elements had the largest change when the temperature exceeded 90°C. Moreover, the FTIR-ATR-analysis showed change in peak heights at the same temperatures, which led to the conclusion that a reaction connected to soap formation occurred.

To examine if the inclination of the rig affected the deposit formation, experiments with the rig tilted to 30° were performed in the same temperature range as with the horizontal rig. Similar trends and elements could be seen as with the horizontal rig, leading to the conclusion that sedimentation did not affect the morphology or reactions but had an impact on the total number of deposits on different locations.

The effect of engine oil on the deposit formation was investigated by addition of both fresh and used oil to the test fuel. Sulphuric acid was also added to the fresh engine oil to ensure that it contained sulphate ions. Additionally, some experiments were performed without addition of calcium and sodium concentrate to

examine if it could have an influence on the deposit formation. Crystals were successfully formed when both oils were added to the test fuel but to a larger extent with the fresh engine oil with sulphuric acid. The crystal formation affected the formation of soap deposits since less soaps were observed when many crystals were formed. The number of crystals increased with temperature and led to a smaller amount of soap deposits at higher temperatures. The FTIR-ATR analysis confirmed the crystal formation since a peak connected to sulphate crystals were found in the spectra. Both $CaSO_4$ and $ZnSO_4$ crystals were identified. It was found that different types of deposits were formed in different temperature ranges. At low temperatures below 90°C, $ZnSO_4$ could be seen. At temperatures between 90-150°C, soap deposits and $CaSO_4$ crystals were observed. Lastly, at higher temperatures above 150°C, $CaSO_4$ was formed to a large extent and competed with the soap formation. A layer structure was observed on a sample from the used engine oil addition with a thin bottom layer of carbon all over the aluminium foil, and more oxygen on top of the carbon layer. When no calcium and sodium concentrate was added, less deposits and crystals were observed but more elements possibly because the compositions of calcium and sodium were lower. Moreover, $ZnSO_4$ was formed to a larger extent than $CaSO_4$.

Through this study, new information regarding the deposit formation was obtained. It was shown that engine oil contamination could contribute to the deposit formation. This made the proposed mechanism about a firstly formed crystal layer, followed by adhesion of soft particles reasonable. However, the results showed that soap deposits adhere before the crystals, possibly due to a too smooth surface for the crystals to adhere. FTIR-ATR also offered new information about how the temperature affects the deposit formation and showed that reactions occur in which the deposits went from organic to more inorganic.

7. Future studies

For future studies, it could be of relevance to investigate both higher temperatures and higher pressures. Moreover, it could be of interest to examine different fuel types since only B7 was investigated in this study. The experiments on the solubility of $CaSO_4$ could also have been made more thoroughly with analyses on the filtrate. This would have offered more understanding about how much of the $CaSO_4$ that was dissolved. Additionally, it would have been of interest to perform more ion milling experiments to investigate layer structures thoroughly. Lastly, it would be interesting to run experiments with a vertical rig since it is more comparable to the injectors used in the field.

8. Reference List

[1] U. Nations, 'Causes and Effects of Climate Change', *United Nations*. https://www.un.org/en/climatechange/science/causes-effects-climate-change (accessed Feb. 13, 2023).

[2] N. Abas, A. Kalair, and N. Khan, 'Review of fossil fuels and future energy technologies', *Futures*, vol. 69, pp. 31–49, May 2015, doi: 10.1016/j.futures.2015.03.003.

[3] 'Transport emissions', *European Commission*. https://climate.ec.europa.eu/eu-action/transport-emissions_en (accessed Feb. 13, 2023).

[4] 'CO_2 emission performance standards for cars and vans', *European Commission*. https://climate.ec.europa.eu/eu-action/transport-emissions/road-transport-reducing-co2-emissions-vehicles/co2-emission-performance-standards-cars-and-vans_en (accessed Feb. 13, 2023).

[5] U. Schümann, S. Berndt, R. Wicht, and B. Buchholz, 'Avoiding Internal Injector Deposits by Using Biodiesel', *ATZheavy Duty Worldw.*, vol. 14, no. 1, pp. 44–49, Mar. 2021, doi: 10.1007/s41321-020-0403-1.

[6] 'The 17 Goals', *The Global Goals*. https://www.globalgoals.org/goals/ (accessed Feb. 14, 2023).

[7] H. Hittig, 'Introduction meeting to Internal Injector Deposits-project', Scania CV AB, Jan. 09, 2023.

[8] J. S. Lamb *et al.*, 'Internal Diesel Injector Deposit Chemical Speciation and Quantification Using 3D OrbiSIMS and XPS Depth Profiling', *SAE Int. J. Adv. Curr. Pract. Mobil.*, vol. 3, no. 1, pp. 349–364, Sep. 2020, doi: 10.4271/2020-01-2098.

[9] S. Berndt, U. Schümann, and S. Cepelak, 'JFTOT Diesel II Vorhaben Nr. 1285: Application and validation of a laboratory test method for classifying diesel fuels according to their tendency to form deposits in injection components as a function of temperature', Forschungsvereinigung Verbrennungskraftmaschinen e.V., Frankfurt am Main: FVV, 2020.

[10] Priya, P. S. Deora, Y. Verma, R. A. Muhal, C. Goswami, and T. Singh, 'Biofuels: An alternative to conventional fuel and energy source', *Mater. Today Proc.*, vol. 48, pp. 1178–1184, 2022, doi: 10.1016/j.matpr.2021.08.227.

[11] C. Bomb, K. McCormick, E. Deurwaarder, and T. Kåberger, 'Biofuels for transport in Europe: Lessons from Germany and the UK', *Energy Policy*, vol. 35, no. 4, pp. 2256–2267, Apr. 2007, doi: 10.1016/j.enpol.2006.07.008.

[12] A. Stanislaus, A. Marafi, and M. S. Rana, 'Recent advances in the science and technology of ultra low sulfur diesel (ULSD) production', *Catal. Today*, vol. 153, no. 1–2, pp. 1–68, Jul. 2010, doi: 10.1016/j.cattod.2010.05.011.

[13] E. Lois, E. L. Keating, and A. K. Gupta, 'Fuels', in *Encyclopedia of Physical Science and Technology*, Elsevier, 2003, pp. 275–314. doi: 10.1016/B0-12-227410-5/00268-4.

[14] H. Aatola, M. Larmi, T. Sarjovaara, and S. Mikkonen, 'Hydrotreated Vegetable Oil (HVO) as a Renewable Diesel Fuel: Trade-off between NO_x, Particulate Emission, and Fuel Consumption of a Heavy Duty Engine', *SAE Int. J. Engines*, vol. 1, no. 1, pp. 1251–1262, 2009.

[15] O. P. Bhardwaj, A. F. Kolbeck, T. Kkoerfer, and M. Honkanen, 'Potential of Hydrogenated Vegetable Oil (HVO) in Future High Efficiency Combustion System', *SAE Int. J. Fuels Lubr.*, vol. 6, no. 1, pp. 157–169, 2013.

[16] A. Sonthalia and N. Kumar, 'Hydroprocessed vegetable oil as a fuel for transportation sector: A review', *J. Energy Inst.*, vol. 92, no. 1, pp. 1–17, Feb. 2019, doi: 10.1016/j.joei.2017.10.008.

[17] D. Huang, H. Zhou, and L. Lin, 'Biodiesel: an Alternative to Conventional Fuel', *Energy Procedia*, vol. 16, pp. 1874–1885, 2012, doi: 10.1016/j.egypro.2012.01.287.

[18] A. C. Pinto *et al.*, 'Biodiesel: an overview', *J. Braz. Chem. Soc.*, vol. 16, no. 6b, pp. 1313–1330, Nov. 2005, doi: 10.1590/S0103-50532005000800003.

[19] S. K. Hoekman, A. Broch, C. Robbins, E. Ceniceros, and M. Natarajan, 'Review of biodiesel composition, properties, and specifications', *Renew. Sustain. Energy Rev.*, vol. 16, no. 1, pp. 143–169, Jan. 2012, doi: 10.1016/j.rser.2011.07.143.

[20] H. Hittig, 'Meeting about Engine systems in Internal Injector Deposits-project', Scania CV AB, Jan. 18, 2023.

[21] A. P. Vyas, J. L. Verma, and N. Subrahmanyam, 'A review on FAME production processes', *Fuel*, vol. 89, no. 1, pp. 1–9, Jan. 2010, doi: 10.1016/j.fuel.2009.08.014.

[22] C. H. Brito Cruz, G. M. Souza, and L. A. Barbosa Cortez, 'Biofuels for Transport', in *Future Energy*, Elsevier, 2014, pp. 215–244. doi: 10.1016/B978-0-08-099424-6.00011-9.
[23] R. Boukhanouf, 'Small combined heat and power (CHP) systems for commercial buildings and institutions', in *Small and Micro Combined Heat and Power (CHP) Systems*, Elsevier, 2011, pp. 365–394. doi: 10.1533/9780857092755.3.365.
[24] P. Breeze, 'Piston Engine–Based Power Plants', in *Power Generation Technologies*, Elsevier, 2019, pp. 99–119. doi: 10.1016/B978-0-08-102631-1.00005-5.
[25] P. Breeze, 'Diesel Engines', in *Piston Engine-Based Power Plants*, Elsevier, 2018, pp. 47–57. doi: 10.1016/B978-0-12-812904-3.00005-7.
[26] S. Fallah, *Electric and Hybrid Vehicles - Technologies, Modeling and Control: A Mechatronic Approach*. 2014.
[27] 'Diesel engine', *Britannica*. https://www.britannica.com/technology/diesel-engine (accessed Feb. 14, 2023).
[28] M. J. Tindal and O. A. Uyehara, 'Diesel Engines', in *Internal Combustion Engines*, Elsevier, 1988, pp. 101–155. doi: 10.1016/B978-0-12-059790-1.50009-2.
[29] J. Barker *et al.*, 'The Application of New Approaches to the Analysis of Deposits from the Jet Fuel Thermal Oxidation Tester (JFTOT)', *SAE Int. J. Fuels Lubr.*, vol. 10, no. 3, pp. 741–755, 2017.
[30] H. Hittig, 'A fuel system that is designed to cope with soft particles is the key to the future', Scania CV AB, Jan. 09, 2023.
[31] M. K. Edney, J. Barker, J. Reid, D. J. Scurr, and C. E. Snape, 'Recent Advances in the Analysis of GDI and Diesel Fuel Injector Deposits', *Fuel*, vol. 272, p. 117682, Jul. 2020, doi: 10.1016/j.fuel.2020.117682.
[32] H. Hittig, 'Mechanism deposits', Scania CV AB, Jan. 09, 2023.
[33] J. Barker, C. Snape, and D. Scurr, 'A Novel Technique for Investigating the Characteristics and History of Deposits Formed Within High Pressure Fuel Injection Equipment', *SAE Int. J. Fuels Lubr.*, vol. 5, no. 3, pp. 1155–1164, 2012.
[34] H. Hittig, 'Hot surface deposit rig', Scania CV AB, Jan. 09, 2023.
[35] J. Reid, S. Cook, and J. Barker, 'Internal Injector Deposits From Sodium Sources', *SAE Int. J. Fuels Lubr.*, vol. 7, no. 2, pp. 436–444, 2014.
[36] M. Berger, 'Meeting about Engine oil in Internal Injector Deposits-project', Scania CV AB, Jan. 24, 2023.
[37] S. Berndt, U. Schümann, T. Sadlowski, R. Junk, C. Fink, and H. Harndorf, 'JFTOT Diesel Vorhaben Nr. 1198: Development of a laboratory test method for the assessment of diesel fuels or diesel fuel additives with regard to their tendency to form internal diesel injector deposits (IDID)', Forschungsvereinigung Verbrennungskraftmaschinen e.V., Leipzig: FVV, 1198, 2017.
[38] 'Use of an additive for dispersing calcium sulfate in a lubricating oil for diesel engines', Jun. 17, 1996 Accessed: Feb. 10, 2023. [Online]. Available: https://patents.google.com/patent/EP0835924B1/en
[39] B. Liu and X. Hu, 'Hollow Micro- and Nanomaterials: Synthesis and Applications', in *Advanced Nanomaterials for Pollutant Sensing and Environmental Catalysis*, Elsevier, 2020, pp. 1–38. doi: 10.1016/B978-0-12-814796-2.00001-0.
[40] U. Schümann, S. Berndt, S. Cepelak, and B. Buchholz, 'JFTOT-Diesel Fuel II', Frankfurt am Main, Sep. 26, 2017.
[41] J. Klettlinger, R. Rich, C. Yen, and A. Surgenor, 'Thermal stability testing of Fischer-Tropsch fuel and various blends with Jet A, as well as aromatic blend additives', in *IEEE 2011 EnergyTech*, Cleveland, OH, USA: IEEE, May 2011, pp. 1–6. doi: 10.1109/EnergyTech.2011.5948544.
[42] 'Scanning Electron Microscopy (SEM)', *Geochemical Instrumentation and Analysis*. https://serc.carleton.edu/research_education/geochemsheets/techniques/SEM.html (accessed Feb. 06, 2023).
[43] 'FTIR Spectroscopy Basics', *ThermoFisher Scientific*. https://www.thermofisher.com/uk/en/home/industrial/spectroscopy-elemental-isotope-analysis/spectroscopy-elemental-isotope-analysis-learning-center/molecular-spectroscopy-information/ftir-information/ftir-basics.html (accessed Feb. 07, 2023).
[44] M. A. Mohamed, J. Jaafar, A. F. Ismail, M. H. D. Othman, and M. A. Rahman, 'Fourier Transform Infrared (FTIR) Spectroscopy', in *Membrane Characterization*, Elsevier, 2017, pp. 3–29. doi: 10.1016/B978-0-444-63776-5.00001-2.

[45] P. Mohamed Shameer and P. Mohamed Nishath, 'Exploration and enhancement on fuel stability of biodiesel: A step forward in the track of global commercialization', in *Advanced Biofuels*, Elsevier, 2019, pp. 181–213. doi: 10.1016/B978-0-08-102791-2.00008-8.
[46] K. Robards and D. Ryan, 'Gas chromatography', in *Principles and Practice of Modern Chromatographic Methods*, Elsevier, 2022, pp. 145–245. doi: 10.1016/B978-0-12-822096-2.00005-0.
[47] 'Pyrolysis Gas Chromatography/Mass Spectrometry (Pyro-GC-MS)', *eurofins: EAG Laboratories*. https://www.eag.com/techniques/mass-spec/pyrolysis-gc-ms/ (accessed Feb. 08, 2023).
[48] T. Hatano, S. Nakaba, Y. Horikawa, and R. Funada, 'A combination of scanning electron microscopy and broad argon ion beam milling provides intact structure of secondary tissues in woody plants', *Sci. Rep.*, vol. 12, no. 1, p. 9152, Jun. 2022, doi: 10.1038/s41598-022-13122-3.
[49] A. Mohammed and A. Abdullah, 'Scanning Electron Microscopy (SEM): A Review', Jan. 2019.
[50] A. Nanakoudis, 'EDX Analysis with SEM: How Does it Work?', *ThermoFisher Scientific*, Nov. 28, 2019. https://www.thermofisher.com/blog/materials/edx-analysis-with-sem-how-does-it-work/ (accessed Feb. 06, 2023).
[51] D. Titus, E. James Jebaseelan Samuel, and S. M. Roopan, 'Nanoparticle characterization techniques', in *Green Synthesis, Characterization and Applications of Nanoparticles*, Elsevier, 2019, pp. 303–319. doi: 10.1016/B978-0-08-102579-6.00012-5.
[52] C. Berthomieu and R. Hienerwadel, 'Fourier transform infrared (FTIR) spectroscopy', *Photosynth. Res.*, vol. 101, no. 2–3, pp. 157–170, Sep. 2009, doi: 10.1007/s11120-009-9439-x.
[53] 'FTIR Applications', *ThermoFisher Scientific*. https://www.thermofisher.com/uk/en/home/industrial/spectroscopy-elemental-isotope-analysis/spectroscopy-elemental-isotope-analysis-learning-center/molecular-spectroscopy-information/ftir-information/ftir-applications.html (accessed Feb. 07, 2023).
[54] 'Pyrolysis-GC/MS: 1. Introduction', *Frontier Lab*. https://www.frontier-lab.com/technical-information/methodology/index/ (accessed Feb. 08, 2023).
[55] K. Robards, P. R. Haddad, and P. E. Jackson, 'Gas Chromatography', in *Principles and Practice of Modern Chromatographic Methods*, Elsevier, 2004, pp. 75–177. doi: 10.1016/B978-0-08-057178-2.50006-6.
[56] J. Melngailis, 'Focused ion beam technology and applications', *J. Vac. Sci. Technol. B Microelectron. Nanometer Struct.*, vol. 5, no. 2, p. 469, Mar. 1987, doi: 10.1116/1.583937.
[57] K. L. House, L. Pan, D. M. O'Carroll, and S. Xu, 'Applications of scanning electron microscopy and focused ion beam milling in dental research', *Eur. J. Oral Sci.*, vol. 130, no. 2, Apr. 2022, doi: 10.1111/eos.12853.
[58] T. Ishitani and T. Yaguchi, 'Cross-sectional sample preparation by focused ion beam: A review of ion-sample interaction', *Microsc. Res. Tech.*, vol. 35, no. 4, pp. 320–333, Nov. 1996, doi: 10.1002/(SICI)1097-0029(19961101)35:4<320::AID-JEMT3>3.0.CO;2-Q.
[59] R. M. Langford and A. K. Petford-Long, 'Broad ion beam milling of focused ion beam prepared transmission electron microscopy cross sections for high resolution electron microscopy', *J. Vac. Sci. Technol. Vac. Surf. Films*, vol. 19, no. 3, pp. 982–985, May 2001, doi: 10.1116/1.1368198.
[60] L. A. Giannuzzi and F. A. Stevie, 'A review of focused ion beam milling techniques for TEM specimen preparation', *Micron*, vol. 30, no. 3, pp. 197–204, Jun. 1999, doi: 10.1016/S0968-4328(99)00005-0.
[61] 'EN 590 Diesel Fuel Specifications (ULSD)', *Crown Oil*. https://www.crownoil.co.uk/fuel-specifications/en-590/ (accessed Jun. 12, 2023).
[62] H. Hittig, 'Follow-up meeting 2 to Internal Injector Deposits-project', Scania CV AB, Apr. 12, 2023.
[63] G. Azimi and V. Papangelakis, 'Chemical Modelling of Calcium Sulphate Phase Equilibria in Multicomponent Electrolyte Solutions', *AIChE Annu. Meet. Conf. Proc.*, Nov. 2008.
[64] H. Hittig, 'Follow-up meeting to Internal Injector Deposits-project', Scania CV AB, Feb. 27, 2023.
[65] 'IR Spectrum Table & Chart', *Sigma Aldrich*. https://www.sigmaaldrich.com/SE/en/technical-documents/technical-article/analytical-chemistry/photometry-and-reflectometry/ir-spectrum-table (accessed Feb. 24, 2023).
[66] M. Pach, H. Hittig, A. Cronhjort, and H. Bernemyr, 'Characterization of Internal Diesel Injector Deposits from Heavy-Duty Vehicles', presented at the 15th International Conference on Engines & Vehicles, Sep. 2021, pp. 2021-24–0062. doi: 10.4271/2021-24-0062.

Appendices

Appendix A: Temperature Profile inside the Rig

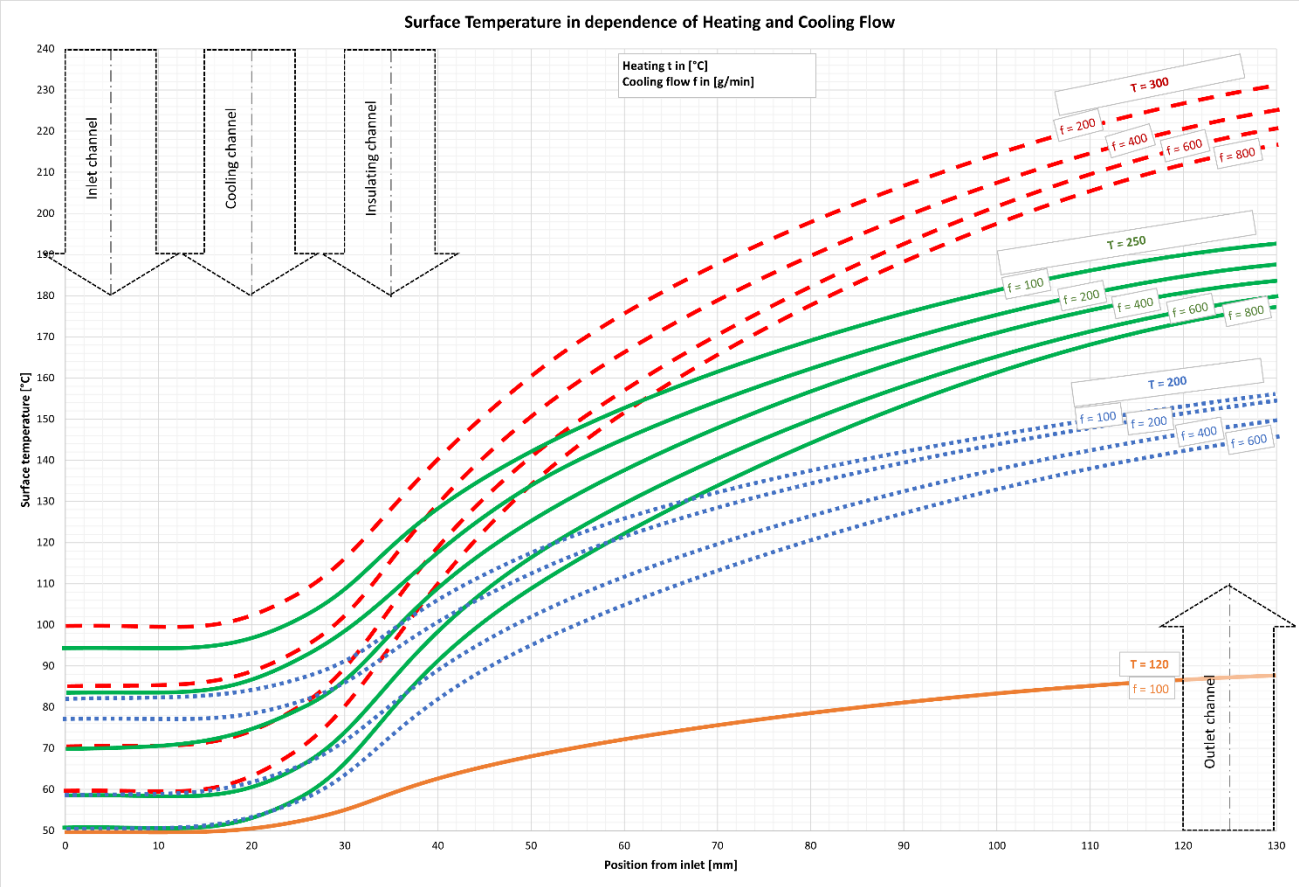

Appendix B: Calculation on H_2SO_4 for the Fresh Engine Oil TDT Experiments

TBN = 9.9 mg KOH/g engine oil

1 wt% engine oil corresponds to an addition of 8.4 g oil. Therefore, the weight of KOH in the engine oil is 0.08 g.

M_{KOH}=56.1 g/mol

$$n_{KOH} = \frac{m}{M} = \frac{0.08\ g}{56.1\ g/mol} = 0.0015\ mol$$

The molar ratio of KOH and OH^- is 1:1.

$$n_{OH^-} = 0.0015\ mol$$

To neutralise half of the hydroxide ions, 0.00074 mol H^+ is needed.

The molar ratio of H^+ and H_2SO_4 is 1:2.

$$n_{H_2SO_4} = \frac{n_{H^+}}{2} = \frac{0.00074\ mol}{2} = 0.00037\ mol$$

M_{H2SO4}=98.1 g/mol

$$m_{H_2SO_4} = M \times n = 98.1\ g/mol \times\ 0.0037\ mol\ =\ 0.036\ g$$

The H_2SO_4 solution is 95-97 wt%.

$$m_{H_2SO_{4,sol}} = \frac{0.036\ g}{0.95} = 0.038\ g$$

Before adding the sulphuric acid to the engine oil, dilution with distilled water was made with 1 part sulphuric acid and 2 parts water.

$$m_{H_2O} = 0.038\ g\ \times 2 = 0.077\ g$$

The total mass of the diluted sulphuric acid solution is therefore:

$$m_{H_2SO_{4,dil.sol}} = m_{H_2SO_{4,sol}} + m_{H_2O} = 0.115\ g$$

Appendix C: Investigation of the Solubility of Calcium Sulphate Dihydrate in Engine Oil

Trial	$CaSO_4$ before [g]	$CaSO_4$ after [g]	Difference [g]	Difference [%]	Type of engine oil	Temperature
1di	0.48	0.44	-0.04	-8%	Fresh engine oil A	Room temperature
2di	0.48	0.59	0.11	23%	Fresh engine oil B	Room temperature
3di	0.53	0.4	-0.13	-25%	Fresh engine oil A	100°C
4di	0.5	0.4	-0.1	-20%	Fresh engine oil A	100°C
5di	0.21	0.13	-0.08	-38%	Fresh engine oil B	100°C
6di	0.48	0.53	0.05	10%	Used engine oil	Room temperature
7di	0.52	0.57	0.05	10%	Used engine oil	Room temperature
8di	0.66	0.53	-0.13	-20%	Used engine oil	100°C
9di	0.46	0.34	-0.12	-26%	Used engine oil	100°C

Appendix D: Investigation of the Solubility of Calcium Sulphate Anhydrous in Engine Oil

Trial	$CaSO_4$ before [g]	$CaSO_4$ after [g]	Difference [g]	Difference [%]	Type of engine oil	Temperature [°C]
1an	0.51	0.38	-0.13	-25%	Fresh engine oil B	Room temperature
2an	0.52	0.32	-0.2	-38%	Fresh engine oil B	Room temperature
3an	0.49	0.33	-0.16	-33%	Fresh engine oil B	100
4an	0.55	0.31	-0.24	-44%	Fresh engine oil B	100
5an	0.55	0.39	-0.16	-29%	Used engine oil	Room temperature
6an	0.5	0.24	-0.26	-52%	Used engine oil	Room temperature
7an	0.59	0.34	-0.25	-42%	Used engine oil	100
8an	0.55	0.35	-0.2	-36%	Used engine oil	100

Appendix E: Investigation of the Solubility of Calcium Sulphate in B7

Trial	$CaSO_4$ before [g]	$CaSO_4$ after [g]	Difference [g]	Difference [%]	Temperature [°C]	Type of $CaSO_4$
1	0.48	0.52	0.04	8%	Room temperature	Dihydrate
2	0.46	0.4	-0.06	-13%	120	Dihydrate
3	0.6	0.45	-0.15	-25%	120	Dihydrate
4	0.5	0.11	-0.39	-78%	Room temperature	Anhydrous
5	0.56	0.49	-0.07	-13%	Room temperature	Anhydrous
6	0.68	0.65	-0.03	-4%	Room temperature	Anhydrous
7	0.58	0.48	-0.1	-17%	120	Anhydrous
8	0.46	0.49	0.03	7%	120	Anhydrous

Appendix F: Comparison of Composition with Temperature for each Element

T [°C]	C [At%]	O [At%]	Na [At%]	Ca [At%]
50	73	23	3.6	0.23
62	74	22	3.3	0.27
72	76	21	3.3	0.30
78	73	22	4	0.30
84	75	21	3.3	0.40
88	73	23	3.6	0.30
94	72	22	5.7	0.50
128	73	22	4.2	0.50
152	67	26	7.7	0.50
169	68	25	6.9	0.70
184	64	28	7.6	0.80
192	64	26	8.8	0.80

Appendix G: Comparison of Composition between Tilted and Non-tilted

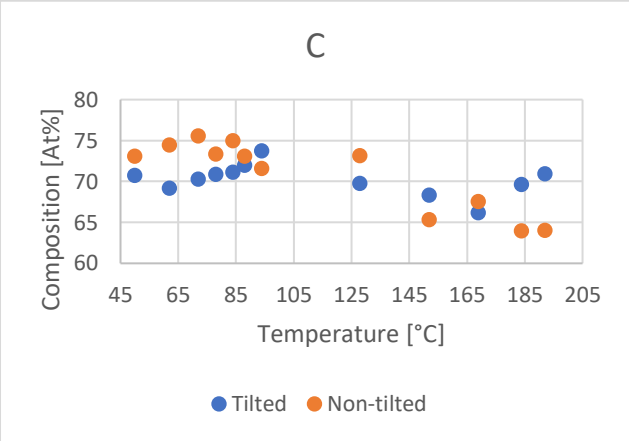

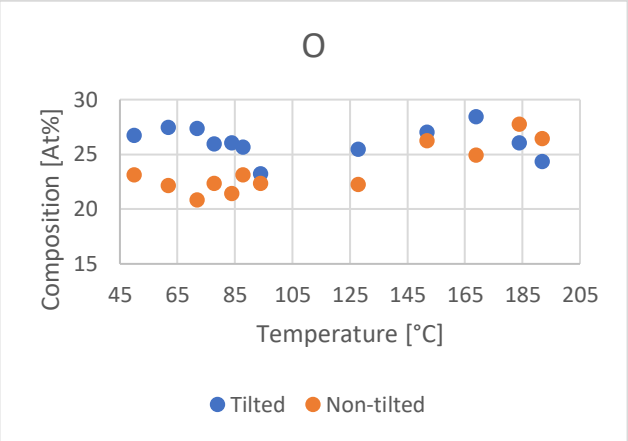

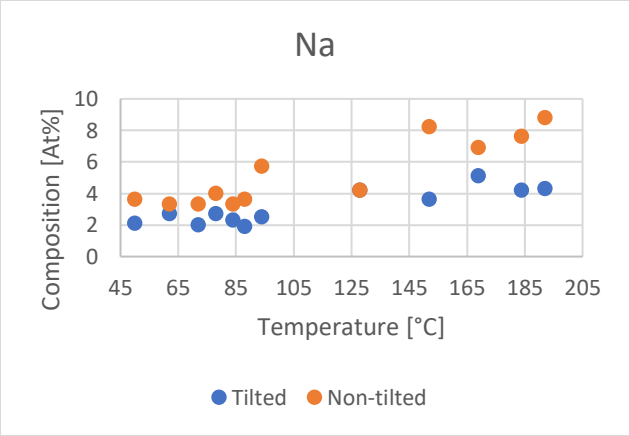

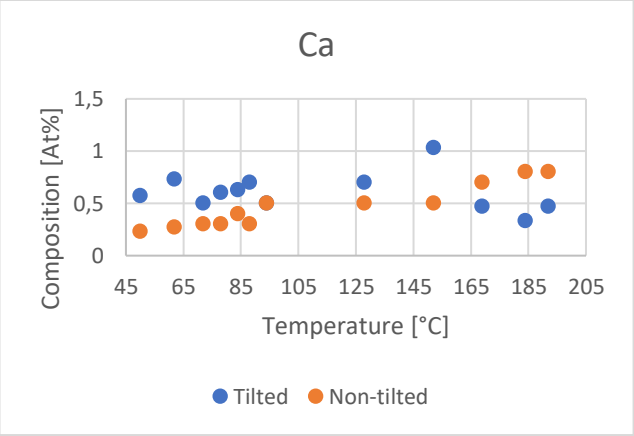

Appendix H: Comparison of Composition in the Trials on Fresh Oil Addition

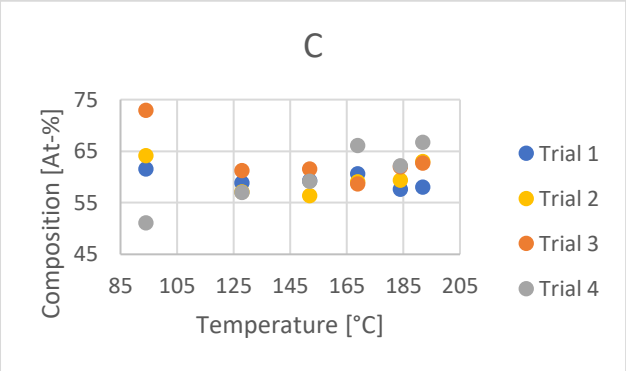

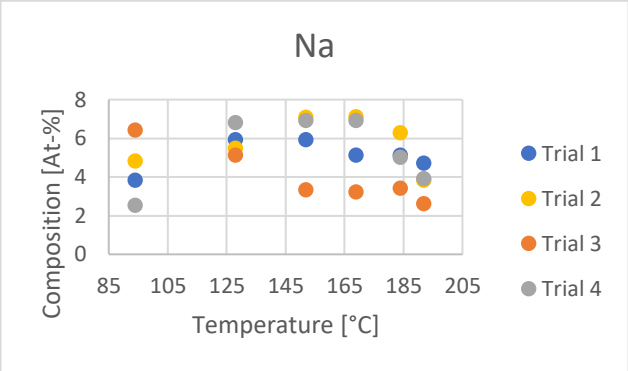

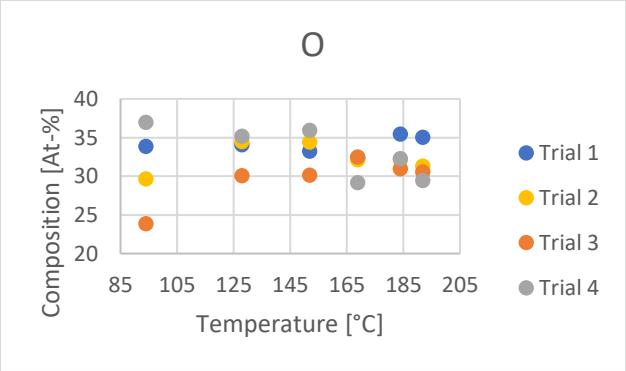

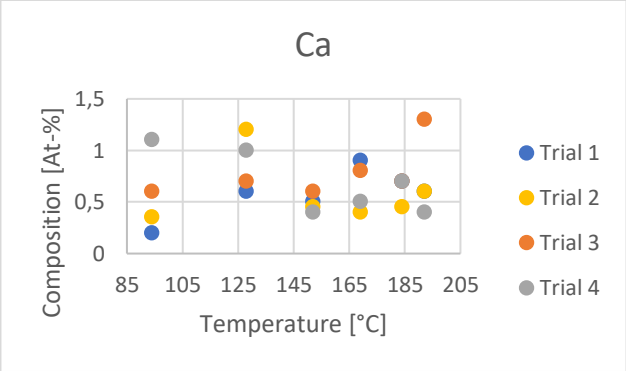

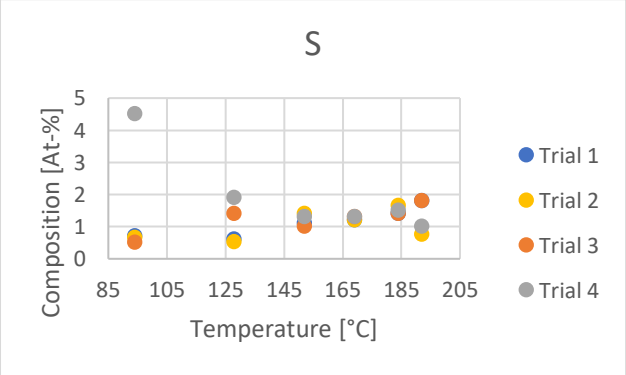

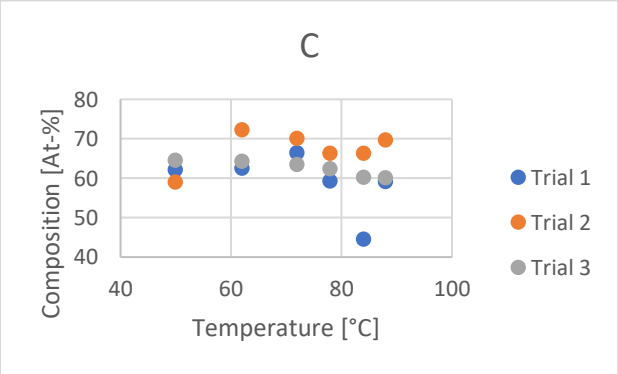

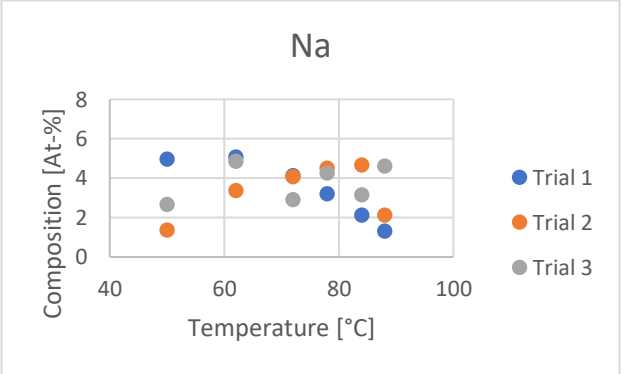

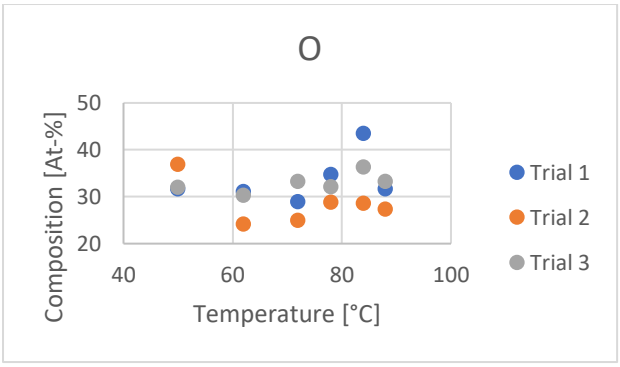

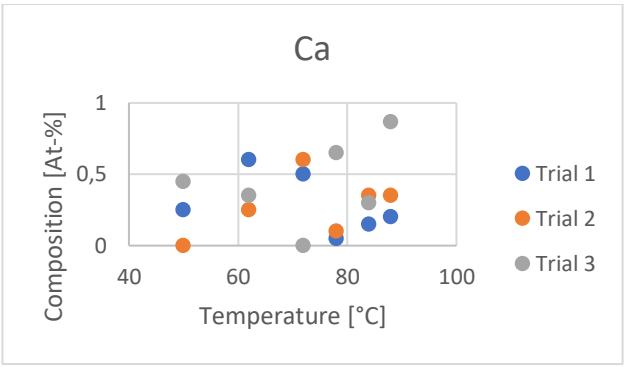

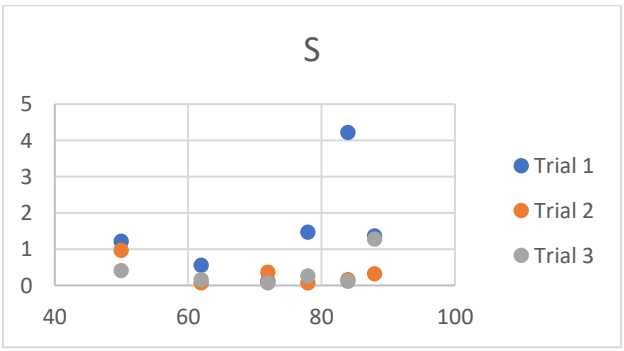

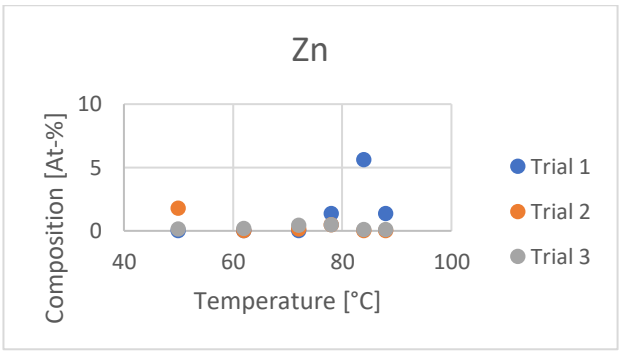

Appendix I: Comparison of Composition with and without Oil Addition

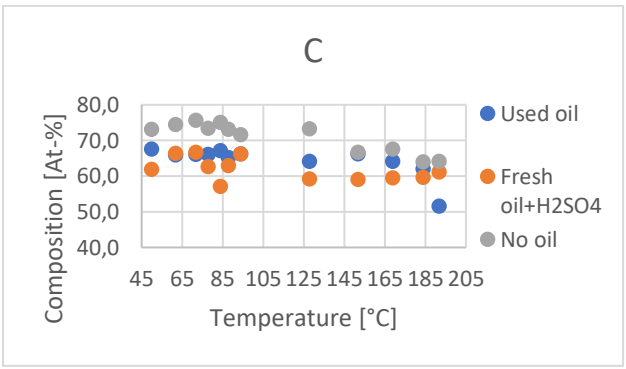

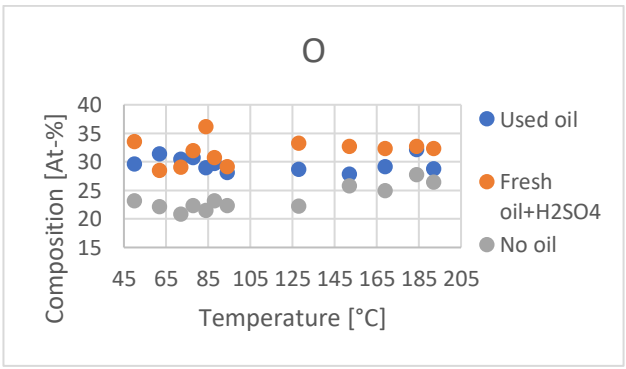

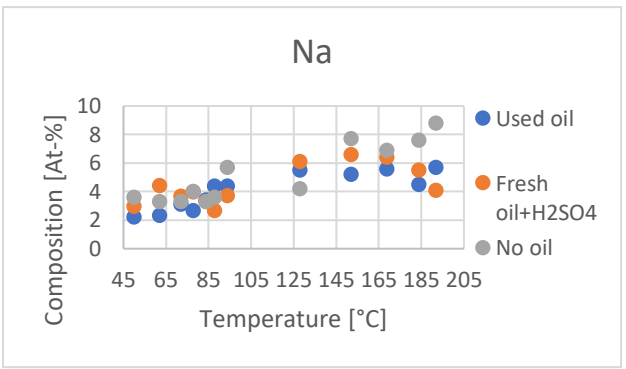

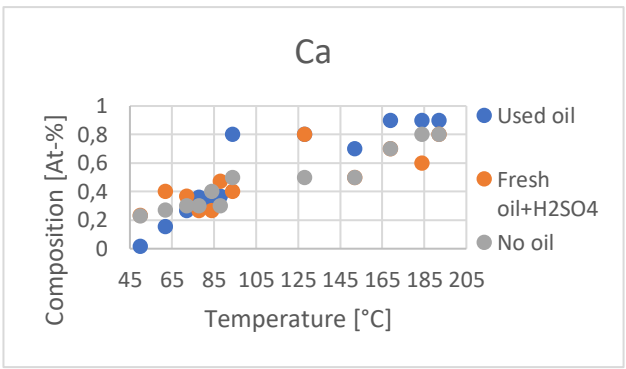

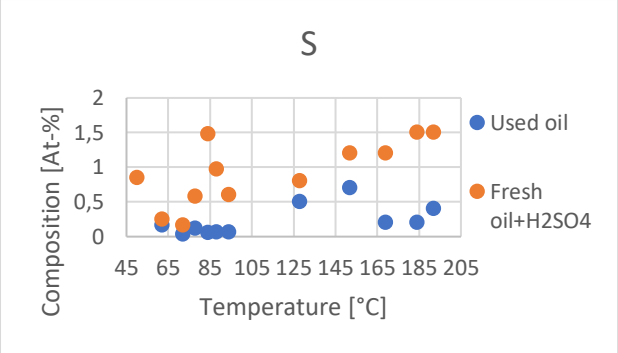

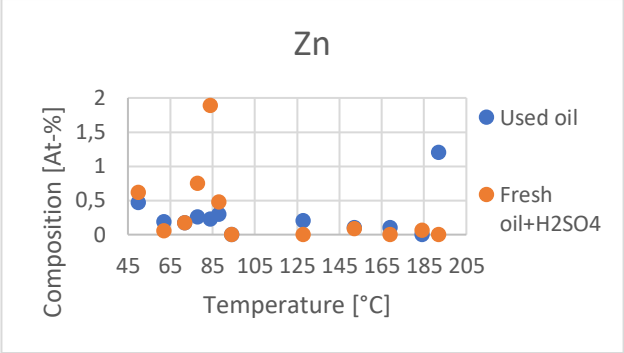

Appendix J: Comparison of Composition with Fresh Engine Oil without Concentrate

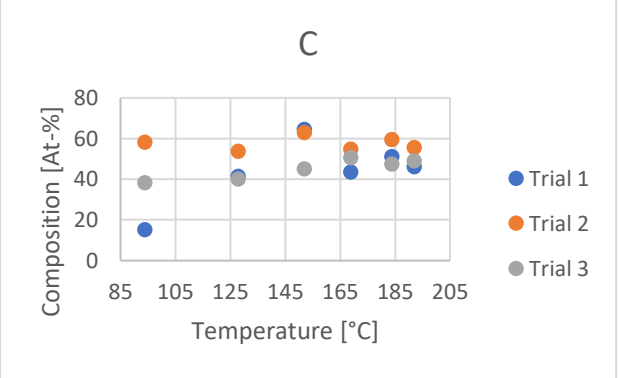

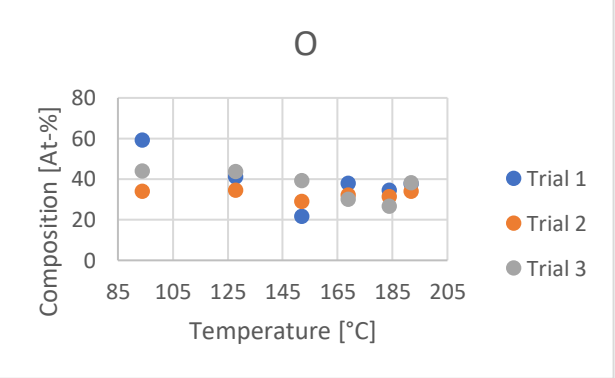

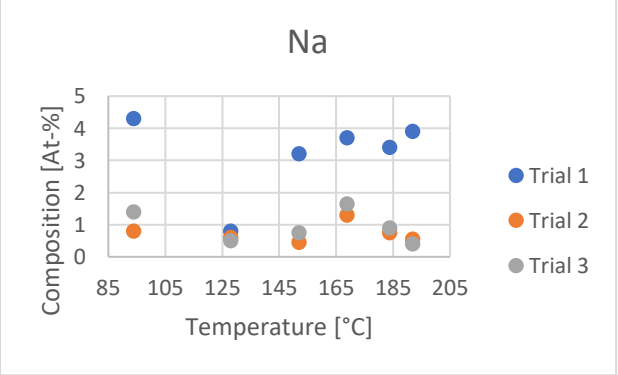

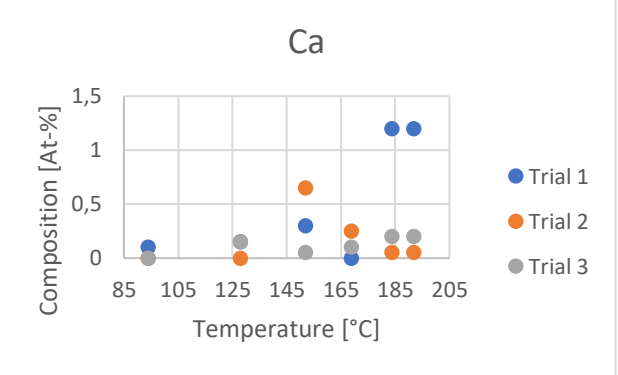

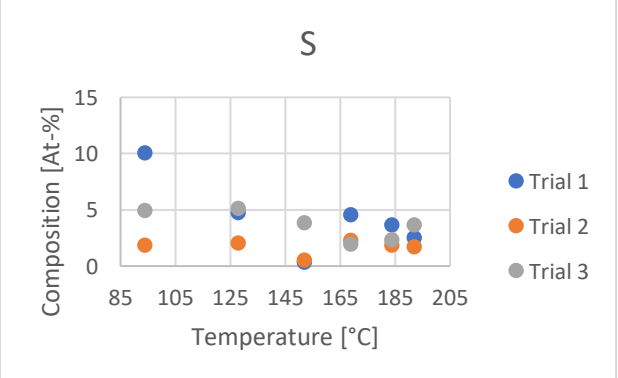

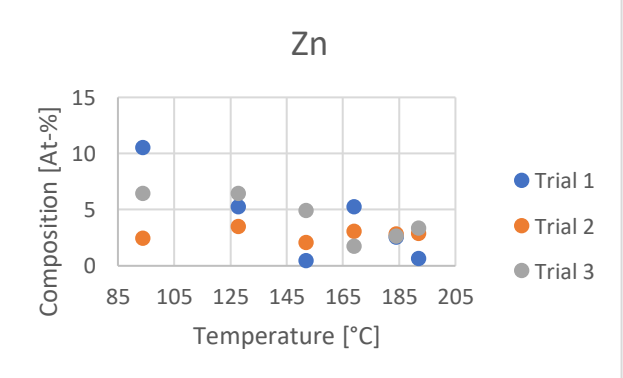

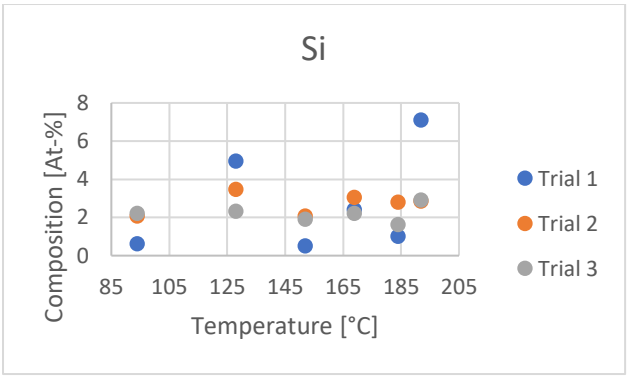

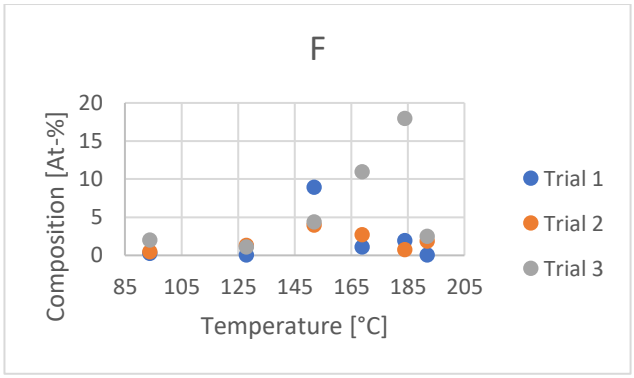

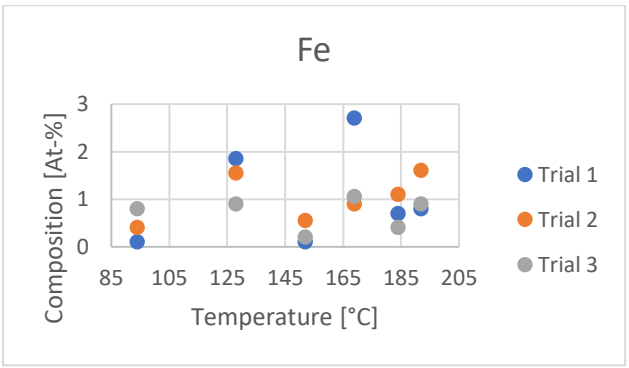

Appendix K: Comparison of Composition with Fresh Engine Oil with and without Concentrate

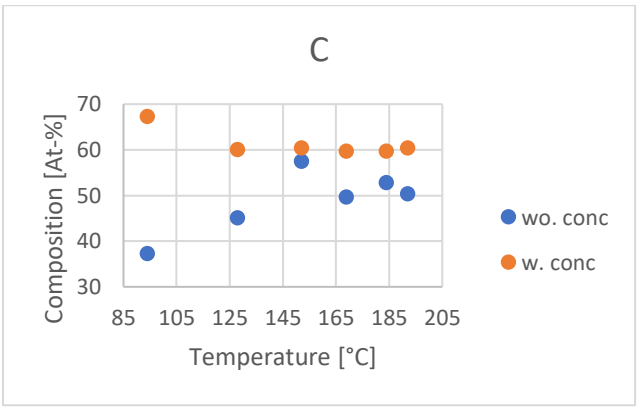

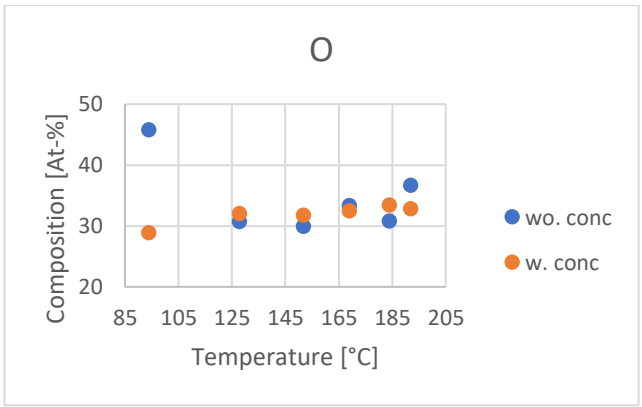

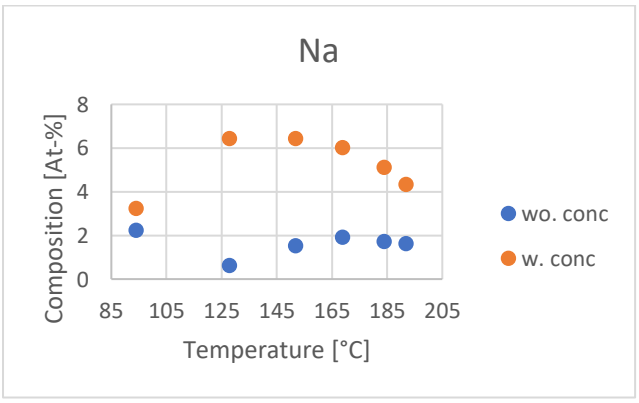

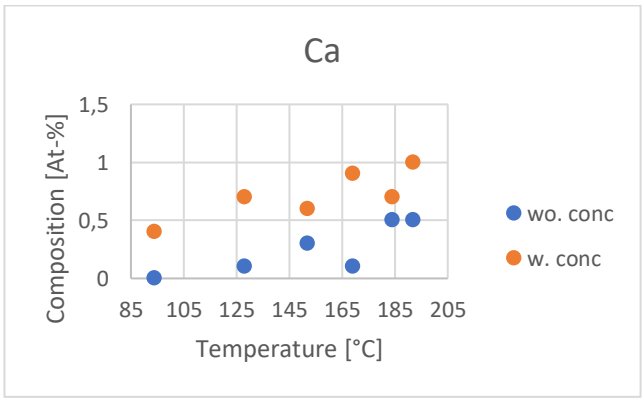

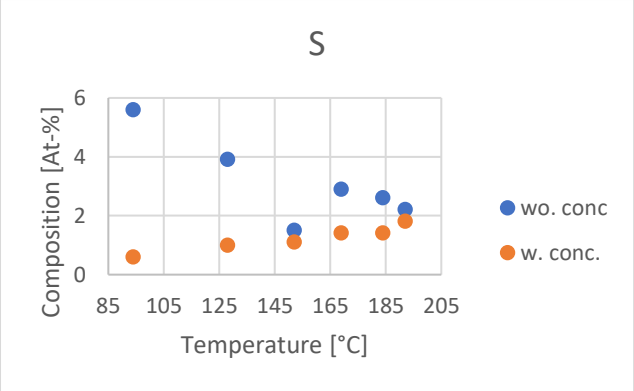

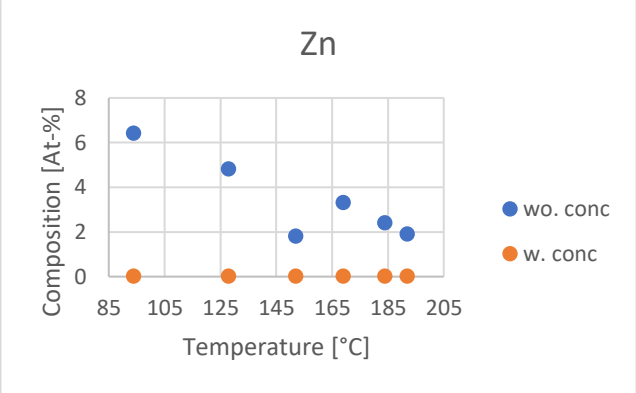

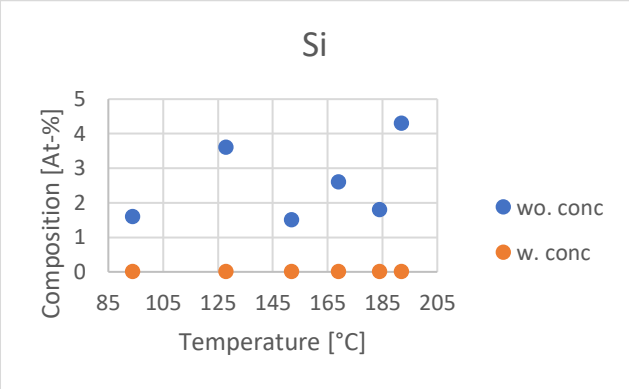

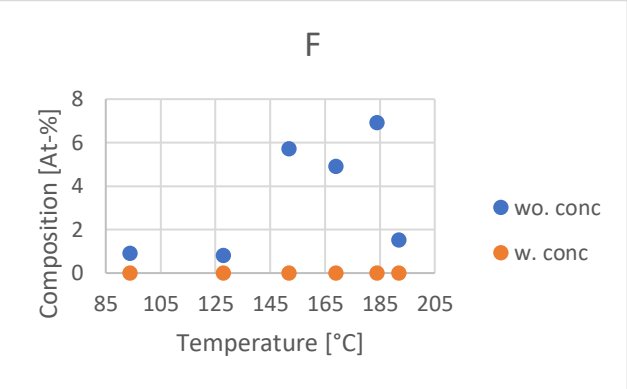

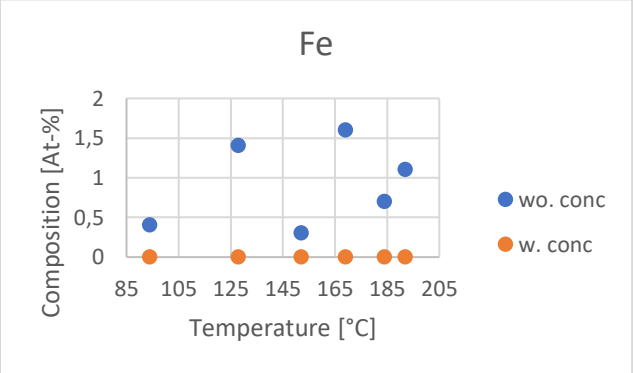

Appendix L: Comparison of FTIR spectra with Addition of Fresh Engine Oil with and without Addition of Concentrate

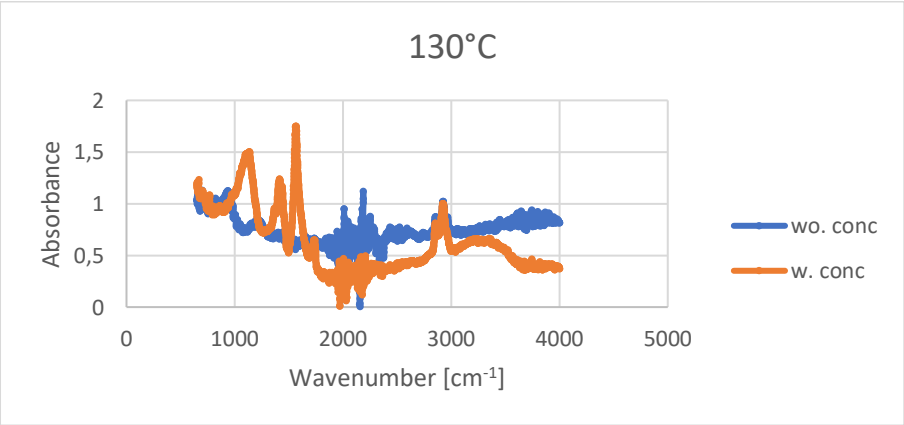

Appendix M: Comparison of Composition in the Trials on Used Oil Addition

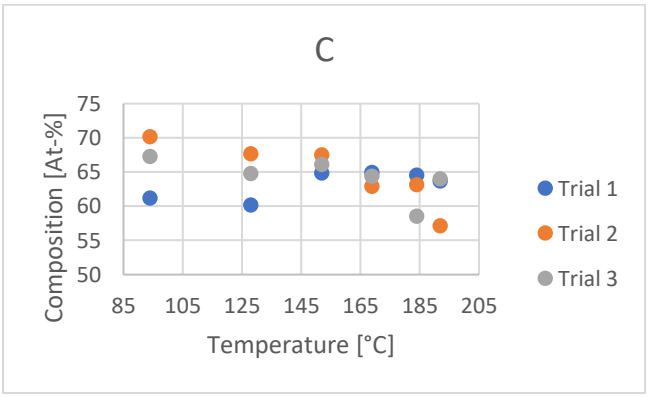

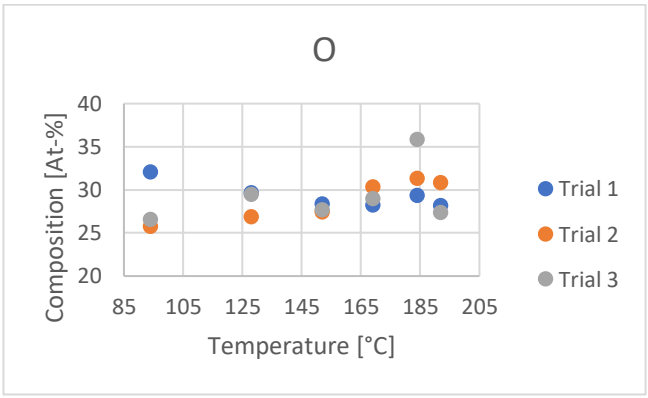

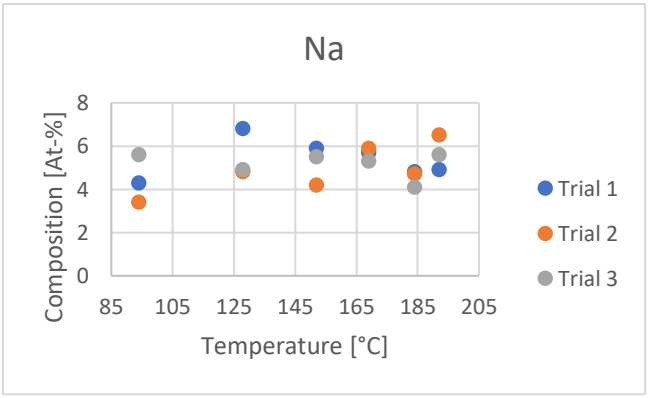

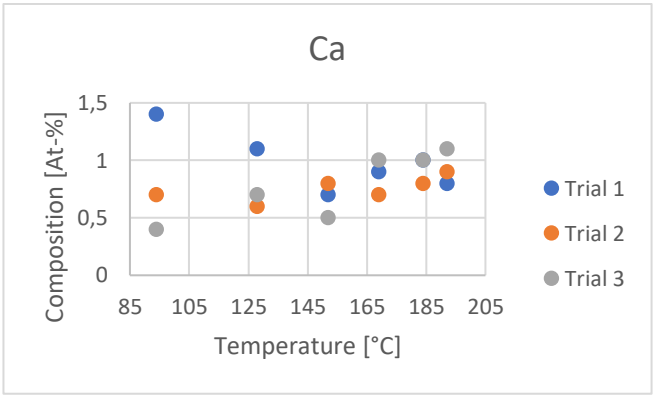

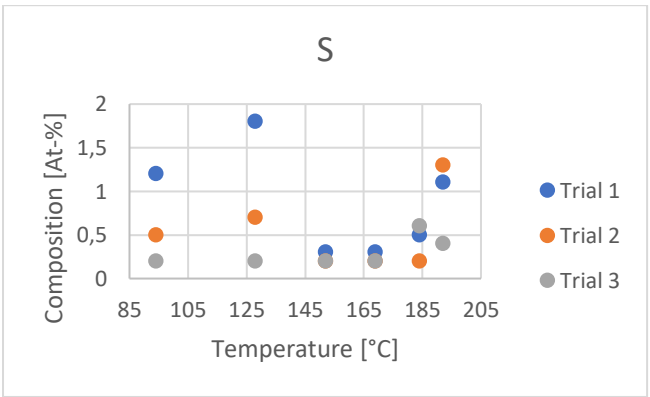

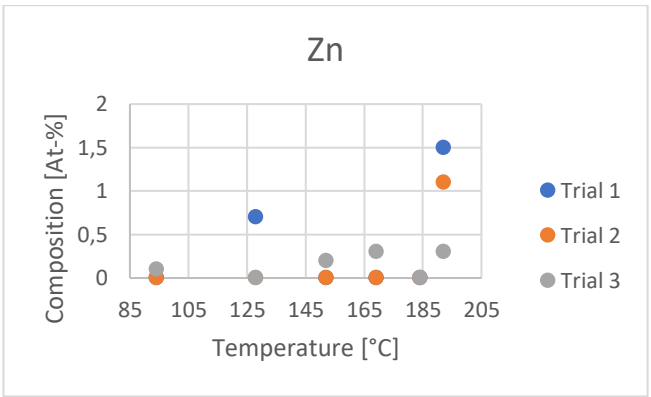

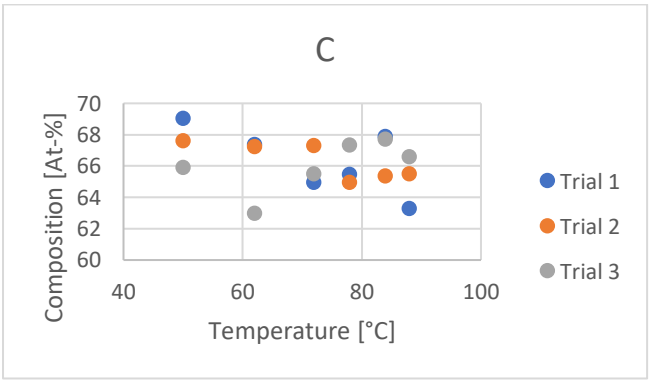

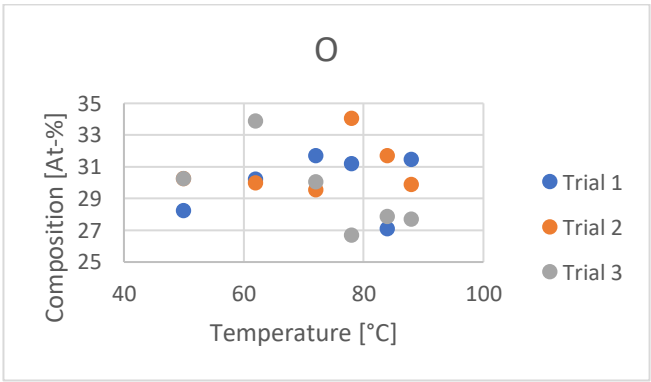

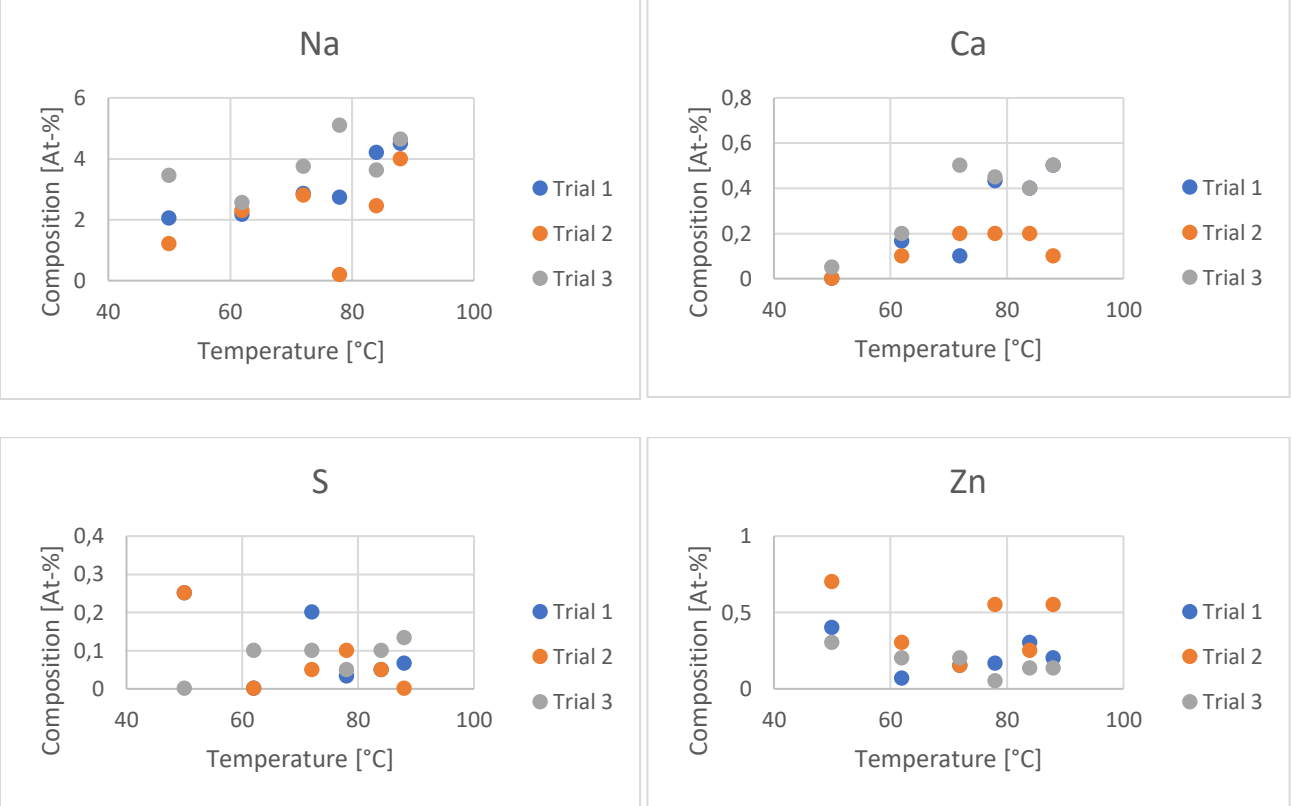

Appendix N: SEM-EDX Mapping of the Cross-sectional Area with Used Engine Oil with Concentrate

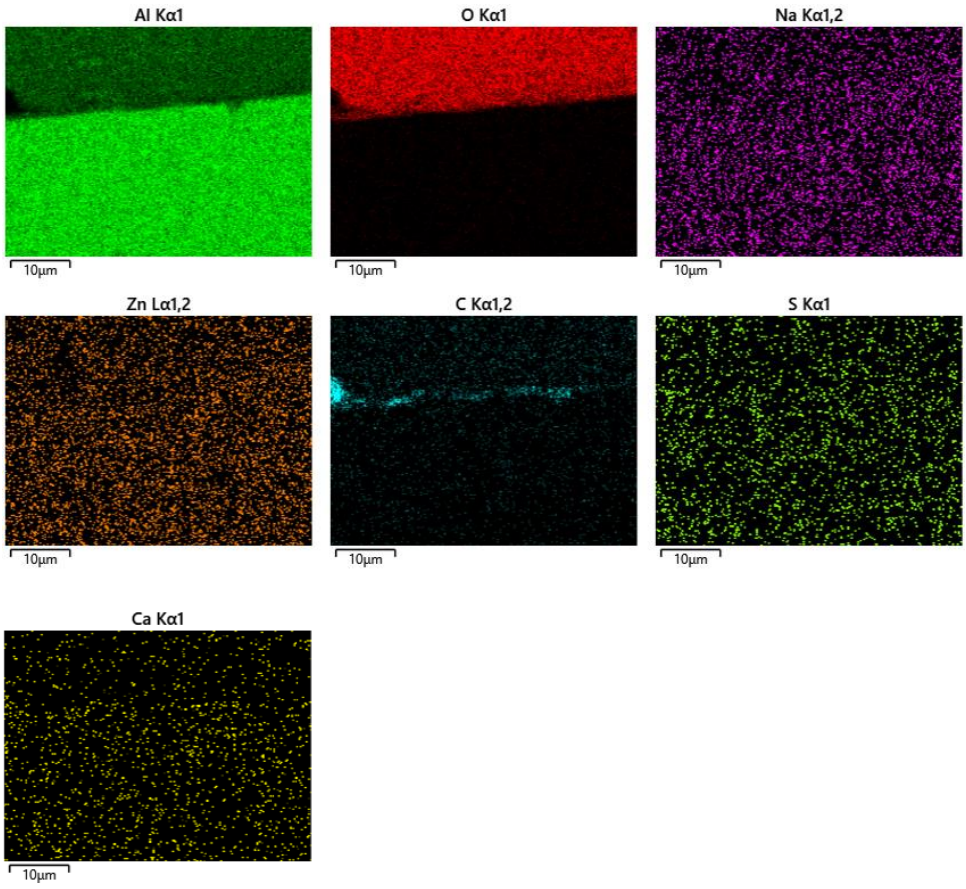

Appendix O: Comparison of Composition with Used Engine Oil without Concentrate

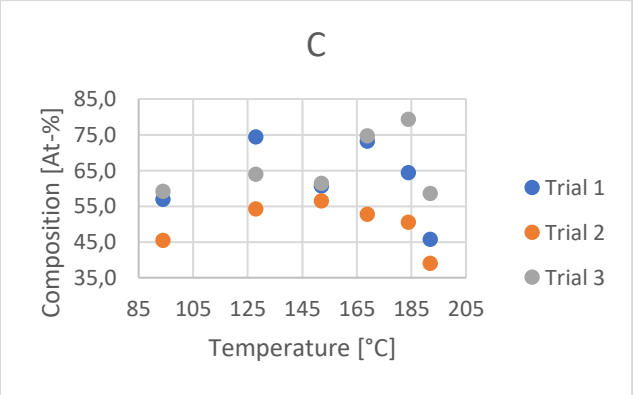

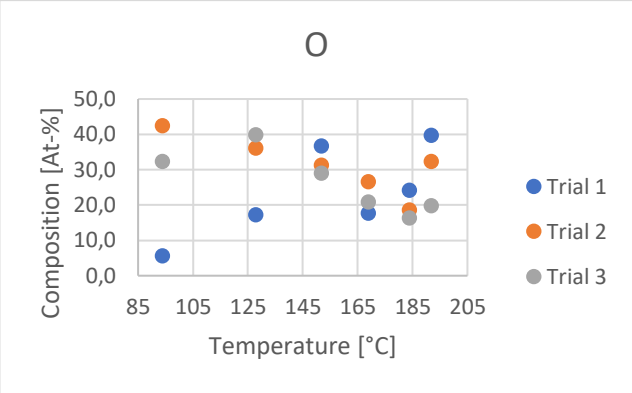

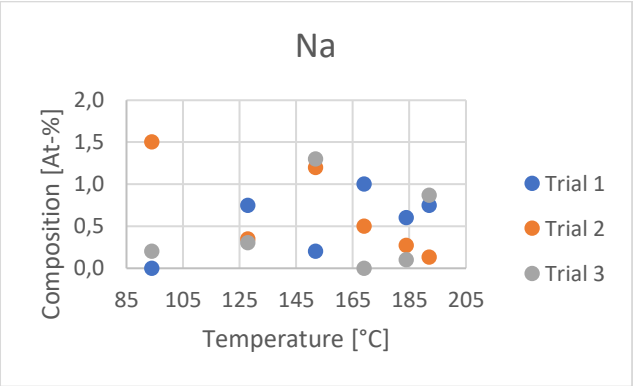

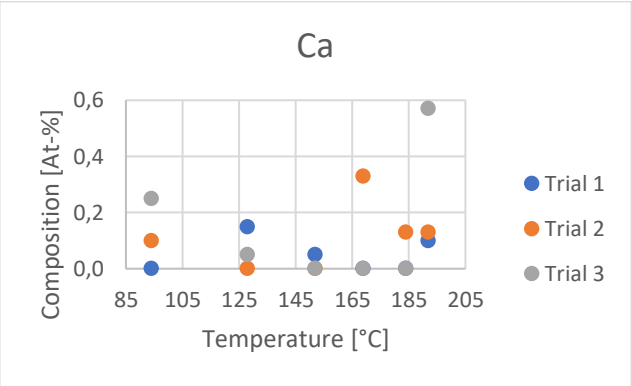

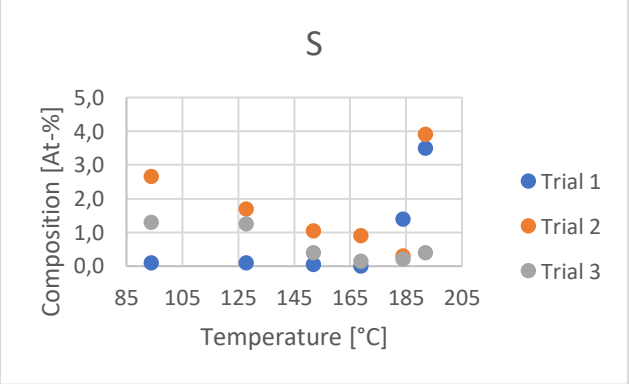

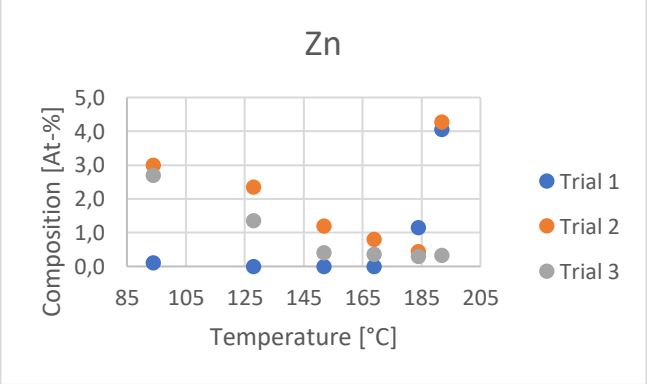

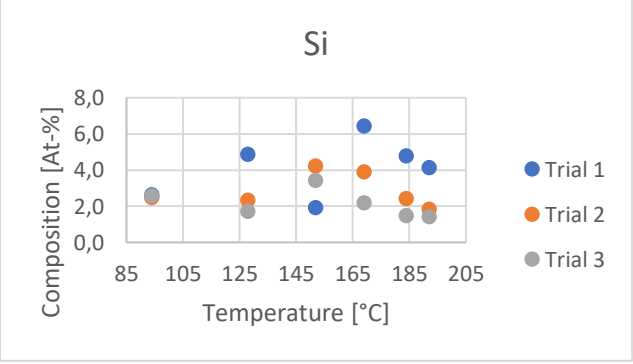

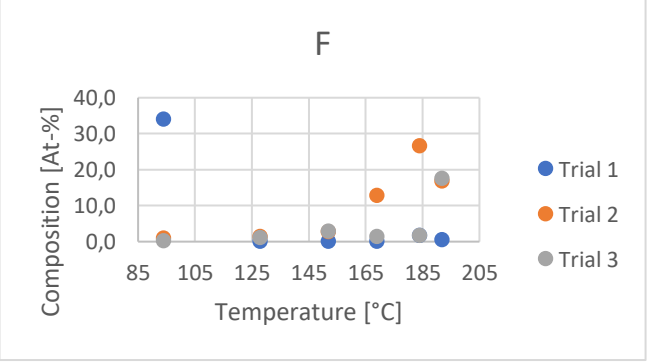

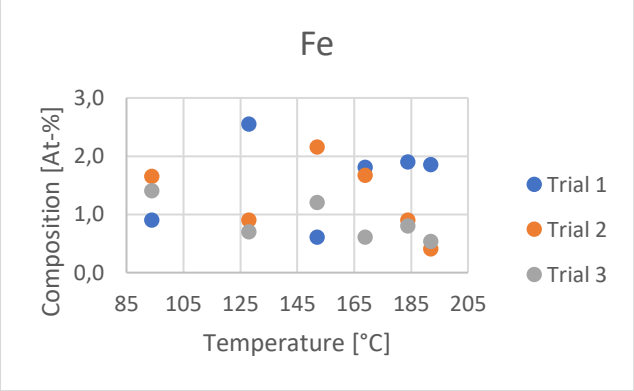

Appendix P: Comparison of Composition with Used Engine Oil with and without Concentrate

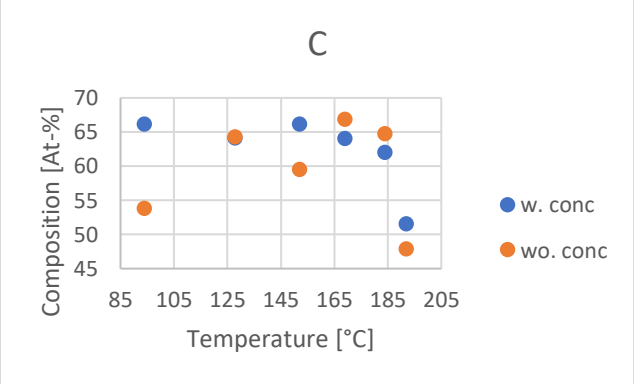

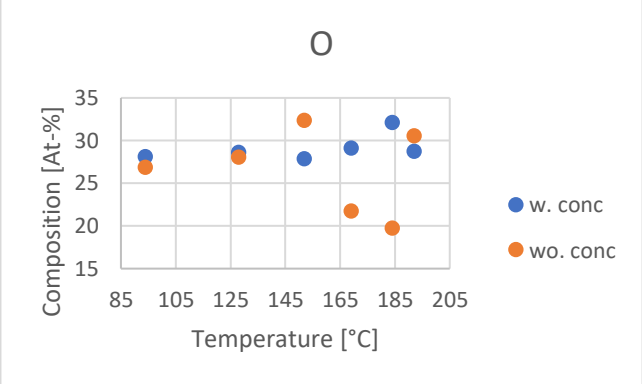

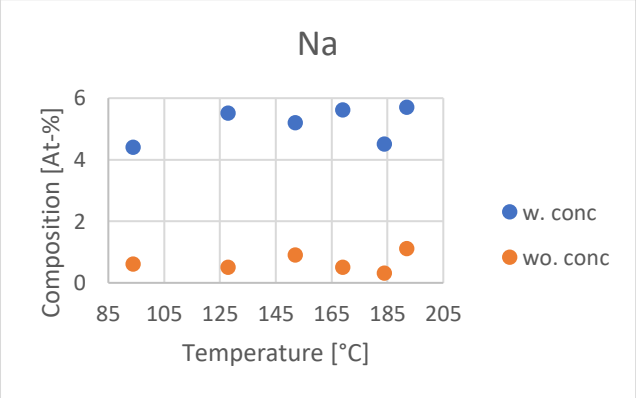

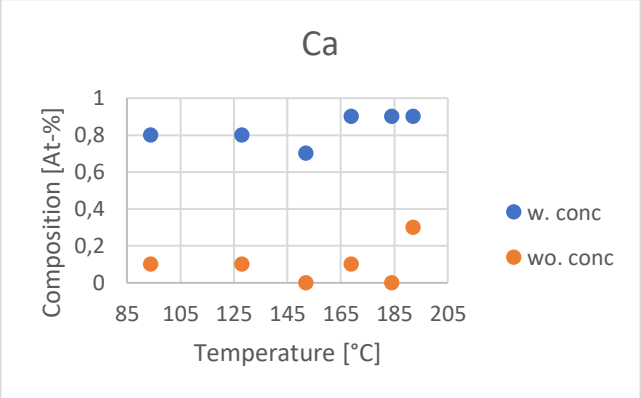

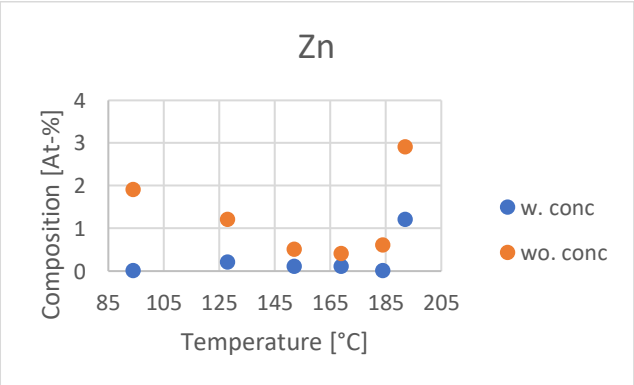

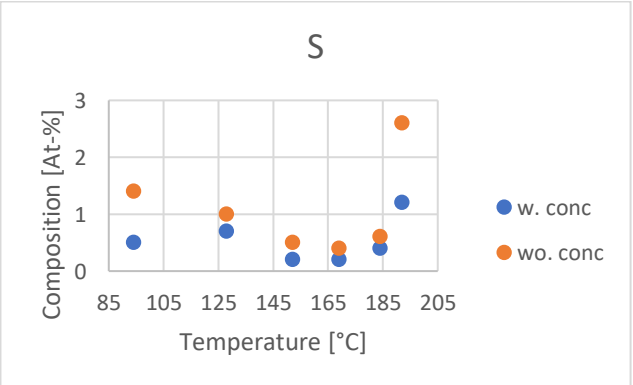

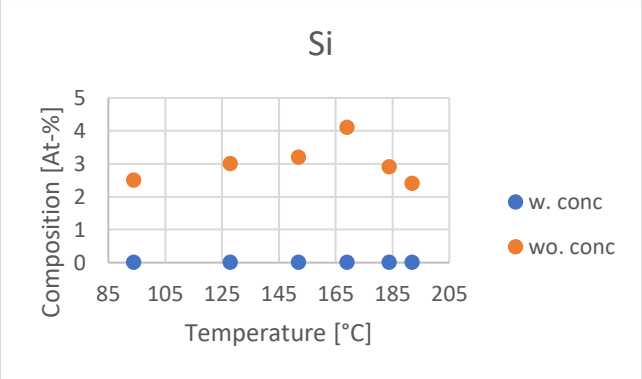

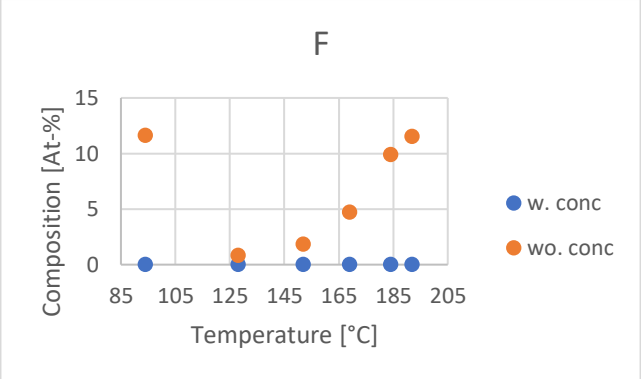

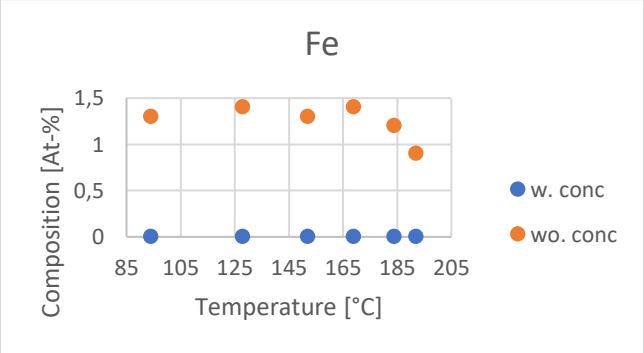

Appendix Q: FTIR spectra from the investigations on Used Engine Oil without Concentrate